



MASTER THESIS

MODELLING SHIP WAVES FOR OVERTOPPING ASSESSMENT PURPOSES

Daan Kampherbeek

Faculty of Engineering Technology
Marine and Fluvial systems

EXAMINATION COMMITTEE
Dr. J.J. Warmink
Dr. Ir. G.H.P. Campmans
Ir. M.P. Benit

17 December 2020

 **ARCADIS**

**UNIVERSITY
OF TWENTE.**

Er kwam een schip gevaren;
het kwam van Lobith terug,
met grint en rivierzand geladen.
Het richtte zijn boeg naar de brug.
Met boegbeeld en naam kwam het nader,
de ophaalbrug ging omhoog;
een deining liep door het water
dat over de kade bewoog.

Aangepast uit:
Het Schip – Ida Gerhardt

Modelling ship waves for overtopping assessment purposes

MSc. Thesis

of

Daan Kampherbeek

Student number: 1577972
Project duration: July 20, 2020 – December 17, 2020
Thesis committee: Dr. J. J. Warmink, University of Twente, supervisor
Dr. Ir. G. H. P. Campmans, University of Twente
Ir. M. P. Benit, Arcadis



**UNIVERSITY
OF TWENTE.**

ABSTRACT

In the Netherlands, inland waterways are an important part of the transport infrastructure. On the Waal alone, 120-140 million tonnes of freight gets transported annually. Every ship sailing on these waterways causes waves. Along low lying quays and dikes, overtopping by ship waves can pose hazards for pedestrians and vehicles.

Although a lot of effort has been spent on quantifying the effects of ship waves since 1949, there is no accurate way of estimating overtopping by ship waves. With models for overtopping being available, the problem lies in the availability of a model that can estimate ship-induced wave conditions at the bank. The analytical methods that are available for this purpose are limited in their accuracy and validity. This thesis aims to clarify whether the non-hydrostatic, non-linear shallow water flow model SWASH is a suitable tool for modelling ship-induced wave conditions at the bank for the purpose of overtopping.

Based on earlier research, there are indications that SWASH should be able to model both primary and secondary components of the ship wave. Up till now, the short, secondary ship waves were the limiting factor of comparable models. In SWASH the dispersion of secondary waves should be accurately represented. To test this hypothesis, three main steps are undertaken with as aim to find out how SWASH performs when modelling ship-induced waves for overtopping.

The first step is the implementation of the pressure field method in SWASH. In the pressure field method, a ship is represented as a time-varying atmospheric pressure field. The time-varying pressure field mimics the sailing ship. Implementing the pressure field method in SWASH proved to be possible. With a suitable numerical scheme, it was shown that the model can simulate a ship passage without crashing due to numerical instability. This is a proof of concept for simulating ship passages in SWASH. The spin-up effects can be separated from the actual wave signal by launching the ship first, and then accelerating it. For testing the implementation of the pressure field method, model settings were varied. The generated wave signal proved to be sensitive to the horizontal resolution of the computational grid. Important wave overtopping parameters like bottom roughness and turbulence only have a small influence on the ship wave signal. The biggest limitations for application of the model are the required computational effort and the numerical instability.

The second step in this research is the validation of the model to measurements and comparison of SWASH to existing analytical methods. In a towing tank, SWASH can reproduce primary components of the wave signal, but it overestimates the secondary wave height. The simulations of real passages in the Port of Rotterdam and the Nauw van Bath show that SWASH can model the wave signal in complex geometries. The uncertainties in the measurements and simulations make it hard to draw a quantitative conclusion about the accuracy of SWASH. When comparing estimated wave characteristics with conventional methods, SWASH outperforms both Dutch and German guidelines.

The third step in this research is a step towards extending the ship-wave model to include overtopping. Here, it was shown that with the full grid at a resolution useful for overtopping, the calculation time becomes unworkable. Options for grid refinement are local refinement around the overtopping area or splitting the model into a ship-wave generation part and an overtopping part. In this study, stability issues prevented SWASH from simulating the overtopping caused by a ship passage.

Overall, SWASH is a promising tool for estimating ship-induced wave conditions. The model has proven to be able to generate both primary and secondary ship waves. Wave signals and components can be estimated more accurately than with other methods. For the purpose of overtopping, SWASH can be used to generate the wave signal that serves as input for an overtopping model. To use SWASH in a standardized engineering methodology, further study on the certainty and sensitivity in the outcomes of the wave signals modelled by SWASH is necessary to increase the reliability of the model to levels acceptable for engineering applications. For this kind of study, measurements on the ship-induced surface excursion and flow velocities at the banks would be a useful addition.

CONTENTS

- Abstract** **1**
- List of Tables** **3**
- List of Figures** **4**
- 1 Introduction** **7**
 - 1.1 Ship-induced water motions 7
 - 1.2 Current ship-induced hazard estimation 10
 - 1.3 Problem statement and research questions 11
 - 1.4 Reading guide 12
- 2 Background** **13**
 - 2.1 History of ship wave effect estimation 13
 - 2.2 Modelling overtopping 14
 - 2.3 SWASH 15
 - 2.4 Ship wave effect estimation with SWASH 17
- 3 Research methodology** **19**
 - 3.1 Methodology outline 19
 - 3.2 Data sets 19
 - 3.3 Pressure field method implementation 22
 - 3.4 Validation 25
 - 3.5 First step to overtopping 31
- 4 Implementing the pressure field method** **32**
 - 4.1 Input grids 32
 - 4.2 Ship to pressure field 32
 - 4.3 Horizontal boundary conditions 35
 - 4.4 Numerical schemes and stability 36
 - 4.5 Reaching a steady state 38
 - 4.6 Model settings 40
 - 4.7 Further implementation characteristics 43
 - 4.8 Summary 46
- 5 Validation of wave generation** **47**
 - 5.1 MASHCON towing tank tests 47
 - 5.2 ROPES measurements 49
 - 5.3 Bath measurements 54
 - 5.4 Validation to analytical results 59
 - 5.5 Summary 64
- 6 First step towards modelling ship-induced overtopping** **65**
 - 6.1 Illustrative case study 65
 - 6.2 Options for refinement 65
 - 6.3 Summary 68

7 Discussion	69
7.1 Potential insights and limitations	69
7.2 Engineering applicability	70
7.3 Further research and opportunities	70
8 Conclusion	72
References	73
A Wave signal processing	77
A.1 Filtering method	77
A.2 Example results	77
B Example calculation time estimation	80
B.1 Uniform grid	80
B.2 Locally refined grid	80
C Case study layout	82
C.1 Geometry	82
C.2 Passage settings	82
C.3 Grid layout	83
D SWASH input file: MASHCON experiment F	84
E SWASH input file: MASHCON experiment E	86
F SWASH input file: ROPES simulation	88
G SWASH input file: Bath simulation	90

LIST OF TABLES

- 3.1 Properties of the model for the MASHCON data (Lataire et al., 2009). 20
- 3.2 Characteristics of the passage of the Bath validation experiment 27

- 4.1 Visible reflection in the horizontal boundary condition test cases. The launch wave indicates the disturbances caused by launching the ship. Reflection of the primary wave is not displayed because the model was created to be so wide that the primary waves don't reach the sides of it. 36

- 5.1 Simulations done for the ROPES experiment. As visible only simulation 2 ran successfully, so this simulation is used in further analysis. 51
- 5.2 Simulations done for the Bath experiment 55
- 5.3 Ship wave characteristics as calculated by several calculation methods 60
- 5.4 Ship wave characteristics as calculated by several calculation methods 61
- 5.5 Ship wave characteristics as calculated by several calculation methods 62

- C.1 Speed, secondary wave length and resolution for the different cases in the case study . . 83

LIST OF FIGURES

- 1.1 A canal dike example for which ship waves can be normative for overtopping. 7
- 1.2 Characteristic ship-induced water movements in a canal (BAW, 2010). Named in the figure are the return current and the propeller jet. The secondary waves are named as ‘Diverging bow wave’ and ‘Diverging stern waves’. The primary waves are named as ‘bow swell’, ‘Drawdown’ and ‘transversal stern wave’. 8
- 1.3 Typical wave signal at the bank caused by a ship passing through a relatively wide channel. The red box shows the primary wave, the green box the secondary bow wave and the blue box the secondary stern wave. 9
- 1.4 Typical wave signals for a ship sailing through a narrow channel. 10
- 1.5 The contribution of this research to improving the design of flood defences. 11

- 2.1 Measurements of squat being done for Schijf (1949). 13
- 2.2 Vertical grid definition in SWASH (Zijlema and Stelling, 2005). 16
- 2.3 The relation between water depth and vessel speed for two wave shortnesses, and between water depth and maximum possible vessel speed. 18

- 3.1 A short summary of the research setup as presented in Section 3.1. 19
- 3.2 The model as used in the MASHCON towing tank experiments (Lataire et al., 2009). . . . 20
- 3.3 The general locations in the Port of Rotterdam of the measurements done for ROPES campaign. 21
- 3.4 The general locations of the measurements done for the Bath measurements. 21
- 3.5 A visualisation of a ship sailing through a geometry. 22
- 3.6 Geometries from Lataire et al. (2009) as tested in SWASH 24
- 3.7 The geometry of Lataire et al. (2009), Experiment E as used in SWASH. 26
- 3.8 Passing distance calculation method for the Bath experiment. 29
- 3.9 The outcome of Equation 3.7 for 100 iterations, starting at $\Delta\bar{h} = 0$ 31

- 4.1 The waypoints and the track that is calculated from them for the ROPES measurements. 33
- 4.2 A frame model from SEAWAY. 34
- 4.3 Example interpolation of a ship on a pressure grid 34
- 4.4 The difference between the water levels as expected by pressure specification and the water levels as calculated by SWASH. 35
- 4.5 One of the unstable test runs. Visible are the wiggles behind the ship that should not be there in reality. 37
- 4.6 The pressure factor against time as used in the ROPES measurements. 38
- 4.7 Water level excursion in Experiment F from Lataire et al. (2009) as modelled by SWASH. 40
- 4.8 Wave signals for different grid cell sizes 41
- 4.9 Influence of the bottom friction on wave signal results. 42
- 4.10 Influence of the viscosity model on wave signal results 43
- 4.11 Depth averaged flow velocity magnitude in Lataire et al. (2009) experiment F. The main observations here are the return current along the ship, the wave-like pattern underneath the ship and the flow in track of the ship. 44
- 4.12 Difference between the water level as specified by the pressure grid and actual water levels as calculated by SWASH. The extra depth is the squat, which is 0.55 cm. Visible is the half-cell shift that could also be observed when simulating a stationary ship. Also visible is the mesh-like pattern underneath the ship which is not present in reality. 44
- 4.13 The performance of a SWASH model for simulations. 46

5.1	Water level excursion over the full domain in Lataire et al. (2009), Experiment E. The ship is sailing right to left.	48
5.2	Measured and modelled wave signals in Lataire et al. (2009), Experiment E.	48
5.3	Characteristics of the ship wave in Lataire et al. (2009), Experiment E. H_i is the secondary wave	49
5.4	Grid size distribution in i and j direction for the grid in the ROPES measurements.	50
5.5	Bathymetry, ship track and measurement locations for the ROPES simulation	50
5.6	Water level excursions as modelled in the ROPES passage.	52
5.7	Water level excursions in the measurement gauges for ROPES run 902. The time axis alternately hours:minutes or seconds.	53
5.8	Ship wave characteristics at the stern of the Jaeger Arrow for ROPES run 902. The differences between measurements and SWASH will be discussed in the text.	54
5.9	Cumulative grid cell size distribution for the simulation done at Bath.	54
5.10	An overview of the Bathymetry, ship track and measurement locations for the Bath measurement.	55
5.11	A visualisation of the water level excursion as modelled in the Bath passage.	56
5.12	Water level signal in the location of the AWAC as measured and modelled by SWASH	57
5.13	Characteristics of the ship wave components for the Bath experiment	58
5.14	The flow velocities as measured by the AWAC and the Vector in the Bath passage.	59
5.15	Comparison between measurements, SWASH, DIPRO and BAW guidelines (1)	60
5.16	The cross-sections of the ROPES geometry as used in the different calculation methods. In the case of DIPRO+, the displayed cross-section represents the average cross section.	61
5.17	Comparison between measurements, SWASH, DIPRO and BAW guidelines (2)	62
5.18	The cross-sections as used in the different calculation methods. In the case of DIPRO+, the displayed cross-section represents the average cross section.	63
5.19	Comparison between measurements, SWASH, DIPRO and BAW guidelines (3)	63
6.1	Location of the basis for the overtopping case study cross sections	66
6.2	The model of a CEMT-Va ship that is used in the case study	66
6.3	Run-up on the 0.5m resolution test grid for the casestudy.	67
6.4	Grid cell area in the overtopping case study.	67
A.1	The wave signals after filtering and the points at which the characteristics were determined, for the measurements in Lataire et al. (2009), Experiment E.	78
A.2	The wave signals after filtering and the points at which the characteristics were determined, for the model of Lataire et al. (2009), Experiment E.	78
A.3	The wave signals after filtering and the points at which the characteristics were determined, for the measurements on the Bath passage.	78
A.4	The wave signals after filtering and the points at which the characteristics were determined, for the model of the Bath passage.	79
C.1	Cross sections for the overtopping case study.	82

1 INTRODUCTION

In the Netherlands, inland shipping forms an important part of many logistical supply chains. Along the Rhine, 150-200 million tons of freight is transported, with the Waal accounting for 120-140 million tonnes annually (CCNR, 2019). This cargo is carried by around 8000 inland cargo vessels. The waterways are further populated by recreational boats. All these ships sailing along waterways interact. With each other, but also with the waterway causing waves and currents. In turn, these water movements influence the waterways they are in. Ship waves influence the morphology of the Western Scheldt (Aldershof, 2020) and can cause accidents with fishermen (Terlingen, 2011) or beach-goers (PZC, 2019).

Waves form an important part in the design of flood defences. Overtopping waves are the main cause of failure of flood defences (van Bergeijk et al., 2020). As the waves overtop a dike, the landward slope gets saturated and loses stability. Overtopping waves can also erode a cover layer (van Bergeijk et al., 2020). These failure mechanisms have their impact during a longer period of overtopping, for example during a storm. On large lakes, wide rivers and at sea, the main cause for overtopping are wind waves during storms. However, on smaller canals or next to low quays (Figure 1.1), ship waves can be normative. Ship waves are unlikely to cause failure of the flood defence. A ship passes, some waves overtop, but



Figure 1.1: A canal dike example for which ship waves can be normative for overtopping.

the repetitive overtopping that is necessary for failure doesn't take place. But even without failure of the flood defence, overtopping due to ship waves can cause problems. Cities like Deventer, Arnhem and Grave have buildings so close to the river that overtopping can cause damage before the flood defence fails (van Os, 2016). And most importantly, wave overtopping can cause hazardous situations for people on or immediately behind a flood defence. The amount of damage or danger is dependent on the characteristics of the overtopping waves (Van der Meer et al., 2018). It is therefore important to be able to calculate the characteristics of overtopping generated by ship waves.

1.1 Ship-induced water motions

Before overtopping can happen, a ship needs to generate waves. Once generated, these waves propagate towards the bank. At the bank they can cause overtopping. The first step: understanding ship-induced water motions is crucial for estimating overtopping. A ship sailing through a confined channel will cause several hydrodynamic effects. The Rock Manual (Ciria, 2007) distinguishes four parts: the return current, the primary waves, the secondary waves and the propeller jet. These parts are presented in Figure 1.2. All four parts will be shortly discussed.

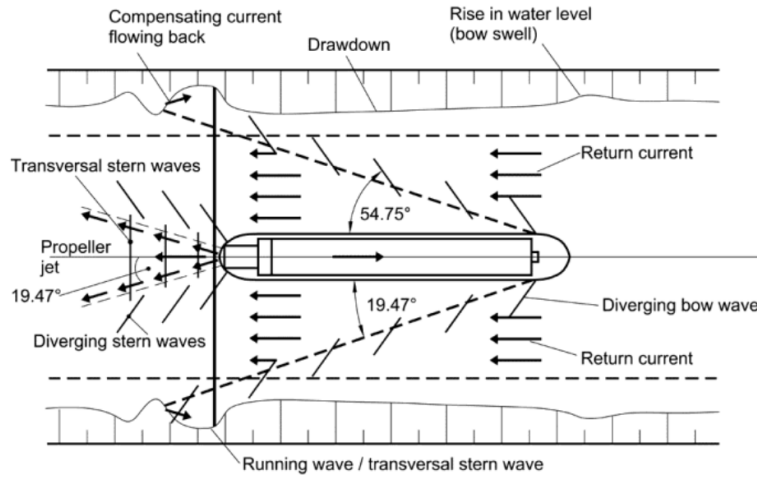


Figure 1.2: Characteristic ship-induced water movements in a canal (BAW, 2010). Named in the figure are the return current and the propeller jet. The secondary waves are named as 'Diverging bow wave' and 'Diverging stern waves'. The primary waves are named as 'bow swell', 'Drawdown' and 'transversal stern wave'.

1.1.1 Return current

The return current is caused by the ship displacing water as it sails along. Water is moved away from the ship at the bow, and attracted at the stern. In combination with the primary water level drop, return current can be calculated using the 1D continuity equation (1.1) and the 1D Bernoulli equation (1.2) (Talstra, 2012):

$$V_s A_c = (V + u)(A_c - A_s - Bz) \quad (1.1)$$

$$h + \frac{V_s^2}{2g} = h - z + \frac{(V_s + u)^2}{2g} \quad (1.2)$$

In which A_c is the channel cross sectional area, A_s is the ship cross section area, B is the channel surface width, V_s is the vessel speed, h is the undisturbed water level, g is the gravity constant and z and u are the water level depression and return flow velocity to be computed. As visible, the return current is dependent on the ratio between the channel cross sectional area and the vessel cross-sectional area and the vessel velocity.

1.1.2 Primary waves

The primary waves are related to the return current. They consist of a transverse front, a water level depression alongside the ship and a transverse stern wave. The z in equations 1.1 and 1.2 is the same water level depression as used for the return current. The increased speed in the return current causes a pressure drop according to Bernoulli, which in turn causes a water level decrease. Because of this, the magnitude of the water level depression is dependent on the same characteristics as the return current. The primary waves form over the total length of the ship. The magnitude of the primary flow effects is dependent on the distance to the ship. Further away from the ship, the primary waves will get less pronounced. If the ship sails close to a bank, the primary waves will get constant along the distance between ship and bank.

1.1.3 Secondary ship waves

The secondary waves are caused by interference between diverging waves from bow and stern, and transverse waves along and behind the ship. The crests of the secondary waves form at a line with an angle of 19° from the pressure point that causes the diverging waves. The crest orientation is 55° from the sailing direction. The secondary waves propagate at an angle of 35° from the sailing direction (Wal, 1990). The height of the secondary waves is influenced by the bow shape (Habben Jansen, 2016). Opposite to the primary waves which are pressure effects, the secondary waves can further be described as gravity waves (Ciria, 2007).

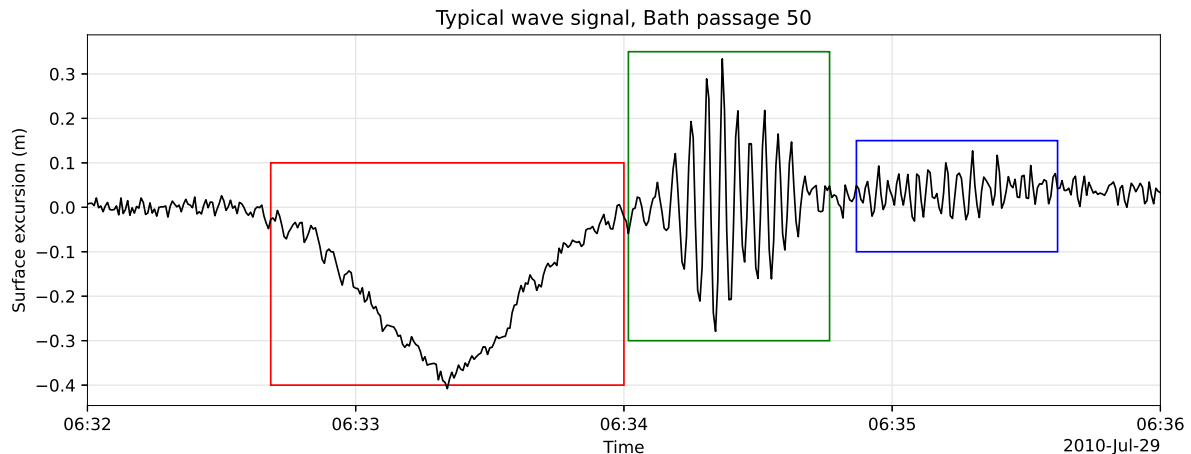


Figure 1.3: Typical wave signal at the bank caused by a ship passing through a relatively wide channel. The red box shows the primary wave, the green box the secondary bow wave and the blue box the secondary stern wave.

1.1.4 Propeller jet

During sailing, the propeller causes a turbulent flow in the opposite direction of sailing. This propeller jet is created behind the ship. The propeller jet has no direct influence on the bank, but it influences the magnitudes of the other ship wave components (Talstra, 2012). When no propeller jet is present, the water around the ship behaves differently. A ship being towed creates an inequality between the water level at the front of the ship and the water level at the back. The water being pushed away at the bow has to flow to the back of the ship where it fills the volume the back of the sailing ship leaves behind. Meanwhile, with no propeller present, a water level difference provides the driving force. A propeller compensates this effect and creates an equality between the water level at the front of the ship and at the back. The propeller increases the flow speeds in the primary wave, and therefore increases primary wave magnitude.

1.1.5 Wave effects at the bank

Depending on the channel geometry, the typical wave signal at the bank may differ. With the primary wave forming along the length of the ship and decaying in a wider canal, distance to the bank mainly influences the water level depression height. With the secondary wave forming at 19° from the bow or stern, distance to the bank mainly influences the wave timing. Figure 1.3 shows a typical wave signal for a wide channel. Here, the primary water level depression is visible but the primary bow and stern waves have decayed so much that they cannot be identified anymore. The secondary waves arrive after the primary wave has passed.

For a narrow channel, the wave signal differs a little from the signal in a wide channel. A typical signal for a narrow channel is pictured in Figure 1.4. Here, the primary bow and stern wave as well as the water level depression perpendicular to the ship can be seen in 1.4 a). Most notable is the deep depression at the bow and stern of the ship with a less deep depression in the middle. 1.4 b) shows the secondary bow and stern wave signal. In both narrow and wide channels, the secondary waves form a train that first increases in height, reaches a peak and then decreases in height again while wave period stays the same.

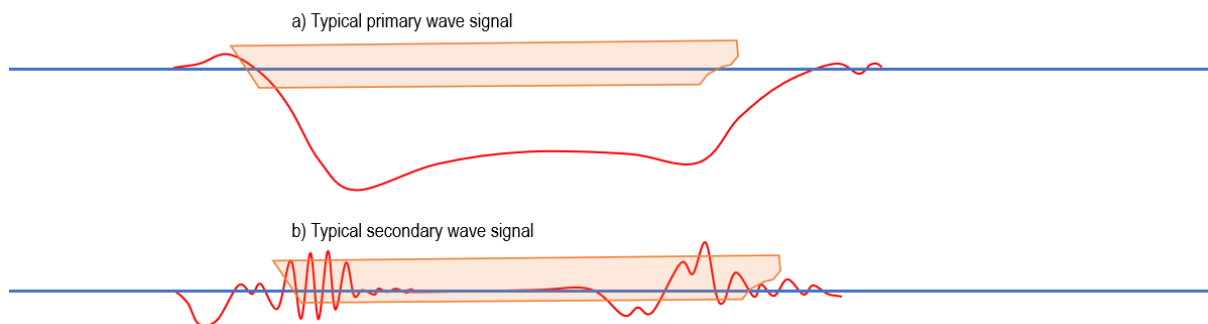


Figure 1.4: Typical primary and secondary wave signals for a ship sailing through a narrow channel. The x-axis represent x position. The y-axis is height. The blue line is the still water level. The red line is the wave signal. a) shows the primary bow and stern wave as well as the primary water level drop. b) shows the secondary bow and stern wave just next to the ship. Source: Wal (1990).

1.2 Current ship-induced hazard estimation

Currently, the estimation of overtopping hazard caused by ships is based on empirical equations and a coupling to wind waves. The hazard estimation process consists roughly of two steps:

1. Estimation of wave conditions at the bank
2. Estimation of overtopping characteristics

These overtopping characteristics are then linked to the hazard, which can be compared to an acceptable hazard level.

For the estimation of wave conditions of the bank, several empirical methods are available. First and most easy is taking the maximum wave height from guidelines like 'The Rock Manual' (Ciria, 2007) or the 'Technisch Rapport Ontwerpbelastingen Rivierengebied' (ENW, 2007). These guidelines give set numbers for the maximum ship-induced wave heights that can occur, independent of location. The second method for estimation of wave conditions at the bank is calculating them according to empirical methods like DIPRO+ (Waterloopkundig Laboratorium, 1997) or the BAW guidelines (BAW, 2010). In these methods, the waterway geometry and ship characteristics are taken into account in a simplified form. DIPRO+ is only valid for inland ships in geometries where the ship length is larger than the channel width. In complex geometries, the primary water motions can be modelled by using shallow water flow models (de Jong, 2010), (Zhou et al., 2013), (Verheij and van Prooijen, 2007). However, due to their nature these models cannot accurately predict the secondary ship waves or the overtopping caused by the waves. The simplified geometries and the lack of a model that can estimate all ship waves components causes uncertainty in the estimation of wave conditions at the bank.

For the estimation of overtopping characteristics, an engineer can now resort to existing empirical relations for wind waves. For example the equations in the 'Overtopping Manual' (Van der Meer et al., 2018) or the 'Leidraad Kunstwerken' (TAW, 2003). These equations give time-averaged overtopping discharge which can be related to other characteristics like single wave overtopping volume. These relations are mainly applicable for the secondary waves. There are no relations specifying overtopping caused by the combination of ship wave components.

The differences between wind waves and ship-induced waves cause further uncertainty between the characterisations done based on time-averaged overtopping discharge. As indicated by (Altomare et al., 2020), overtopping flow speeds and layer thicknesses are the determinant factor for the safety of pedestrians. Not time-averaged overtopping discharge. A relation for overtopping flow-speed and layer thickness is lacking, but it can be modelled by for example the non-linear, non-hydrostatic shallow water flow model SWASH (Suzuki et al., 2014).

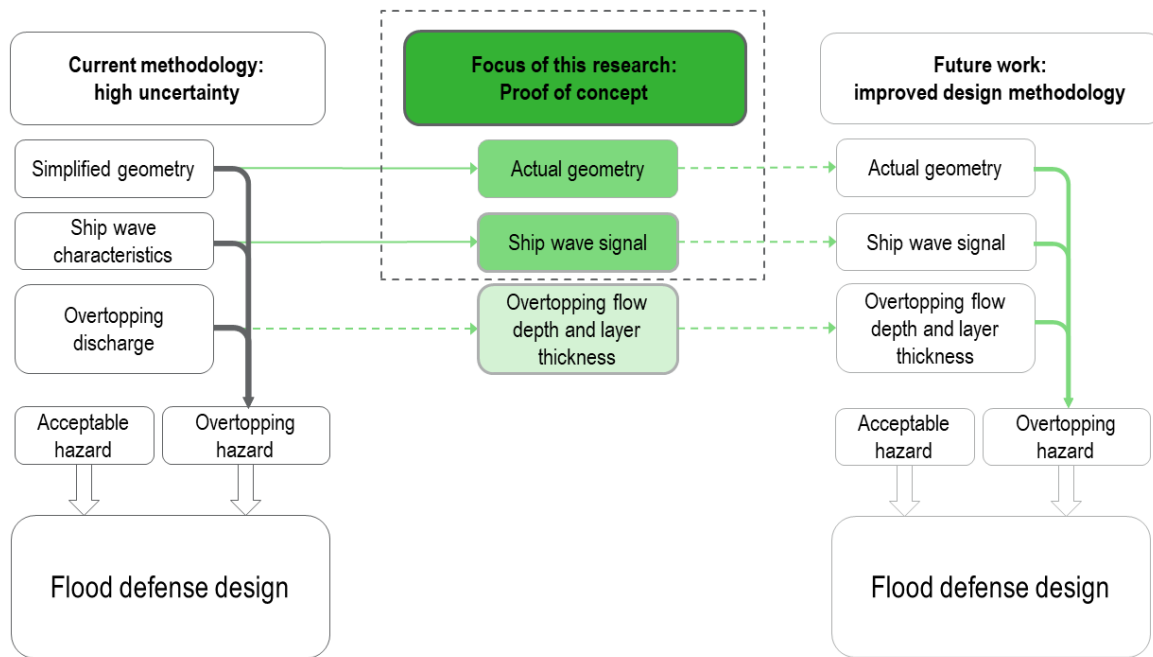


Figure 1.5: The contribution of this research to improving the design of flood defences.

1.3 Problem statement and research questions

Figure 1.5 shows the position of this research into the broader context of risk-based design. Currently, there is no good method to estimate overtopping hazard caused by sailing ships. A good method will accurately quantify this hazard. In simple geometries, Rijkswaterstaat advises to use DIPRO+ (ENW, 2007). The ship wave characteristics as calculated by DIPRO+ can then be used for overtopping estimation using the same relations as used for wind waves. These relations are mainly aimed at overtopping hazard during storms and not necessarily useful for the hazards caused by ship waves. Also, the software is no longer supported. In complex geometries, the primary ship-induced water motions can be modelled with models based on the shallow water equations. For the secondary waves no suitable model is available yet. As will be explained in Chapter 2, SWASH is expected to be able to model both primary and secondary ship wave effects. SWASH has already been validated for overtopping flow speeds and layer thicknesses. The objective of this research project therefore is:

To find out how SWASH performs when modelling ship-induced waves for the purpose of overtopping, by recreating ship wave generation in SWASH, validating the generated wave signals and putting a first step to modelling ship-induced overtopping with SWASH.

The objective is broken down into several research questions. When these questions are answered, the objective is reached. The research questions follow the structure of the objective:

1. In what way can the pressure field method be implemented in SWASH, and how do the settings that influence overtopping influence ship wave generation?
2. To what extent can SWASH reproduce the ship wave components relevant for simulating overtopping?
3. What is the first step towards extending the ship-wave model in SWASH to include overtopping?

In the larger picture, this research will contribute to a proof of concept for estimating the ship-induced overtopping hazard, eventually leading to less uncertainty in flood defence design.

1.4 Reading guide

In Chapter 2, existing knowledge on ship waves will be summarised, together with an explanation of SWASH and the grounds for the expectation that SWASH will be able to model ship waves. Also, a short summary on the modelling of overtopping will be given here. Chapter 3 will describe the research methodology. It will start with an outline, a description of the data sets and then the methodology used to answer the research questions. Chapter 4 will describe how the sailing ships can be implemented in SWASH. A global description of the model performance using these settings will also be presented. The chapter will be finalized with a conclusion summarizing the information necessary for answering the first research question. Chapter 5 will describe the validation experiments, how they were implemented in SWASH and how the results were compared with other measurements. The comparison with conventional calculation methods will be done for Experiment F from Lataire et al. (2009). The chapter will be finalized with a conclusion summarizing the information necessary for answering the first research question. Chapter 6 will present an illustrative case study to identify the problems regarding modelling ship-induced overtopping with SWASH. The chapter will be finalized with a conclusion summarizing the information necessary for answering the first research question. The overall results will be discussed in Chapter 7, and the research questions will be answered in Chapter 8.

2 BACKGROUND

The focus of this chapter lies on the background of the research: which relevant work has been done before? With the aim of this research to find out how SWASH performs when modelling ship-induced waves for the purpose of overtopping, the background will focus on the estimation of ship-induced waves, on modelling overtopping and on SWASH. To start, a short history of ship wave effect estimation will be given. Then, the different options for modelling overtopping will be discussed. After this, a description of SWASH will be given and the chapter is finalised by a description of the reason why SWASH is expected to be able to model the full ship wave.

2.1 History of ship wave effect estimation

Ship induced water motions have been studied in the Netherlands since just after the second World War. Schijf (1949) was the first to describe the water movements around a ship sailing in a canal. He introduced a simple formula for squat in a confined channel: the lowered water pressure next to a ship that is caused by the ship sailing. Figure 2.1 shows a picture of the measurement campaign.



Figure 2.1: Measurements of squat being done for Schijf (1949).

Later, in the 1970s and 1980s, Rijkswaterstaat commissioned another measurement campaign for ship-induced water motions, described in Verheij and Laboyrie (1988). The results from this measurement campaign formed the basis for new bank protection design norms in the Netherlands. The computer program DIPRO, in which the formulae from Verheij and Laboyrie (1988) were implemented was created as

a design tool for bank protections. The formulations in DIPRO are in turn integrated in 'The Rock Manual' (Ciria, 2007). DIPRO has since seen several updates (Wal, 1990) increasing its applicability and user friendliness. DIPRO is developed for inland shipping situations, in geometries which can be schematized as trapezoids. Given the fact that the formulae from DIPRO were not well applicable for complex geometries, Raven (2001) and Verheij et al. (2001) tried to develop a numerical model that could simulate ship-induced water motions. This model was a coupling between the model potential flow model RAPID and the boussinesq model TRITON. The coupled models could well estimate ship wave generation and propagation. At the time calculation capacity was too expensive to continue this model development. In 2007, Rijkswaterstaat commissioned a report for the improvement of DIPRO by comparing it with the shallow water flow model FINEL2D (Verheij and van Prooijen, 2007). This report found unexplainable differences between the water movements as calculated by DIPRO and those calculated by FINEL2D, possibly due to the fact that the case studied was with a sea-going vessel instead of an inland vessel for which DIPRO is designed. In more recent years, studies on ship-induced water motions were done with XBeach (Zhou et al., 2013), (de Jong et al., 2013) and Delft3D (Zhou et al., 2013). These studies found that the primary flow effects caused by ships could be modelled well by shallow water flow models. The secondary waves were still a challenge. Being based on the shallow-water equations, these models are mainly useful for modelling long, non-dispersive, shallow-water waves. The secondary waves are shorter and can be dispersive. Due to the formulations in the models, the secondary waves will be either not generated or their speed will be underestimated.

Next to studies on ship-induced water motions in canals, in recent years, some studies have been done on the effects that ship waves have on the morphology of estuaries. Measurements done at the Nauw van Bath by Huisman et al. (2010) indicate that both primary and secondary ship waves can temporarily cause a significant increase in bottom shear stress, and that ship waves will influence the erosion of the banks. This same conclusion was drawn by Aldershof (2020). Although not the scope of this research, these conclusions create extra relevance for the modelling of ship waves.

2.2 Modelling overtopping

In many construction projects, overtopping is calculated using empirical relations as described by the Overtopping Manual (Van der Meer et al., 2018). The main relation employed is:

$$\frac{q}{\sqrt{gH_{m0}^3}} = a \exp \left[- \left(b \frac{R_c}{H_{m0}} \right)^c \right] \quad \text{for } R_c \geq 0 \quad (2.1)$$

In this formula, q is the time-averaged overtopping discharge per meter width. g is the gravity constant. H_{m0} is the significant wave height at the toe of the structure. a , b , and c are parameters for the structure, which describe the effects of wave-structure interaction on overtopping. R_c is the crest height of the structure. The outcome of this main relation is time averaged overtopping volume, dependent on wave and structure characteristics.

In combination with wave parameters, the time averaged overtopping discharge forms the basis for classification of other overtopping characteristics such as individual maximum overtopping volume V_{max} , and stability characteristics. As a storm progresses, overtopping waves cause saturation of the landward side of flood defences, leading to failure (van Bergeijk et al., 2020). This process is very dependent on time-averaged overtopping discharge. For quantifying the risk of ship-induced wave overtopping, time averaged wave overtopping volume may not be a good criterion. As ships cause only a limited number of waves, inundation or structural failure of the flood defence is not likely. More relevant are hazards for people and vehicles immediately behind the flood defence. The safety of pedestrians is linked to a combination of flow speed and layer thickness during overtopping. Not to time averaged discharge or single wave overtopping volume (Altomare et al., 2020), (Hujii et al., 1994). Mares-Nasarre et al. (2019) indicates that flow speed and layer thickness are not correlated. Both are relevant to determine the safety of people flood defences during overtopping. This confirms the statement done by Allsop et al. (2008) that mean discharge is not a good characteristic for evaluating the safety of people. Being able to model overtopping flow speeds and layer thicknesses would therefore be an improvement over current calculation methods when estimating the safety of pedestrians and vehicles in the case of overtopping ship waves.

Next to the empirical relations for estimating overtopping effects, numerical models are used for testing geometries. In a benchmark test of numerical modelling for wave overtopping, Lashley et al. (2020) distinguish two types of models for wave effects: phase averaged models and phase resolving models. For

ship waves, the primary flow effects and the small amount of secondary waves make a phase averaged wave model less suitable. Within the phase-resolving models, several approaches to modelling the water movements can be taken. The most accurate models with the least theoretical limitations solve the fully nonlinear, reynolds-averaged Navier-Stokes equations. These models solve the full flow structure. van Bergeijk et al. (2020) already demonstrated that it is possible to estimate overtopping flow velocities and layer thickness with such a model. The largest drawbacks of these accurate models is the computational effort that is required for the simulations. To reduce the required computational averaged, a model can be made depth-averaged.

2.3 SWASH

SWASH is a non-hydrostatic shallow water flow model developed for simulating water motion in complex geometries. It is applicable in coastal regions up to the shore. It is begin developed at the TU Delft since the early 2000's. When using the classification as described above, SWASH falls under the phase-resolving models. When run with one vertical layer, it is also depth-averaged. Until yet, SWASH has been used for a wide range of studies, ranging from the investigation of the effect that harbor navigation channels have on waves (Dusseljee et al., 2014), to sand dune breaching (Miani et al., 2015), wave run up in urban areas (Guimarães et al., 2015) and landslide-generated waves (Mulligan et al., 2019).

The applicability of SWASH for calculating wave overtopping has already been demonstrated by Suzuki et al. (2014), Suzuki et al. (2017) and Vanneste et al. (2014). Here, SWASH was found to produce a reasonable estimate of overtopping for a dike with a shallow foreshore as well as for a quay wall. In these studies, several methods have been used for characterising the wave overtopping. Among these methods are the use of layer thickness and flow velocity for the calculation of overtopping volume. SWASH is therefore expected to be a suitable tool for simulating the overtopping characteristics relevant for wave overtopping caused by ship waves.

2.3.1 Governing equations

The governing equations in SWASH are the non-linear, non-hydrostatic shallow water equations, as given by:

$$\frac{\partial u}{\partial x} + \frac{\partial v}{\partial y} + \frac{\partial w}{\partial z} = 0 \quad (2.2)$$

$$\frac{\partial u}{\partial t} + \frac{\partial u^2}{\partial x} + \frac{\partial vu}{\partial y} + \frac{\partial wu}{\partial z} + \frac{g}{\rho_0} \frac{\partial \zeta}{\partial x} + \frac{g}{\rho_0} \frac{\partial q}{\partial x} + c_f \frac{u\sqrt{u^2 + v^2}}{h} = \frac{1}{h} \left(\frac{\partial h\tau_{xx}}{\partial x} + \frac{\partial h\tau_{xy}}{\partial y} \right) \quad (2.3)$$

$$\frac{\partial v}{\partial t} + \frac{\partial uv}{\partial x} + \frac{\partial v^2}{\partial y} + \frac{\partial wv}{\partial z} + \frac{g}{\rho_0} \frac{\partial \zeta}{\partial y} + \frac{g}{\rho_0} \frac{\partial q}{\partial y} + c_f \frac{v\sqrt{u^2 + v^2}}{h} = \frac{1}{h} \left(\frac{\partial h\tau_{yx}}{\partial x} + \frac{\partial h\tau_{yy}}{\partial y} \right) \quad (2.4)$$

$$\frac{\partial w}{\partial t} + \frac{1}{\rho_0} \frac{\partial q}{\partial z} = 0 \quad (2.5)$$

$$\tau_{xx} = 2v_t \frac{\partial u}{\partial x}, \tau_{xy} = \tau_{yx} = v_t \left(\frac{\partial v}{\partial x} + \frac{\partial u}{\partial y} \right), \tau_{yy} = 2v_t \frac{\partial v}{\partial y} \quad (2.6)$$

In these equations, t is time, u , v and w are velocities in x , y and z direction, ζ is the surface elevation, measured from the still water level d . ρ_0 is the water density. q is non-hydrostatic pressure. c_f is a dimensionless friction coefficient, depending on the bottom friction model. $h = \zeta + d$ is water depth and τ_{xx} , τ_{xy} , τ_{yx} and τ_{yy} are horizontal turbulent stress with v_t as local effective viscosity. The value of v_t is governed by the selected horizontal eddy viscosity model. From the formulas can be noted that hydrostatic and non-hydrostatic pressure are separate terms. Because of this, the equations presented above see too many unknowns for solving the system of equations. To make the system solvable, q is solved from a different set of equations. The equation system for q can be found in Zijlema et al. (2011). A further description of the governing equations of SWASH is given in Zijlema et al. (2011), Zijlema and Stelling (2008) and Zijlema and Stelling (2005).

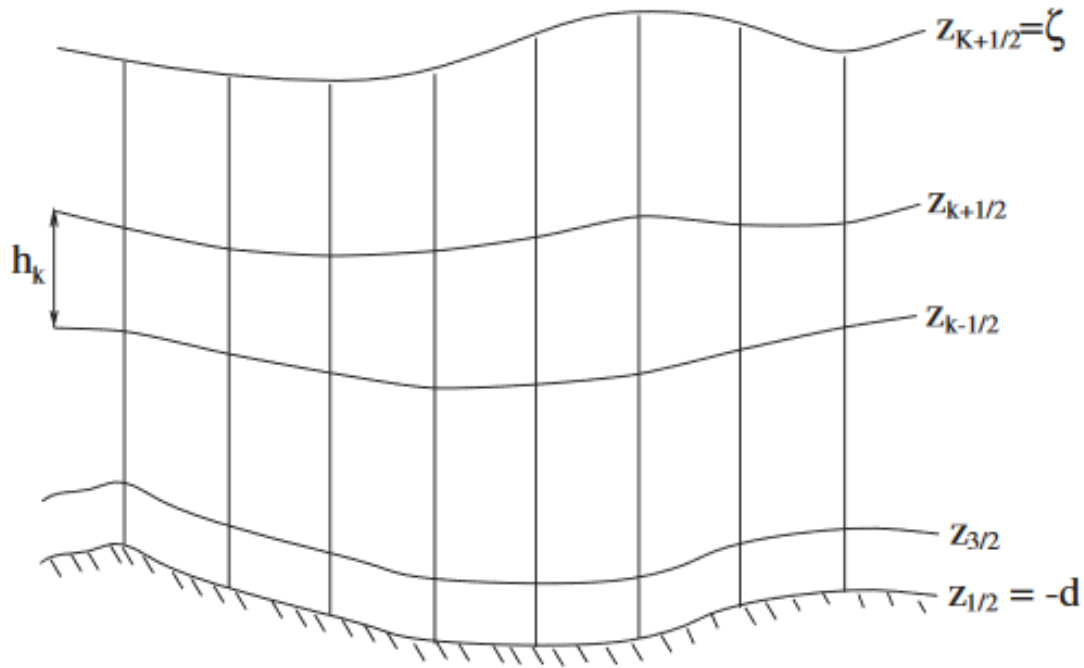


Figure 2.2: Vertical grid definition in SWASH (Zijlema and Stelling, 2005).

2.3.2 Discretizations

The discretization of the governing equations in SWASH is done using a finite difference method on a staggered, orthogonal curvilinear grid (Zijlema et al., 2011). The velocity is computed at the cell centres, while the other variables are computed at the grid points. The velocity is also evaluated at a half between the timestep. For the time-integration, by default an explicit leapfrog scheme is used. Implicit time integration is also possible but this requires more memory. When the flow is pressurized in some point in the simulation, implicit time integration is necessary. The default discretization of the momentum equation uses a second order explicit time step for advection, a first order explicit time step for the viscosity term and a first order implicit time step for the non-hydrostatic part (Zijlema et al., 2011). In SWASH, the space discretizations of the momentum equations can be set. These settings will be discussed in Section 4.4.

2.3.3 Vertical layers

In the default settings of SWASH, the vertical layers are implemented terrain following. This means that the layer thickness is always relative to the water depth. Figure 2.2 illustrates how the vertical layers follow terrain and water surface. The number of vertical layers determines the dispersive qualities of the model. More vertical layers means better dispersive qualities for short waves. The shortness of a wave is expressed in kh value, which is the wave number (k) times the still water depth (h). A low kh value means a long wave relative to the water depth. A higher kh value means a shorter wave relative to the water depth. Zijlema et al. (2011) indicates that SWASH accurately solves wave dispersion for $kh < 3$ in depth averaged mode and $kh < 16.4$ with three vertical layers.

2.3.4 Time-step

The time-step of SWASH is dynamically controlled by the Courant number:

$$Cr = \Delta t \left(\sqrt{gh} + \sqrt{u^2 + v^2} \right) \sqrt{\frac{1}{\Delta x^2} + \frac{1}{\Delta y^2}} \leq 1 \quad (2.7)$$

For dynamic selection of the time-step, SWASH looks at the maximum Courant number of all wet grid cells. By doubling or halving the time-step, SWASH will stay between the minimum allowed Courant

number (Cr_{min}) and the maximum allowed Courant number (Cr_{max}). As visible, in the equation, at a constant Courant number, the time-step decreases if the cell size decreases. As SWASH looks at all wet grid cells, one smaller cell already reduces the time-step for the entire model. This implicates that a small local refinement will cause a decreased time-step for the entire model, and therefore a significantly increased computational effort.

2.4 Ship wave effect estimation with SWASH

In recent years, some modelling of ship waves has been done with various shallow water flow models: see for example Zhou et al. (2013), de Jong et al. (2013) and Talstra (2012) who used the hydrostatic models Delft3D and FINEL2D and the non-hydrostatic model XBeach. With these models, the primary wave effects could be modelled well. Not possible to accurately model were the secondary waves, as the models could not represent the dispersion of the secondary ship waves. The reason why SWASH is expected to perform better than other non-linear shallow water models lies in the dispersion accuracy of the models. Zhou et al. (2013) indicates that XBeach in non-hydrostatic mode calculates accurate dispersion for waves with $kh < 2$ while in SWASH, wave dispersion is off by 1% for $kh < 16.4$ when three layers are used. For SWASH to be able to model the dispersion of secondary ship waves, it is important that it these waves have a low enough kh value. In other words: that they are long enough for accurate dispersion in SWASH.

Using analytical equations to determine the wave characteristics, it can be illustrated that it is likely that SWASH can accurately model the dispersion of the secondary waves. According to Wal (1990), wave length L_s of the secondary waves is dependent on vessel speed:

$$L_s = 0.67 * 2\pi * \frac{V_s^2}{g} \quad (2.8)$$

With V_s as the vessel speed and g as the gravity constant. As visible, secondary wave length is dependent on vessel speed. A higher ship speed will mean longer secondary waves. Using $k = kh/h$ and $k = 2\pi/L$, Equation 2.8 can be rewritten into an equation that relates vessel speed to wave shortness:

$$V_s = \sqrt{\frac{gh}{0.67kh}} \quad (2.9)$$

Solving the equation for $kh = 16$ and a range of depths will give a minimum vessel speed. If ships sail faster than this speed, the secondary wave shortness becomes so low that SWASH should be able to model the dispersion of the secondary waves. But how fast do ships sail through a narrow channel? As the research is on overtopping hazard, the ships with which create the largest hazard are the normative ships. A faster ship will create larger waves. The fastest possible ship in a channel is a ship sailing at its limit speed. Assuming the limit speed as the actual speed for overtopping hazard is therefore a safe option. Rijkswaterstaat (1990) specifies a method for calculating the maximum speed of a vessel in restricted waters: Schijf's method. This method specifies the maximum speed of a ship in restricted waters as:

$$1 - \frac{A_s}{A_c} + \frac{1}{2} \left(\frac{V_l}{\sqrt{gh}} \right)^2 - \frac{3}{2} \left(\frac{V_l}{\sqrt{gh}} \right)^{\frac{2}{3}} = 0 \quad (2.10)$$

In this formula, A_s is the vessel's submerged cross section area, A_c is the channel wet cross section area, and V_l is the physical maximum ship speed. The maximum ship speed depends on both both blockage ratio (A_s/A_c) and water depth. A large ship in a small, shallow channel will have a low limit speed. For open water ($A_s/A_c = 0$) the limit speed will be \sqrt{gh} .

Figure 2.3 shows the results of solving equations (2.9) and (2.10) for different depths, blockage ratios and minimum speed with $kh = 16$. It also shows a comparison with the dispersive characteristics of XBeach. The figure shows why the secondary wave dispersion could not be modelled accurately with XBeach. For many blockage ratios, the ships could not reach speeds necessary for accurate dispersion of the secondary waves. For SWASH the story is different. As visible in the figure, the limit speeds of the vessels are above the minimum speeds that SWASH needs for accurate dispersion modelling. SWASH is therefore a promising tool for estimating secondary wave characteristics and the resulting overtopping.

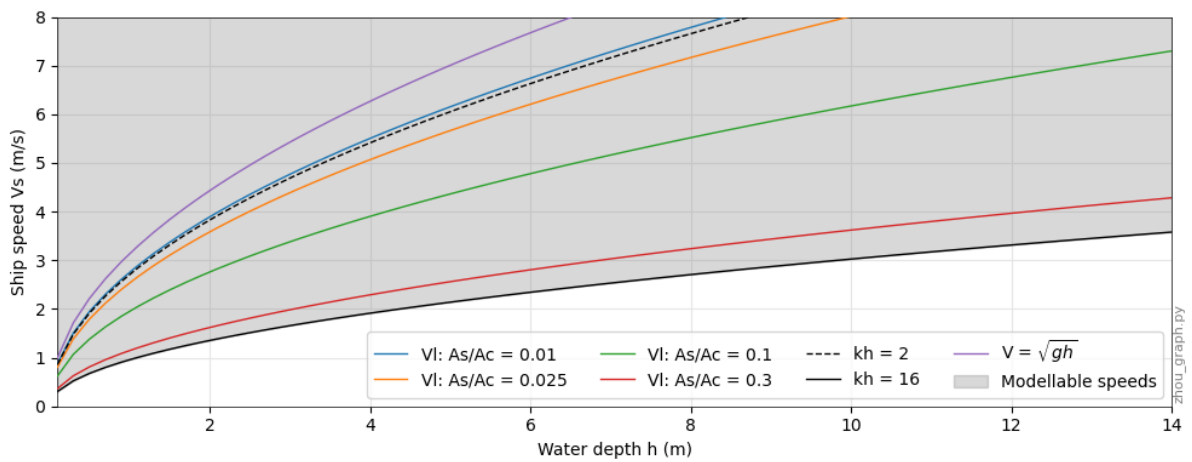


Figure 2.3: The relation between water depth and vessel speed for two wave shortnesses, and between water depth and maximum possible vessel speed. The black lines denote minimum vessel speed needed for long enough waves at various depths. The continuous lines denote vessel limit speed for several blockage ratios. If the limit speed is above the minimum speed for accurate short wave dispersion, SWASH should be able to represent the dispersion of secondary ship waves. The gray area represents the vessel speeds for which SWASH should be able to accurately model secondary wave dispersion when working with three layers.

3 RESEARCH METHODOLOGY

The research methodology describes the steps taken in this research. The chapter starts with an outline of the methodology and a description of the used data sets. Then, more attention will be paid to the individual steps in this research.

3.1 Methodology outline

Figure 3.1 shows a visualisation of the research setup. As visible, the research setup will roughly follow the research questions. In the first part, the pressure field method will be implemented in SWASH. The settings that were found to be relevant in overtopping studies with SWASH will also be tested for their influence on ship wave generation. At the end of the first part, the first research question can be answered. In the second part, the implementation of the pressure field method from the first part will be validated against measurements. The performance of SWASH will also be compared to pre-existing estimation methods for ship waves. At the end of the second part, the second research question can be answered. In the third part, a first step will be put towards modelling ship-induced overtopping. The lessons learnt from this study with regards to the creation of such a model will be discussed. At the end of the third part, the third research question can be answered. Before discussing the methodology to answer the research questions, the data sets that form the basis for this research will be discussed in more detail.

3.2 Data sets

For testing the implementation of the pressure field method and for the validation of the implementation, the outcomes of the SWASH model will be compared to measurements. With the eventual goal of modelling ship-induced overtopping, an ideal data set would contain measurements done on ship induced overtopping. This ideal data set would contain water level, flow speed and pressure measurements at several locations in a transect and on top of an overtopped structure. Such a data set is not available. With the focus of this research being the recreation of ship wave signals, data sets gathered for a comparable goal are useful as well. Opposite to data regarding ship-induced overtopping, data on ship-induced wave signals is available. In this research, the public data from three data sets will be used. These three data sets will be discussed below.

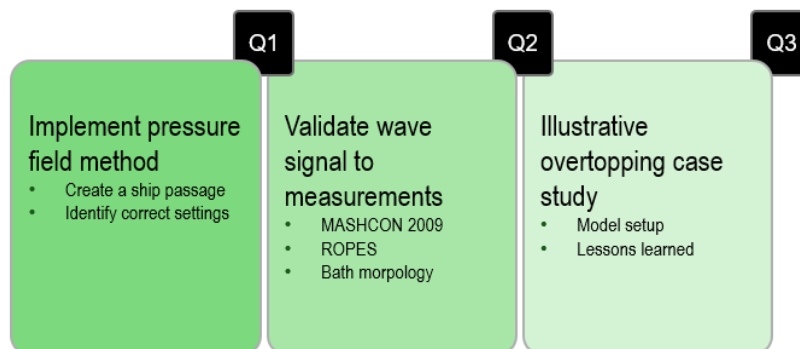


Figure 3.1: A short summary of the research setup as presented in Section 3.1.

Property	Scale model	Prototype model	unit
Length	4.332	350.0	m
Width	0.530	42.9	m
Draught	0.180	14.5	m
Block coefficient	0.65	0.65	-

Table 3.1: Properties of the model for the MASHCON data (Lataire et al., 2009).

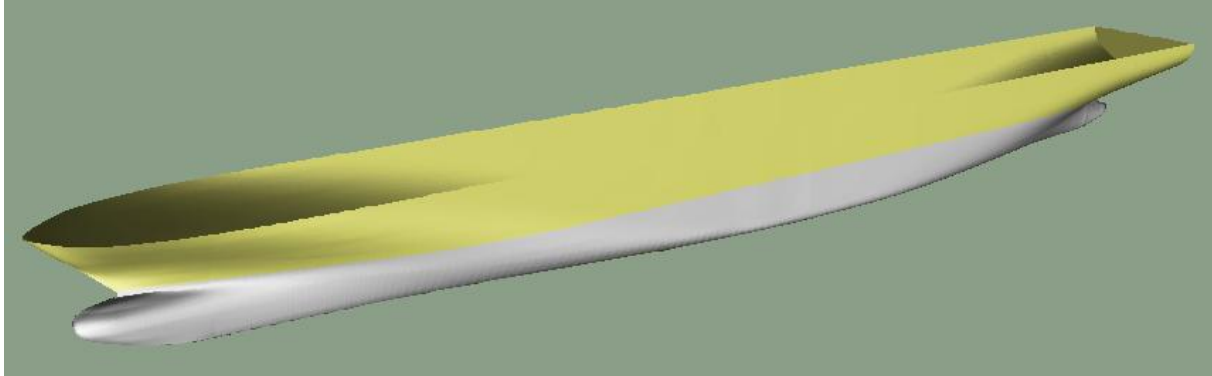


Figure 3.2: The model as used in the MASHCON towing tank experiments (Lataire et al., 2009).

3.2.1 MASHCON

The first data stems from towing tank experiments done for the MASHCON conference Lataire et al. (2009). The tests were done to determine the effects that sailing close to banks has on the manoeuvrability of ships. From some passages, water level measurements are available.

The passages for the water level measurements were done with a container ship model on a 1:81 scale. The model is depicted in Figure 3.2 and its properties can be found in Table 3.1. The water level elevation was recorded in three gauges on a location at which the ship was sailing at a steady speed. The measurement frequency was 40 Hz.

3.2.2 ROPES

The second data set stems from the measurements done for the JIP ROPES program (Wictor, 2012). JIP ROPES stands for Joint Industry Project (JIP) for Research On Passing Effects of Ships (ROPES). The objective of ROPES was to gain insight in the forces on moored ships caused by passing vessels and to increase knowledge on the different methodologies and tools for predicting the resulting vessel motions and mooring loads in lines and fenders (de Jong, 2010).

The measurement data includes the forces on a moored ship, but also pressure, flow speeds en water level signals for several passing ships. Figure 3.3 shows the general location of the ROPES measurements in the Port of Rotterdam.

The measurements were done in November 2011. The forces in mooring lines and fenders that ship passages caused were measured. Additionally, water levels were measured at the bow and stern of the moored ship, named Jaeger Arrow. These water level measurements will be used in this research. The water levels were measured to NAP with ultrasonic level gauges mounted on the quay. Measurements were done with a frequency of 10 Hz. From the passing ships, name, draught and speed were registered. The data is further described in Wictor (2012).

3.2.3 Bath

The third data set that will be used for validation are measurements done near Bath. Figure 3.4 shows the general location. The measurements were done by Deltares to investigate the effect that ships have on the erosion of the 'Slik van Bath' Huisman et al. (2010). During the measurement campaign, 62 ship passages have been analysed in detail. The data from these 62 passages were available for recreation in SWASH. The data sets used in this research include the wave, current, and pressure measurements necessary for the validation of the ship waves as modelled in SWASH.



Figure 3.3: The general locations in the Port of Rotterdam of the measurements done for ROPES campaign at the Scheur in the Port of Rotterdam. The red point indicates the stern gauge and the orange point indicates the bow gauge.

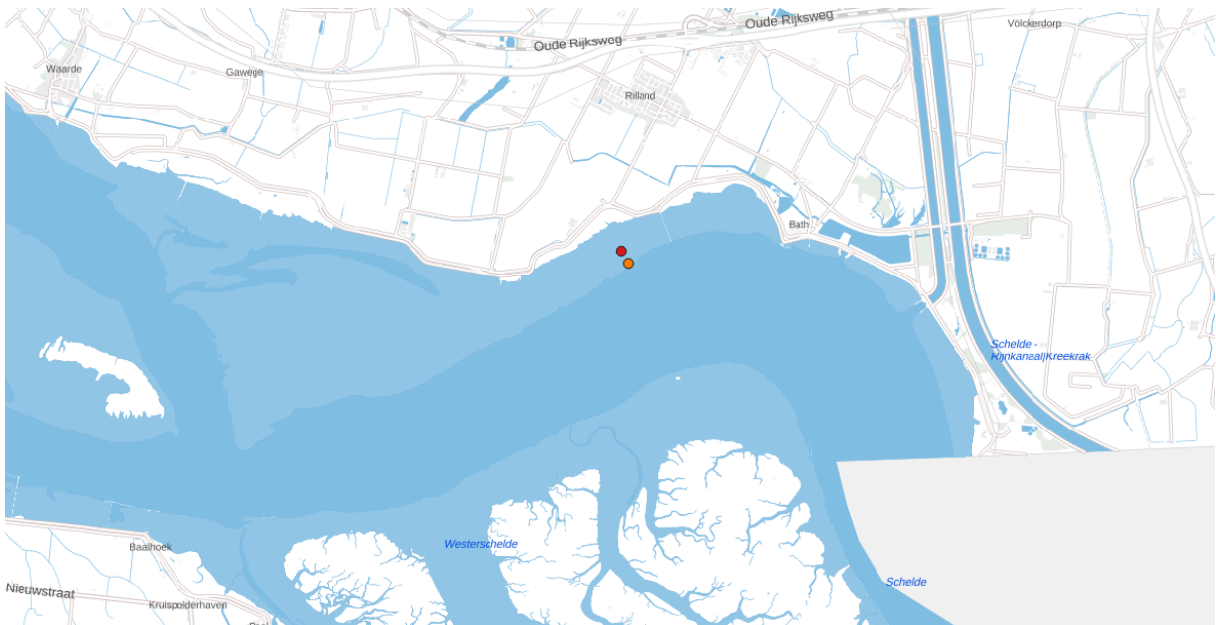


Figure 3.4: The general locations of the measurements done for the Bath measurements in the Western Scheldt. The red point shows the location of the Vector, the orange point shows the location of the AWAC.

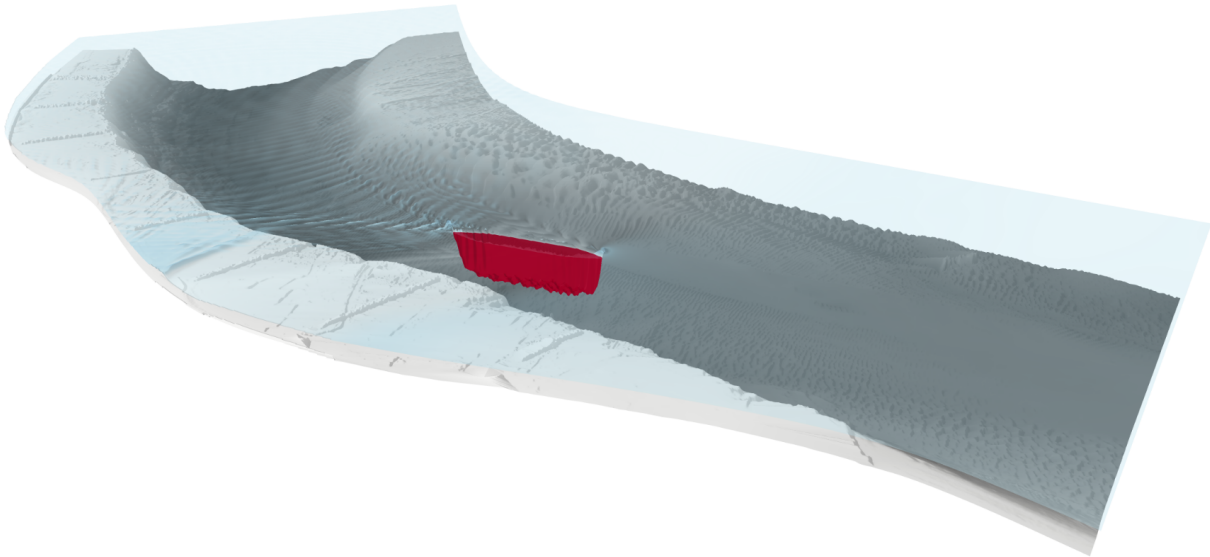


Figure 3.5: A visualisation of a ship sailing through a geometry. The water level at the location of the ship is drawn in red. The blue surface represents the water level. Visible are the ship waves as well as the water following the ship-hull shape. The bottom is represented by the white-gray surface. Here, a darker color means a lower bottom level. For visibility, the vertical scale is enlarged by a factor 10.

During the measurement campaign, the hydraulic conditions were measured at two locations. On the first location (close to the channel), pressure, water level and flow properties were measured by an AWAC measurement device. On the second location, further on the bank, pressure, flow velocity and direction were measured by a Vector measurement device. All measurements were done at 2 Hz. Of the passing ship, direction, length, width and speed were stored as well as characteristics of the ship-induced waves. From the environment variables, water level compared to NAP, flow velocities and direction as well as wind speed and wind-wave characteristics were stored. Of the pressure measurements, the quality of the data could not be verified sufficiently. Those measurements were therefore not used.

3.3 Pressure field method implementation

In reality, the ship-induced waves are generated by a ship sailing through a waterway. The goal of the implementation of the pressure field method in SWASH is to represent the sailing ship as accurately as possible. For accurate representation of such a passage, several elements are important. These elements are displayed in Figure 3.5. The first thing to note from this figure is the geometry in which the ship is sailing. The geometry is a combination of the bottom level (pictured as a white-gray surface) and the horizontal boundaries, in this case all open boundaries. On the water level, there is free surface except in the location of the ship. Under the ship, the flow is pressurized. For the implementation of the pressure field method, the main source of information will be the recent studies done by Zhou et al. (2013), de Jong et al. (2013) and the SWASH user manual. The limited number of publications where SWASH is used calls for an exploratory approach. This section will describe the steps taken to implement the ship sailing through a geometry in SWASH, and which tests will be done to confirm the correct implementation of the model.

3.3.1 Input

For replication of the physical experiments in SWASH, SWASH needs to represent all passage elements: the geometry, the boundaries and the ship. The basis for a calculation in SWASH is the computational grid. On this computational grid, the calculations are done. The extent of the computational grid should be as small as possible, while still allowing a spin-up and passage and without boundary effects influencing the point of interest. In SWASH, passage elements can be specified on the computational grid, as well as on a different grid. If an input grid differs from the computational grid, SWASH will interpolate it to the computational grid. As the geometries and the ships themselves can have steep sides, this interpolation can cause errors or misrepresentation of reality. In this research, all grids will be specified on the computational grid to prevent interpolation in SWASH.

A bottom grid vertically bounds the waterway geometry. For the MASHCON experiments, the cross-sections supplied with the measurements form the basis for the bottom grid. For the ROPES and Bath simulations, the bottom grid will be based on bathymetric data supplied by Rijkswaterstaat. At the horizontal grid boundaries, the boundary conditions should either represent a bank or an open boundary. In the MASHCON experiments, the towing tank has four reflective, closed boundaries. A reflective, closed boundary matches the default boundary setting in SWASH, so no boundary conditions need to be specified here. In the ROPES simulation, the bathymetric data is provided from bank to bank. With the grid extent being on the water line, the boundaries can be represented by closed boundaries. Where the waterway extends beyond the grid edges, the boundaries need to be open boundaries. For the Bath simulation, there are no surface-piercing banks so all boundaries are open. For the representation of these open boundaries, a suitable solution will be found in this research. As indicated by Vasarmidis et al. (2020), SWASH has no boundary condition on which water can flow in and out of the model and on which internally generated directional waves are not reflected. A solution to this problem is the combination of a boundary condition with a sponge layer. In SWASH, a sponge layer is an area which absorbs wave energy to simulate waves leaving the domain freely. To find a boundary specification that simulates an open boundary, four boundary conditions will be tested in combination with various sponge layer widths:

1. An imposed water level at the boundary
2. An imposed velocity at the boundary
3. A sommerfeld radiation condition
4. A weakly reflective boundary condition

For the sponge layer, the SWASH user manual advises using a width of three times the length of the most energetic wave component. In this research, the secondary wavelength is used as a basis for the sponge layer. To test the absorption of the secondary wave in the sponge layer, three thicknesses will be tested:

1. No sponge layer
2. 1 time the secondary wave length
3. 3 times the secondary wave length.

All combinations of sponge layer thickness with boundary conditions will be simulated, giving 12 simulations to complete. The tests will be done in a rectangular geometry with a uniform depth and a rectangular box representing the ship. All boundaries will be specified by the same boundary condition.

With the geometry sorted, the ship needs to be implemented in SWASH. For the representation of a ship, SWASH offers two main options: a floating object grid and a pressure grid. A floating object grid specifies the maximum water level at a grid point. The free surface cannot exceed this maximum level. If the water is at the maximum level, the flow becomes pressurized. In SWASH, it is not possible to make the floating object grid time-varying. A pressure grid specifies a spatially varying atmospheric pressure. This pressure is input as extra pressure on the surface. Opposite to the floating object grid, the pressure grid can be time-varying. The pressure grid will therefore be the main method for representing the ship in the model. The movement of the ship will be implemented by varying the pressure field in time. After determining the times at which a pressure grid is specified, the location of the ship at these times can be found. These locations will then be used to translate the ship to a set of pressure fields.

Next to the physical aspects that need to be implemented in SWASH, the model needs input regarding the computational properties. First, the model must be stable so that it will not crash while simulating a passage. The settings that create a sufficiently stable model will be found by experimenting with different numerical schemes, ship shapes and vertical layer settings. Using an unstable model, the influence that each of these parameters has on the stability will be tested by looking at the moment the model crashes. For each of the parameters, the setting that leads to the longest time before crashing will be used in the final model implementation.

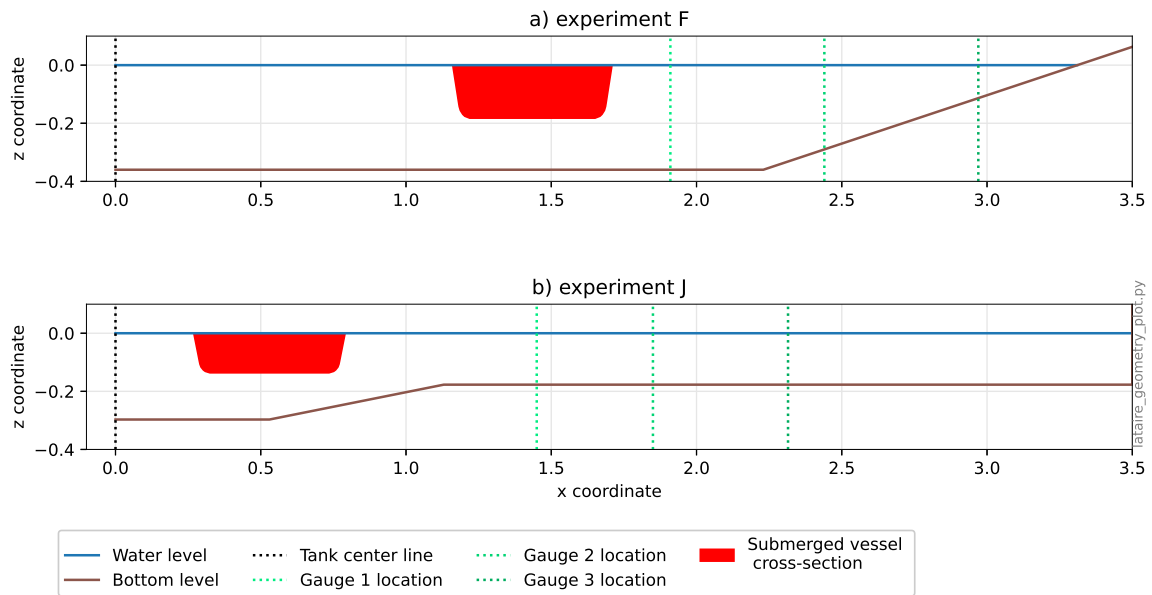


Figure 3.6: The cross-sections from Lataire et al. (2009). On the left side of the centerline, the tank cross-section is rectangular.

The final input for the model is the spin-up procedure. In reality, a ship will pass the measurement points or overtopping location at a constant speed. The model cannot be started with a ship sailing at a constant speed. To reach a state in which the ship is sailing at a constant speed and the effects from the acceleration don't influence the measurements, the model needs to be spun-up up using a spin-up procedure. Two spin-up procedures will be tested:

1. First launching the ship, then accelerating
2. Launching the ship at speed

These spin-up procedures will be judged on computational effort necessary for the procedure, and on the possible influence that the spin-up procedures have on the results.

3.3.2 Testing model settings

When the model can simulate a ship passage, the effect that settings for which the overtopping is sensitive have on wave generation will be tested.

The MASHCON towing tank experiments will form the basis for these tests. In the simulations, the wave signals generated with different settings are compared with the measured wave signals. The first experiment in the tests is MASHCON experiment F. This experiment has before been recreated in XBeach and Delft3D by Zhou et al. (2013). The second experiment recreated for these tests is MASHCON experiment J. The wave signals from SWASH will be compared to the measurements by visual inspection. The geometries of Lataire et al. (2009) test F and test J are pictured in Figure 3.6. Regarding the ship, some concessions are needed to be able to represent the shape in SWASH. As the original ship model has a bulb it cannot be used for the modelling in SWASH. Therefore, a model without a bulb, similar dimensions and a slightly larger volume has been selected. The speed of the vessel was 0.801 m/s in both experiments.

The settings that will be tested are identified from recent literature such as Vanneste et al. (2014), Suzuki et al. (2014), Suzuki et al. (2017) and Lashley et al. (2020). These papers describe how overtopping can be calculated with SWASH.

The first influential setting found is the grid cell size. Suzuki et al. (2014) simulate wave overtopping for a two-dimensional SWASH model. They conclude that grid cell size does not influence wave transformation, but find a large influence on wave overtopping. A smaller cell size gives a better overtopping

estimation. Lashley et al. (2020) support the earlier conclusion about grid cell size. They conclude that for good overtopping the grid cell size needs to be smaller than 100 cells per wavelength on deep water as the waves will get shorter in shallower water. The influence of grid cell size on ship wave generation will be tested by simulating (Lataire et al., 2009), experiment F with 5cm and 2cm grid cells. The cell size was uniform in both x and y directions. The 5cm resolution is the closest to the XBeach test done by Zhou et al. (2013). The 2cm resolution is the smallest fraction of the towing tank dimensions that would still have a reasonable calculation time. For SWASH it is relevant to know how many cells per wavelength this translates to. When using Equation 2.8, a speed of 0.801 m/s gives a secondary wave length of 0.27 m. 5cm and 2cm cell size, therefore, mean 5.4 and 13.5 cells per wavelength (CPW). Further conclusions of Suzuki et al. (2014) are that bottom friction has a significant influence on wave overtopping flow speed and layer thickness. The second setting to be tested is therefore bottom friction. The influence of bottom friction on wave generation is tested by simulating Lataire et al. (2009) experiment J with the default bottom friction in SWASH and with a manning-friction coefficient of $n = 0.012$. The third and final setting to be tested is the viscosity model which is used to simulate sub-grid turbulence. Zhou et al. (2013) uses a viscosity model to calibrate the primary water level depression in XBeach. Lashley et al. (2020) uses a turbulence model to take into account vertical mixing in a depth-averaged overtopping model in SWASH. The influence of the viscosity settings on wave generation will be tested by recreating Lataire et al. (2009), experiment F three times. Once with default viscosity settings, once with the Smagorinsky viscosity model with a viscosity constant of 0.9 and once with the $\kappa - \epsilon$ viscosity model as used in Lashley et al. (2020).

3.3.3 Further model characteristics

Next checking the performance on wave generation, trust in the implementation of the pressure field method can be increased if the model also correctly calculates other characteristics of the ship movement. The model will therefore be tested for one characteristic that should be inherently included. Also, the performance of the model regarding calculation time can be seen as a metric of performance of the model. As these characteristics are both relevant in the eventual usage of the model, they will also be tested.

The characteristic that will be tested is squat. The squat is the vertical, downward displacement of the ship caused by its movement. As a ship is sailing, it continuously displaces water. The bow pushes water away while the stern leaves a gap to be filled. This displacement causes a return current. According to Bernoulli, the return current causes a reduction in hydrostatic pressure and a water level drop around the ship as described in Chapter 2. The reduced water level, in turn, leads to a downward translation of the ship (Lataire et al., 2012). This phenomenon is called squat. In the analytical methods for the estimation of ship-induced water motions, the squat is necessary for calculating the reduced channel cross-section during the passage of the ship. In SWASH, squat should be inherently included. As the pressure field specifies an additional pressure surface, a lowered hydrostatic pressure will mean that the pressure field will let the ship sink in deeper. A correct estimation of the squat by SWASH is an indication for an accurate representation of the ship-induced water motions. To test the performance of SWASH, the squat as calculated by SWASH in Lataire et al. (2009), experiment F is compared to the measured squat and to the squat as calculated by the much-used formula for squat presented by Barrass and Derrett (2012).

The calculation time of the model is discussed by looking at the calculation time of the model for the simulations done for this research. It is expected that using a finer resolution will increase the calculation time. If SWASH performs well, the calculation time will be acceptable for model resolutions suitable for ship wave generation and overtopping.

3.4 Validation

With the pressure field implemented in SWASH, the next step is to validate the model. Four tests will be done to benchmark the performance of SWASH for ship wave generation. First, a passage from the MASHCON data set will be replicated in SWASH. Then, a passage from the ROPES measurements will be simulated as well as a passage from the Bath measurements. Finally, the performance of SWASH will be compared to existing analytical methods for estimating ship waves. For this comparison, the three passages that have been simulated in SWASH will be modelled with these analytical methods. The validation will be finalized with a summary regarding the performance of SWASH on ship wave signal generation. This section will discuss the model setup procedure for the validation experiments.

3.4.1 Passage selection

The creation of a SWASH model to simulate the validation passages starts with the selection of a passage to be modelled. The passages for the three validation simulations are selected based on the measured wave signals. A first selection is done based on a visual inspection of the signals with as criteria:

- High signal to noise ratio: the ratio between the wind waves and ship waves needed to be so high that the ship waves could visually be distinguished.
- Clear ship wave components: the primary and secondary ship waves needed to be visible in the signal

A further selection is done based on the passage characteristics. A large ship will generally cause large water movements and therefore a more distinguishable wave signal. A larger ship is therefore preferred over a smaller ship. A fast ship will cause long secondary waves. As SWASH performs better for longer waves, a faster ship is preferred over a slower.

MASHCON

For the MASHCON data set, this selection procedure yields Experiment E as the validation passage. In this passage, the ship is loaded to its maximum depth and the speed is among the highest of the measurement data. The tank geometry for Experiment E is as found in Figure 3.7. In this experiment, the vessel had a speed of $V_s = 0.687 \text{ m/s}$. This means a secondary wave length of $L_s = 0.20 \text{ m}$.

ROPES

From the ROPES data set, run 902 is selected as the passage to be modelled. For this passage, the wave signal clearly shows primary and secondary waves. Also important for the selection of this passage was that the report of Wictor (2012) contained a detailed analysis of this run. This detailed analysis pictured a part of the ship track so that the track could be easily recreated in SWASH. According to the report, a ferry with a length of 142m and a draught of 8m passed the measurement location at 130 m distance with 11.8 knots (6.07 m/s). From the Arcadis ship database, these dimensions match those of the ferry 'Maersk Exporter'. According to the Arcadis ship database, the Maersk Exporter has a width of 23.2 m. With a speed of 6.07 m/s, the secondary ship wave length is 15.8 m.

Bath

For the Bath measurements, the last passage is selected for modelling in SWASH. Next to the criteria described above, an additional criterion in the selection was the water level. As the bank is around 0 m+NAP and the measurement devices were placed on the bank, the water level needed to be sufficiently high that both measurement locations were submerged as deep as possible so that the wave is less

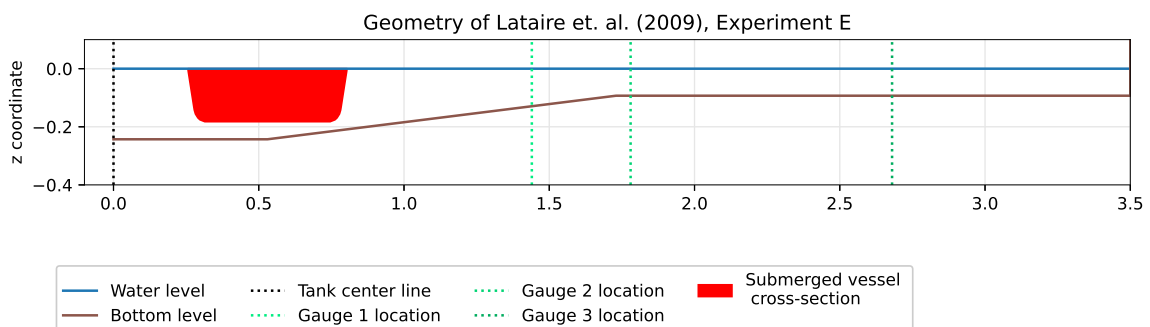


Figure 3.7: The geometry of Lataire et al. (2009), Experiment E as used in SWASH.

Table 3.2: Characteristics of the passage of the Margrit Rickmers as simulated in the Bath validation experiment

Ship			Environment		
Length	294	m	SWL	3.03	m + NAP
Width	32	m	$Hm0_{wind}$	0.14	m
Draught	12	m	$Tm0_{wind}$	2.72	s
Speed	14.7	kn			
Speed	7.56	m/s			

distorted by the bank. The selected passage was of the ship 'Margrit Rickmers'. The characteristics of the passage can be found in Table 3.2. As visible, the vessel speed was 7.56 m/s This gives a secondary wave length of 24.5 m.

3.4.2 Model setup

For the setup of the models, a set procedure is developed so that all models are comparable. The end result of this procedure are the models that will be discussed in Chapter 5. The procedure is based on the implementation as described in Chapter 4. It consists of 5 steps:

1. Grid creation
2. Bottom generation
3. Boundary conditions
4. Ship model selection
5. Track estimation

Each of the steps will be discussed below.

Grid creation

The computational grid consists of a grid extent, a grid type and a resolution. The grid extent is determined by the waterway geometry and the track length. Regarding the width, the grid spans the entire width of the waterway for which bathymetric data is available. Regarding the length, the setting depends on the data set that the simulation is based on. In the MASHCON experiment, the grid will span the entire length of the towing tank. In the ROPES and Bath simulations, the grid spans a length of eight ship lengths before the measurement point and four ship lengths after. This is to make sure that the ship will have enough space to reach a steady speed before reaching the measurement points and that the waves will have reached the measurement point when the ship reaches the end of the grid. This is necessary as the cannot sail out of the grid. A ship sailing out of the model creates errors at the boundaries. The grid type also depends on the data set on which the simulation is based. For the MASHCON experiments, a rectangular grid is used as the towing tank is also rectangular. For the ROPES and Bath experiments, a curvilinear grid forms the basis as this is better suited to follow the track of the ship. For the generation of the curvilinear grids, the Deltares software RGFgrid is used (Deltares, 2020b). RGFgrid is software designed for the generation and manipulation of curvilinear grids. In RGFgrid, a set of splines is drawn around the grid area and these are then used for grid generation. The resolutions are chosen as accurate as possible with an expected computational time of 7-10 days on 12 cores.

Bottom generation

For the MASHCON simulation, the bottom grid is generated by manually specifying the values according to the geometries as presented in Lataire et al. (2009). For the ROPES and Bath simulations, the Bathymetric data comes from bathymetrie.rijkswaterstaat.nl. This data is then interpolated on the curvilinear grid using Quickin (Deltares, 2020a). Quickin is software developed for the generation and manipulation of grid-related parameters such as bathymetry, initial conditions and roughness. The bottom level is specified at the grid points as SWASH also uses it at the grid points.

Boundary conditions

For the boundary conditions, there are two possibilities: closed boundaries and open boundaries. For all places where the banks are surface-piercing in reality, no boundary condition is specified creating a closed boundary. For all locations in which flow can be expected, a Sommerfeld radiation condition is imposed with a sponge layer of three times the length of the secondary waves. This boundary condition best represents a non-reflective, open boundary according to Section 4.3.

Ship selection

As described in Section 4.2.2, the ship model in SWASH cannot have a bulb or other fully submerged shapes. Also, the actual shape of the ships is not available from the measurements. A comparable ship is therefore selected from the Arcadis ship database. For selection of a ship, the ship characteristics from the measurement data sets form the basis. These parameters are then complemented by characteristics from the Arcadis ship database to yield at least the dimensions of the ship and the volume. The Arcadis ship database is then used to find a ship in the same category, and with roughly the same volume at the same dimensions.

Track estimation

The track estimation procedure differs per simulation. For the MASHCON dataset, the position of the ship over time is included in the measurements. For the ROPES measurements, the image of the ship positions from Victor (2012) is used to draw the ship track. For the Bath dataset, no data on the track is available. For an estimate of the passing distance, the wave signal was used. Using the recorded vessel speed, and the time between the start of the primary wave and the peak of the secondary waves the distance the ship has sailed between those two moments can be calculated. From literature, it is known that the primary wave forms along the length of the ship, while the secondary waves form at a line at 19° from the vessel axis Wal (1990). Knowing the sailing distance from vessel speed and timing of the two waves, and knowing the directions of these two waves, an equation for the passing distance can be constructed:

$$y = \tan(19^\circ) * V_s * \Delta t \quad (3.1)$$

The process of calculating the passing distance is visualized in Figure 3.8. For the selected passage, the passing distance between the ship and the AWAC was estimated at 122 m. From this passing distance, the track is constructed so that the ship keeps a constant distance from the bank.

3.4.3 Results

To get a consistent view of the performance of SWASH, the results of all validation experiments will be described in the same order. First, the result of the model setup will be discussed. This includes grid extent and resolution, ship selection and estimated track. Second, the results of the model runs will be discussed. This will be done based on three visualizations:

1. A top view of the wave field
2. A plot of the wave signal
3. A bar graph of the characteristics relevant for overtopping

The top view of the wave field will be used to see if the wave field looks realistic. Realistic is if the primary water level depression forms along the length of the ship and if the secondary waves form a line 19° from the track. It is useful to discuss the top view as it is a very accessible way of data interpretation. From this plot, it is not possible to conclude quantitatively about the correctness of SWASH as there is no information on the wave field in the measurements.

In the plot of the wave signal, the measurement signal will be visualized along with the simulated wave signal in the same location. The plot of the wave signal will be used to see if the timing of the wave components is correctly simulated. In the simulations, the start and end of the water level depression should be at the same moment as in the measurements. The secondary wave train should also arrive at the same time in both measurements and simulation. The wave signal will also contain some information on the launching procedure in the SWASH signal and on the environment waves in the measurement

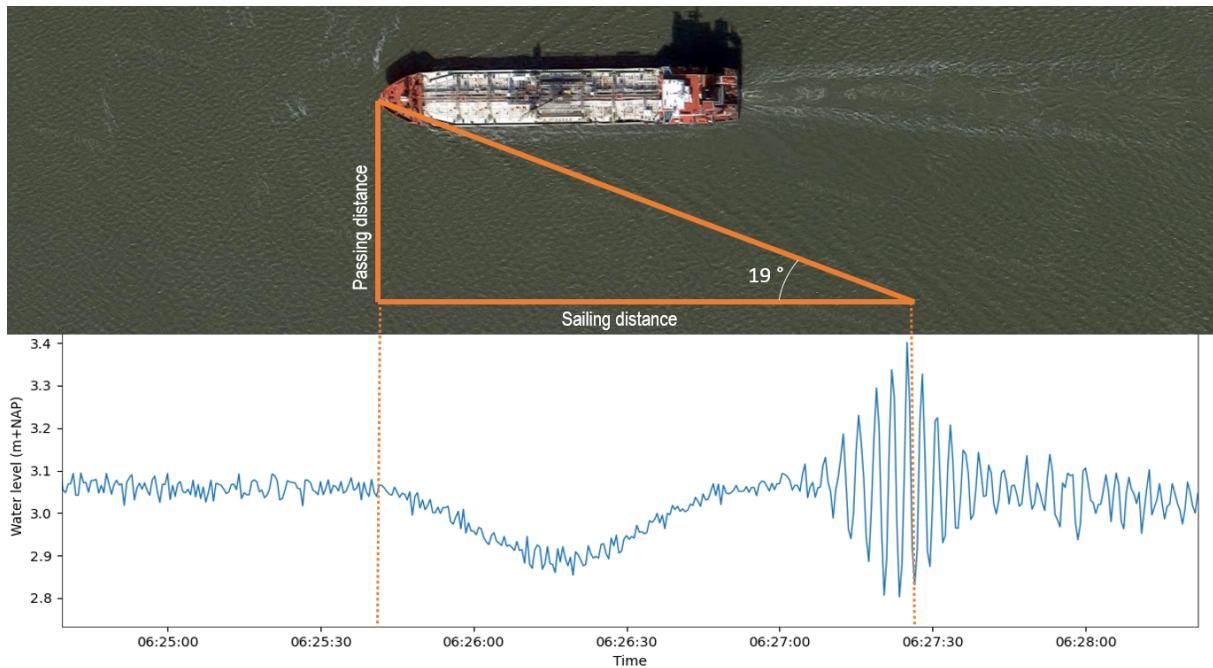


Figure 3.8: Illustration of the passing distance calculation method for the Bath experiment. The sailing distance is computed by multiplying the time between the wave signals with the vessel speed. For the purpose of the illustration, the time in the bottom part is scaled to coincide with the distance in the top part of the figure.

data. If relevant, this information will be discussed. From this plot, it is not possible to give a comparative conclusion about the performance of SWASH, as there is no other method to calculate these wave signals.

The bar graph of the characteristics will be used to compare the magnitudes of the ship wave components as simulated by SWASH with the measured magnitudes. For overtopping, the most relevant characteristics are the secondary waves and the primary stern wave. These two components of the ship-induced water movements can propagate towards the bank and increase the water levels there. They can also arrive at the bank together and reinforce each other. A further relevant characteristic is the primary water level depression as this characteristic forms the basis for the other primary wave components in analytical calculation methods. If this is estimated correctly, then it is already a step forward on existing calculation methods. The characteristics will be identified by the signal analysis process as described in Appendix A. In this process, band filters are used to separate the primary long waves from the shorter secondary waves. This comparison can give insights into the uncertainty of the components modelled by SWASH. In the optimal case, the wave component magnitudes as modelled in SWASH are equal to the magnitudes in the measurements.

3.4.4 Comparison to analytical results

As described earlier, the main method for estimating the effects of ship-induced water motions currently is DIPRO+ (Waterloopkundig Laboratorium, 1997). Alternatively, the formulations in the BAW guidelines (BAW, 2010) can be used. Both methods are based on a simplified geometry and analytical relations for estimating the magnitudes of the ship-wave components. To be able to conclude on the performance of SWASH in comparison with these analytical methods, the magnitudes of the wave components in the validation part of this research will be compared with the results that DIPRO+ and the BAW guidelines give for these situations. The secondary wave height, primary water level drawdown and stern wave height will be calculated according to DIPRO+ and the BAW guidelines. The passages will be recreated two times: once with settings aimed at getting as close as possible to the measured wave magnitudes and once with conservative settings aimed at getting a realistic estimate of the results if DIPRO+ or the BAW guidelines are used in a study. The difference between the two calculations is seen as uncertainty margin. Below, the two methods are introduced.

DIPRO+

In the Netherlands, ship wave impacts are calculated using the software package DIPRO+ (ENW, 2007). The formulae in these norms and calculation methods are based on Schijfs theory, and on measurements done in the 1980's (Wal, 1990). The formulations in DIPRO+ are also described in a more internationally used guideline: The Rock Manual (Ciria, 2007). The first input necessary in DIPRO+ is the canal cross-section. For the canal cross-section, a choice should be made between a trapezoidal input profile, a broken profile, a rectangular profile and a berm, all of which are then schematized as a trapezoidal profile. For an insight in the uncertainty that this causes, DIPRO+ calculations are done with a trapezoidal profile that fits within the actual geometry, a profile which resembles the actual geometry as good as possible and a profile which would enclose the actual geometry. The second input request is the ship. In DIPRO+, the type of ship, its dimensions and the block-coefficient of a mid-ship cross-section of the ship can be selected. The block-coefficient, in this case, is the ratio between the actual cross-sectional area of the ship and the cross-sectional area of a box with the same width and draught. This block-coefficient is not always known, so the simulations are done with both a large and a small block-coefficient to give insight into the uncertainty that this lack of knowledge causes. For the secondary waves, DIPRO+ uses the formulation:

$$H_i = h\alpha_1 \left(\frac{y_{H_i}}{h} \right)^{-1/3} F_h^4 \quad (3.2)$$

Where H_i is the secondary wave height, α_1 is a ship-dependent coefficient, y_{H_i} is the distance of the side of the ship till the bank and F_h the Froude number. The primary water level depression is calculated according to:

$$\Delta h = \frac{V_s^2}{2g} \left[\alpha_s (A_c/A_c^*)^2 - 1 \right] \quad (3.3)$$

$$\Delta \hat{h}/\Delta h = \begin{cases} 1 + 2A_w^* & \text{for } b_w/L_s < 1.5 \\ 1 + 4A_w^* & \text{for } b_w/L_s \geq 1.5 \end{cases} \quad (3.4)$$

Where Δh is the mean water level depression, V_s is the ship speed, α_s is a factor to express the effect of sailing speed in relation to the limit speed, A_c is the channel cross-section and A_c^* is the area of the cross-section next to the ship. $\Delta \hat{h}$ is the maximum water level depression, b_w is the waterway width and L_s is the ship length. The stern wave height is calculated according to:

$$z_{\max} = 1.5\Delta \hat{h} \quad (3.5)$$

BAW guidelines

In Germany, the Bundesamt für Wasserbau (BAW) has published the "BAW code of Practice" BAW (2010) for the design of hydraulic works. The formulae are comparable to the formulations in DIPRO+ but differ on some aspects. The BAW software was not available for this research. Instead, the relations as presented in the BAW code of practice BAW (2010) have been implemented in Python. Here, secondary wave heights are calculated using:

$$H_i = A_W \frac{V_s^{8/3}}{g^{4/3} (u')^{1/3}} f_{cr} \quad (3.6)$$

In this equation H_i is the secondary wave height, A_W is the wave height coefficient which varies between 0.25 and 0.8 depending on ship type and loading condition, V_s denotes the vessel speed, g is the gravity constant, u' is the distance from the ship's side to the bank and f_{cr} is the coefficient of velocity which is 1 if $V_s/\sqrt{gh} < 0.8$.

The maximum water level drawdown is based on the same formulations as implemented in DIPRO+. It is estimated iteratively using:

$$\Delta \bar{h} = \frac{1}{2g} \left[\alpha_1 (V_s + \bar{u}_r)^2 - V_s^2 \right] \quad (3.7)$$

With $\Delta \bar{h}$ as the maximum drawdown in the narrowest flow cross section. α_1 is calculated by:

$$\alpha_1 = 1.4 - 0.4 \frac{V_s}{\sqrt{gh}} \quad (3.8)$$

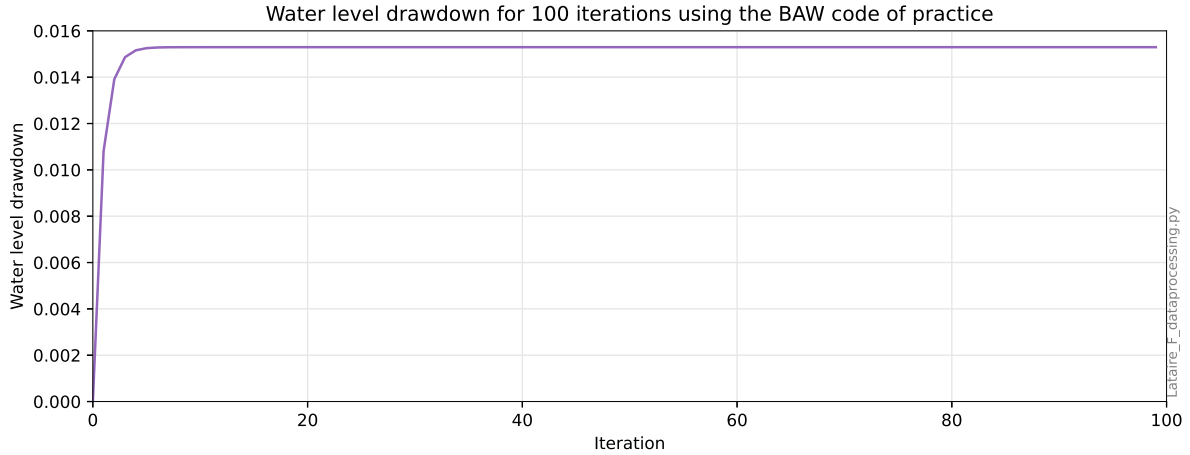


Figure 3.9: The outcome of Equation 3.7 for 100 iterations, starting at $\Delta\bar{h} = 0$.

In Equation 3.7, u_r is calculated by:

$$\bar{u}_r = \frac{\Delta A}{A - \Delta A} V_s \quad (3.9)$$

In which ΔA is the reduction in the cross-section of the canal due to the cross-section area of the ship (A_m) and the depression $\Delta\bar{h}$. As the depression is needed to calculate the depression, this equation is solved iteratively using 100 iterations starting at $\Delta\bar{h} = 0$. From Figure 3.9, it becomes clear that with the routine as implemented, 100 iterations are sufficient to reach a steady outcome. From the maximum drawdown, stern wave height can then be calculated using:

$$z_{max} = \left(2.0 - 2\frac{A'}{A}\right) \Delta\hat{h} \quad (3.10)$$

In this equation, A is the relevant cross-section of the canal. A' is the cross-sectional area between the ship's axis and the bank. $\Delta\hat{h}$ is the maximum drawdown near the bank at the stern. It is calculated by:

$$\Delta\hat{h} = C_H \Delta\bar{h}_u \quad (3.11)$$

In this equation, C_H is the factor for the influence of the type of ship. C_H varies between 1.1 and 1.3 depending on the ship type and loading conditions.

In these relations, the geometry is represented as a rectangular equivalent cross-section. For the calculations, a cross-section is chosen such that it represents reality as close as possible.

3.5 First step to overtopping

The focus of this research lies on the modelling of ship waves for the purpose of overtopping. However, a number of interesting lessons regarding the future modelling of ship-induced overtopping can be learned from this study. To illustrate these lessons, this study contains a first step towards the modelling of ship-induced overtopping with SWASH.

The main lessons to be illustrated in this part of the study concern the resolution necessary to model overtopping with SWASH. The illustration will be done on the basis of a schematized case study. First, this case study will be developed. Then, two options to overcome the resolution issues will be discussed:

1. Local refinement of the grid around the overtopping location
2. Separating the wave generation model from the overtopping model

For both of these options, the problems that are faced in the implementation of the options will be discussed. Due to time constraints, neither of the two options have been implemented. The chapter will be finalized with a summary of the first step towards modelling ship-induced overtopping.

4 IMPLEMENTING THE PRESSURE FIELD METHOD

In reality, ship-induced waves are generated by a ship sailing through a waterway. In SWASH, this ship is represented using a pressure field. The reason for doing so is explained in Chapter 3. The basis for the pressure field method is the possibility to specify an atmospheric pressure field as a boundary condition. This pressure field can be time-varying. This chapter will describe how the pressure field method is implemented in SWASH. It will start with the generation of the pressure field and horizontal boundary conditions and then continue with the search for a stable numerical scheme and a suitable spin-up procedure. The chapter will describe how relevant settings for overtopping influence ship-generated wave signals. The performance of the model is discussed, and the chapter will finalize with a conclusion answering the first research question.

4.1 Input grids

As explained in the Research Methodology, the input grids that are necessary for simulating a passage are a computational grid, a bathymetric grid, the pressure grids representing the sailing ship and possibly a floating object grid. Apart from the pressure grids, the procedure of creating these grids will be summarized here.

The first grid to be implemented in SWASH for this research is a rectangular grid to be used for recreating the MASHCON experiments. For a rectangular grid, SWASH only requires grid extent and resolution as input. More effort was spent to find a way of accurately representing the curved geometries in the ROPES and Bath simulations. To allow the ship to sail along the grid lines, the choice was made to use curvilinear grids. For the creation of these grids, RGFGrid (Deltares, 2020b) was selected due to previous experiences that the author has with this software. The grid was specified in RD-coordinates as in this coordinate system the grid points are specified in the same unit in RGFGrid as they are in SWASH.

As explained in Chapter 3, the bathymetry is specified at the computational grid points to prevent SWASH from interpolating a bottom grid specified at other points. For the MASHCON experiments and the illustrative case study, a function was written to specify the bottom grids. For the ROPES and Bath simulations, the bathymetry data is taken from bathymetrie.rijkswaterstaat.nl. For interpolation of the bathymetric data to the computational grid, the triangular interpolation option in QUICKIN (Deltares, 2020a) has been used. The output of QUICKIN could be chosen such that it could be used in SWASH without conversion.

The floating object grid was used to represent the moored ship in the ROPES simulation. It was created using the same process for the pressure grids.

4.2 Ship to pressure field

In the pressure field method, the ship is specified as a pressure field boundary condition. This means the translation from a ship specified by a hull shape to a pressure field which represents this same hull. The first step for this is locating and rotating the ship. The second step is interpolating the ship hull onto the pressure grid. To prevent interpolation issues within SWASH, a pressure value is required at every grid point, and at all the moments in time at which a pressure field is specified.

4.2.1 Ship location and orientation

The MASHCON simulations are the easiest for ship location and orientation. The heading is constant and the measurements contain the position of the ship in the towing tank at every measurement time. For the ROPES and Bath simulations, the ship location and rotation needs to be done in a different way.

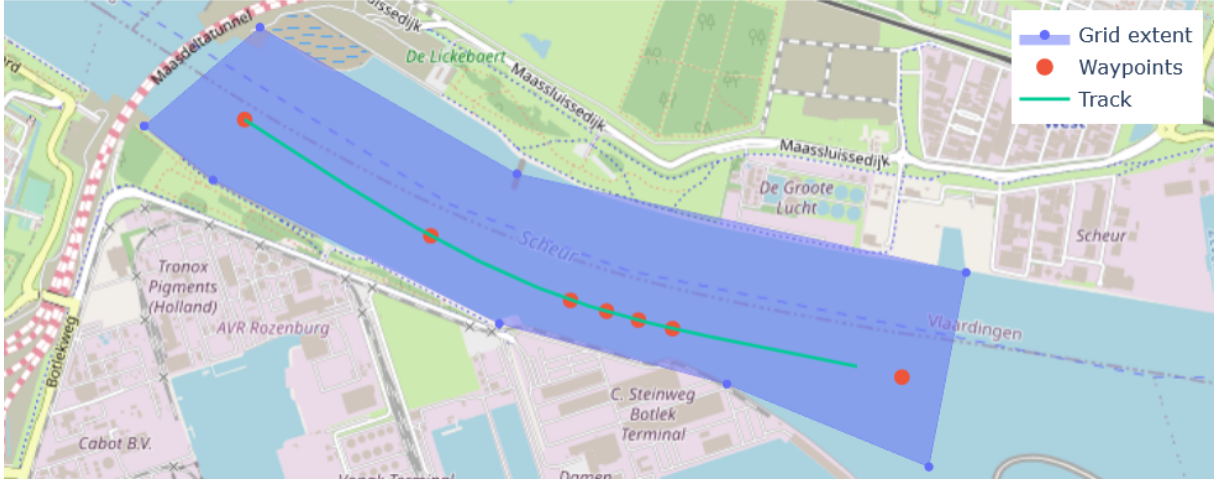


Figure 4.1: The waypoints and the track that is calculated from them for the ROPES measurements. The track doesn't reach the last waypoint because the simulation doesn't run so long that the ship will reach this point.

In this research, the ships sail along a track at a given speed. The track is based on the information that accompanied the measurements and is specified by a number of waypoints. Through these waypoints, a 3rd order spline is fitted. The spline will for the basis for the location calculation. For every grid-specification time step the distance that the ship has sailed is determined. The spline and its derivative are then evaluated for all these distances, giving the positions and headings of the ship. The result is visualised in Figure 4.1.

4.2.2 Ship interpolation

With the ship located and rotated, it can be interpolated to the computational grids. To get an optimal estimation of the wave signal, it is necessary to accurately represent the ship shape from the measurements in the pressure grids. The basis for ship hulls in this research are ship shapes from the program SEAWAY (Journee, 2001). SEAWAY has a database of frame models, like the example visible in Figure 4.2. The points that are visible in the figure form the point cloud that will be interpolated to the pressure grid.

In reality, the ships in the simulations have some complex parts like the rudders, propellers and bulbs. Due to SWASH being based on the non-linear shallow water equations, complex shapes that are fully submerged cannot be represented. For the purpose of modelling overtopping, the bulb is the most important element that cannot be represented, as the bulb is specifically made to decrease secondary wave generation. It can be expected that with a vessel sailing at its design speed, a model without a bulb will generate higher secondary waves than its equivalent with a bulb. For the situations modelled in this research, the ships were likely not sailing at their design speed as they were in a narrow channel. It is therefore expected that the lack of a bulb in the models in SWASH will have negligible effect on the estimated secondary wave height.

For generation of the pressure grids, the point cloud from the SEAWAY hull model has to be interpolated on the computational grid. For each grid, the position and heading of the ship are calculated at the grid time. The point cloud is rotated to the correct heading and then moved to the correct location. The z-coordinate of all hull points is transformed to a pressure value according to equation 4.1:

$$p_{zi} = z_i \frac{\rho g}{100} \text{ hPa} \quad (4.1)$$

In which p_{zi} is the pressure corresponding to the z-coordinate of point i from the point cloud, z is the z-coordinate, ρ is the density of the water, g is the gravity constant, $f_{launch,t}$ is the time-dependent factor used for launching the ship and the division by 100 is done to get to hPa as unit. This unit is chosen for easy addition of the background atmospheric pressure if necessary. The resulting point cloud is then linearly interpolated to the computational grid, and a background pressure grid is added if necessary. In the simulations in this thesis, the background pressure is set to 0 hPa. An example of the result of an interpolation is visible in Figure 4.3.

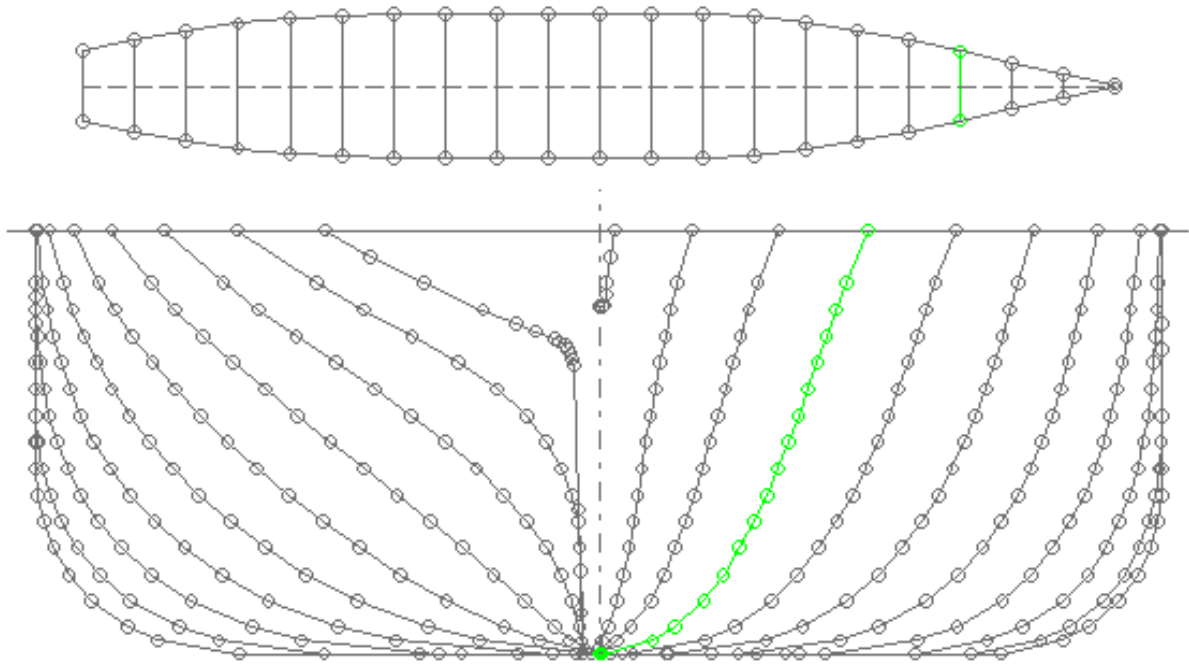


Figure 4.2: A frame model from SEAWAY. The top drawing is a top view of the ship. The bottom drawing is a back/front view of the ship. Left of the middle line is the back view, right of the middle line is the front view. The green line in the in the top drawing is the same line as in the bottom drawing.

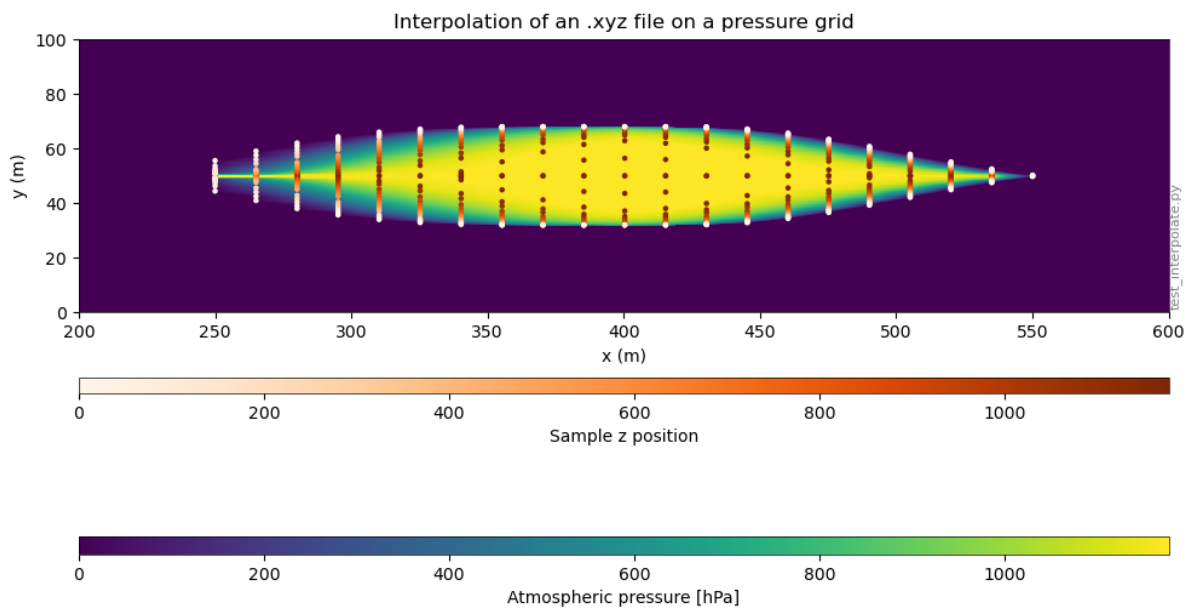


Figure 4.3: Example interpolation of the ship from Figure 4.2 on a pressure grid. The points indicate the hull points from the SEAWAY model. The colored background image is the result of the interpolation.

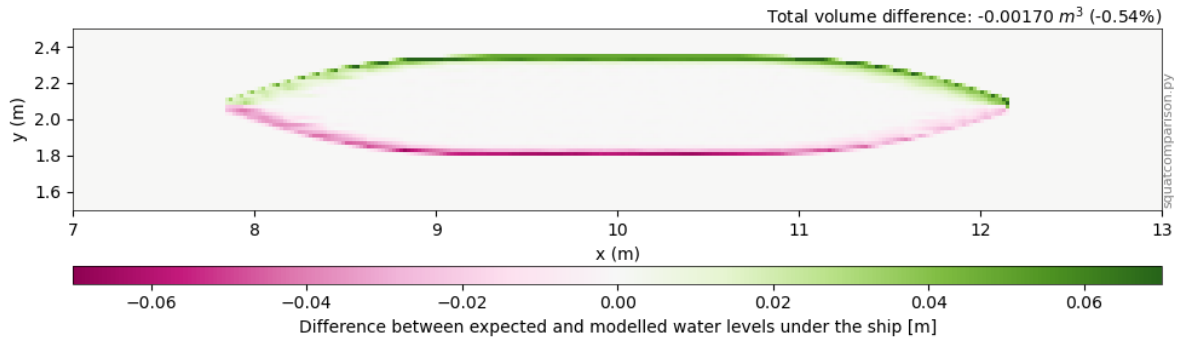


Figure 4.4: The difference between the water levels as expected by pressure specification and the water levels as calculated by SWASH. As visible, the total difference is negligible. The difference at the edges of the ship is probably due to the staggered grid. In both x and y direction, the centre of gravity of the ship has shifted about half a grid cell.

4.2.3 Example results

A first test with this interpolated pressure field is to compare the water levels under a stationary ship as computed by SWASH with what is expected from the pressure field. This comparison is done by translating the pressure grid back to an expected water level grid and comparing this grid with the outcomes of SWASH. Figure 4.4 shows the outcome of this comparison. As visible, there are some differences between water level and expected water level along the edges of the ship. This behaviour is a bit unexpected as both atmospheric pressure input and water level output are specified at the grid points (see 2.3.2). The differences lead to a total volume difference of 0.54 % and a centre of gravity shift of 0.7 cm in the x-direction and 0.8 cm in the y direction. These values are about 0.5 times the cell size, leading to the expectation that the differences are caused by the staggered grid employed in SWASH. The small shift in center of gravity, and small difference in total volume make that the observed shift will not cause problems in further simulations.

4.3 Horizontal boundary conditions

In the simulations for this research, two types of boundary conditions are necessary: a closed boundary for simulating the sides of towing tanks and surface piercing banks and an open boundary for simulating the boundaries where the bank does not meet the surface. These open boundaries need to be defined such that the internally generated, ship-induced waves can propagate over them without reflection. In SWASH, the default boundary is a closed, fully reflective boundary. This can therefore be implemented in the model without any further research. However, for the open boundaries a boundary specification needs to be found that meets the requirements.

In this search, four boundary conditions have been tested:

1. An imposed water level at the boundary
2. An imposed velocity at the boundary
3. A sommerfeld radiation condition
4. A weakly reflective boundary condition

For the water level and boundary condition, both were set at a constant 0. The sommerfeld radiation condition and the weakly reflective boundary condition are given by Equations 4.2 and 4.3 from Zijlema et al. (2011) respectively.

$$\frac{\partial u}{\partial t} \pm \sqrt{gh} \frac{\partial u}{\partial x} = 0 \quad (4.2)$$

$$u_b = \pm \sqrt{\frac{g}{h}} (2\zeta_b - \zeta) \quad (4.3)$$

Table 4.1: Visible reflection in the horizontal boundary condition test cases. The launch wave indicates the disturbances caused by launching the ship. Reflection of the primary wave is not displayed because the model was created to be so wide that the primary waves don't reach the sides of it.

Sponge layer width Boundary condition	$0L_s$	$1L_s$	$3L_s$
Imposed water level	Both launch and secondary wave fully reflected	Both launch and secondary wave partly reflected	Launch wave partly reflected
Imposed velocity	Both launch and secondary wave fully reflected	Both launch and secondary wave partly reflected	Launch wave partly reflected
Sommerfeld radiation condition	Secondary wave fully reflected	Secondary wave partly reflected	No visible reflection
Weakly reflective boundary condition	Both launch and secondary wave fully reflected	Launch wave partly reflected	Launch wave partly reflected

In these equations ζ is the surface elevation at the boundary and ζ_b is the incident wave signal. In these tests, the incident wave signal is set to a constant 0. The sommerfeld radiation condition is designed to allow long waves to travel over the boundary. The weakly reflective radiation condition should also allow waves to travel over the boundary without being reflected. For decreasing the reflections at the boundaries, SWASH allows the specification of sponge layers. These sponge layers are relaxation zones which dissipate wave energy at the boundaries. For full wave dissipation at the boundaries, the SWASH user manual advises to use a sponge layer width of three times the most highly energetic wave component. With no boundaries specified, the secondary waves get reflected on the sides of the model while the long, launch-induced waves get reflected on the model boundary which is crossed by the ship track. These reflections are therefore the relevant reflections to prevent.

For testing the boundary conditions, a rectangular model has been created with a uniform depth and the boundary condition to be tested imposed at all boundaries. The ship is represented by a rectangular box. To test the effect of different boundary conditions in combination with different sponge layer widths, all four boundary conditions as described above are tested in combination with a sponge layer width of 0, 1 and 3 times the secondary wave length. Reflection is identified based on a top view of the water levels at the end of the simulation. As visible in Table 4.1, the sommerfeld radiation condition in combination with a sponge layer three times the secondary wave length allows both the launch-induced waves and the secondary waves to travel over the end of the domain. This is in line with expectations, as the sommerfeld radiation condition is designed to allow long waves to travel over the boundary, while the sponge layer dissipates the secondary waves. These settings will therefore be used for simulating open boundaries where necessary.

4.4 Numerical schemes and stability

In the earlier testing of the model, it became clear that instability of the model was a big risk. During simulation, a wiggle would develop and explode causing water level errors (Figure 4.5). For the stability of the model, grid cell size in combination with the numerical scheme are the main controlling factors. With a finer grid, the ship shape and bathymetry can be described more accurately and with smaller gradients at sharp edges. This will decrease gradients in the model and therefore increase stability. Still only refining the grid was not sufficient for increasing the stability of the model enough to simulate a ship passage. For increasing model stability, there are several options: decreasing gradients in the ship hull, increasing the number of vertical layers, using a flow limiter and choosing a different numerical scheme. To get an insight into the effects of each of these options, some tests have been done on each option individually. For testing the influence of individual adaptations to the model, an instable version of the model used to test the horizontal boundary conditions was used. By comparing the moment at which the model produced a water level error, the increase in stability could be quantified.

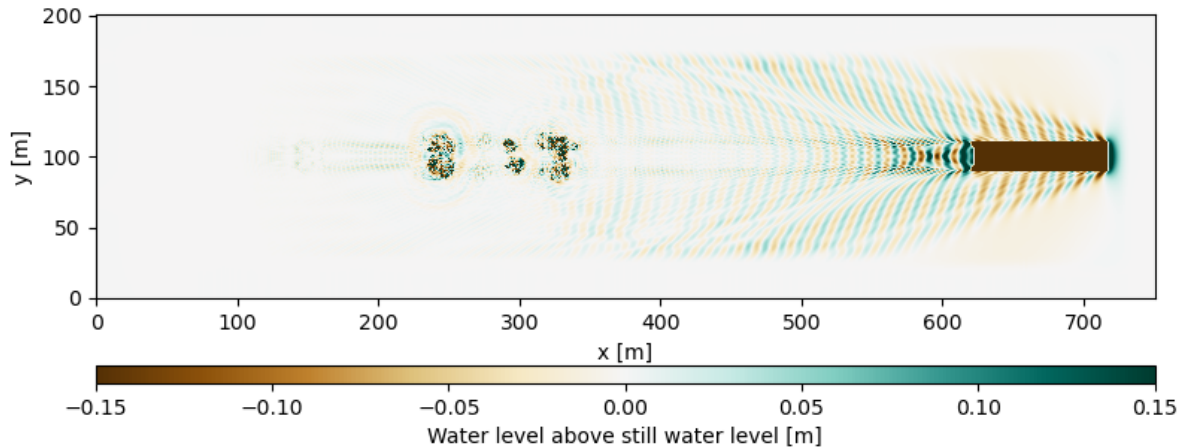


Figure 4.5: One of the unstable test runs. Visible are the wiggles behind the ship that should not be there in reality.

4.4.1 Ship shape

For testing the influence of decreasing gradients in the ship shape, a ship represented by a rectangular box was compared to a ship represented by a model from SEAWAY. Here, the expectation was that the gradients at the edges of the box would cause instabilities while the more smooth ship shape would decrease the formation of instabilities. This expectation was confirmed by the model runs. The model with the SEAWAY ship took double the time it took the model with the rectangular box to get unstable.

4.4.2 Vertical layers

For testing the influence that the number of vertical layers in the model has on stability, the instable test model was ran with one vertical layer, three vertical layers, four vertical layers and four non-equidistant layers. By default, SWASH divides the layers equally over the water column (see 2.3.3). In this setting, the layers are equidistant. When using non-equidistant layers, the user can define the layer thickness as a percentage of the water column. With the purpose of this research being overtopping, the top of the water column is of more relevance than the bottom of the water column. By using non-equidistant layers, the resolution in the top can be increased without increasing computational demand. For this test, the layers were specified as having a thickness of 10, 20 30 and 40 percent of the water column, numbered from the top down. Compared to a simulation with one layer, using four non-equidistant layers improves stability by an order of magnitude.

4.4.3 Flow limiter

A flow limiter increases stability as it prevents the strong flows that an exploding wiggle needs. For the test model, the stability increase could not be quantified as applying a flow limiter caused the simulation to finish without getting instable. However, when the model was expanded to including a surface-piercing bank, the flow limiter caused disappearance of the water at the bank. It is therefore not used in further simulations.

4.4.4 Numerical scheme

In the first proof of concept, the numerical scheme was taken from the SWASH progressive wave example. This was done as the SWASH manual indicated that for short waves local conservation of momentum is required and these settings provided this. Extensive testing provided insight on the stability of different momentum-conservative schemes. The best stability was achieved with the commands:

```
DISCRET UPW UMOM MOM H FRO
DISCRET UPW WMOM H FRO
DISCRET UPW UMOM MOM V BDF
DISCRET UPW WMOM V BDF
```

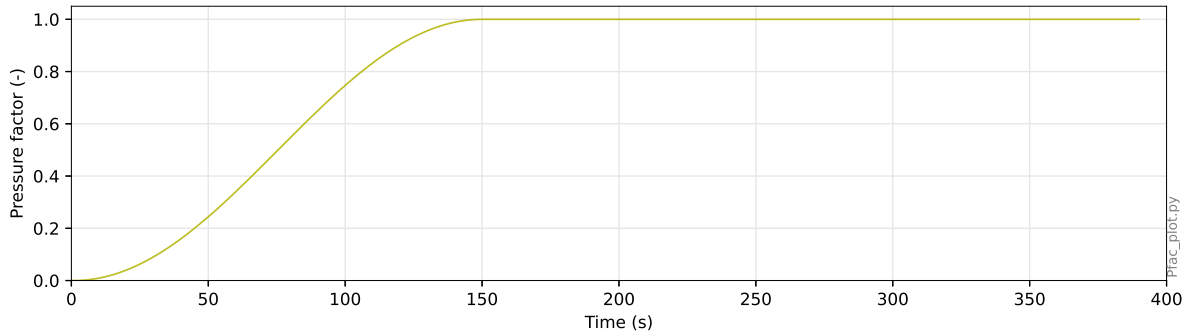


Figure 4.6: The pressure factor against time as used in the ROPES measurements.

The commands indicate that SWASH should conserve momentum in the u/v momentum equations. For the horizontal components of both the u/v and w momentum equations SWASH will use Fromm's scheme. For the vertical components of the momentum equations SWASH uses a backward difference scheme. Time integration is still explicit.

4.5 Reaching a steady state

In reality, the ship sails through the waterway at a constant speed. Effects from the acceleration of the ship do not reach the measurement location. In SWASH, the model does not offer the option to start with the ship already sailing through a geometry. The ship needs to be introduced into the model, creating disturbances in the measurement signal that are not there in reality. To prevent these disturbances from interfering with the measurements, a spin-up procedure needs to be developed that makes it possible to introduce the ship in the model and where the artefacts from the launching can be identified in the wave signal. This spin-up procedure consists of two phases:

1. The ship needs to be launched into the water. Technically, this means the introduction of a volume and therefore the displacement of the water initially in the model.
2. The ship needs to be accelerated from zero to end velocity. This means the introduction of momentum into the model.

4.5.1 Launching the ship

For gradual introduction of the ship into the water, the simplest method is gradually changing the z -coordinate of the hull points. In this research, the ship is launched using a sine function to get a fraction of the z -coordinate of all hull points for each timestep. The factor $f_{launch,t}$ from equation 4.1 will be specified for all pressure grids in a simulation. See Figure 4.6 for an example of the evolution of the $f_{launch,t}$ over time. The translation of this factor to the pressure field, is done by multiplying the pressure value as calculated by Equation 4.1 with a the $f_{launch,t}$. The extended equation then looks as follows:

$$p_{zi,t} = z_i f_{launch,t} \frac{\rho g}{100} \text{ hPa} \quad (4.4)$$

The advantage of using a sine function over launching the ship linearly is the prevention of shocks at the beginning and end of the launching. The start of the sine function is the start of the simulation. When launched in the same time, a larger ship displaces more water than a smaller ship. It will therefore also cause larger disturbances. To decrease the height of these disturbances, a larger ship needs to be launched slower than a smaller ship. When launching, the displacement of the water causes a long wave that moves away from the ship. If the launching time is long enough, this wave will be lower than the waves caused by the ship passing the measurement locations.

4.5.2 Accelerating the ship

For the ship acceleration, both the moment of acceleration and the acceleration function are relevant. Two ways of accelerating the ship were tested, both with their benefits and drawbacks:

1. Launching at speed
2. Acceleration after launching

The benefit of the first procedure is that at the moment the launch is completed, there is no need for an additional acceleration procedure, reducing the simulated time necessary for a passage. The decreased simulated time in turn reduces the computational effort and chances for instability. The drawback is that with the ship moving with the shock wave while being launched, the first procedure will produce a higher shock wave than the second. The higher wave can cause extra oscillations before leaving the domain. These extra oscillations make it hard to determine when the model reaches a steady-state. Before a steady-state, the measurements will be unreliable, so for accuracy purposes, the second procedure is preferred. The choice of launching procedure therefore depends on which of the arguments is deemed more important. If the reduced computational effort and chances for instability are favoured over the increased accuracy, the first launching procedure is favorable. If the extra computational effort does not outweigh the benefits of increased accuracy, the second launching procedure is favourable.

The simulations in this research will use the second procedure as much as possible. The benefits of this approach are that the disturbances created by the launching are separated from those created by the acceleration. This means smaller disturbances that die out quicker. Further, the distance between the starting point of the ship and the measurement location can be smaller. This is because a set distance between disturbances and ship is necessary for reliable output. During the launching, the ship does not move so the distance increases at the speed of the disturbances (\sqrt{gh}). During acceleration, the ship starts slowly so the disturbances move away quickly. A long period of low disturbance is created this way so that the disturbances will not be higher than the ship waves themselves. The drawback of using the second method is the long time the warm-up takes. All this time, the complete grid needs to be simulated considerably increasing the computational effort. The computational effort required for a passing event will be discussed later in this chapter. The values chosen for launching time and acceleration distance will be discussed at the individual simulations.

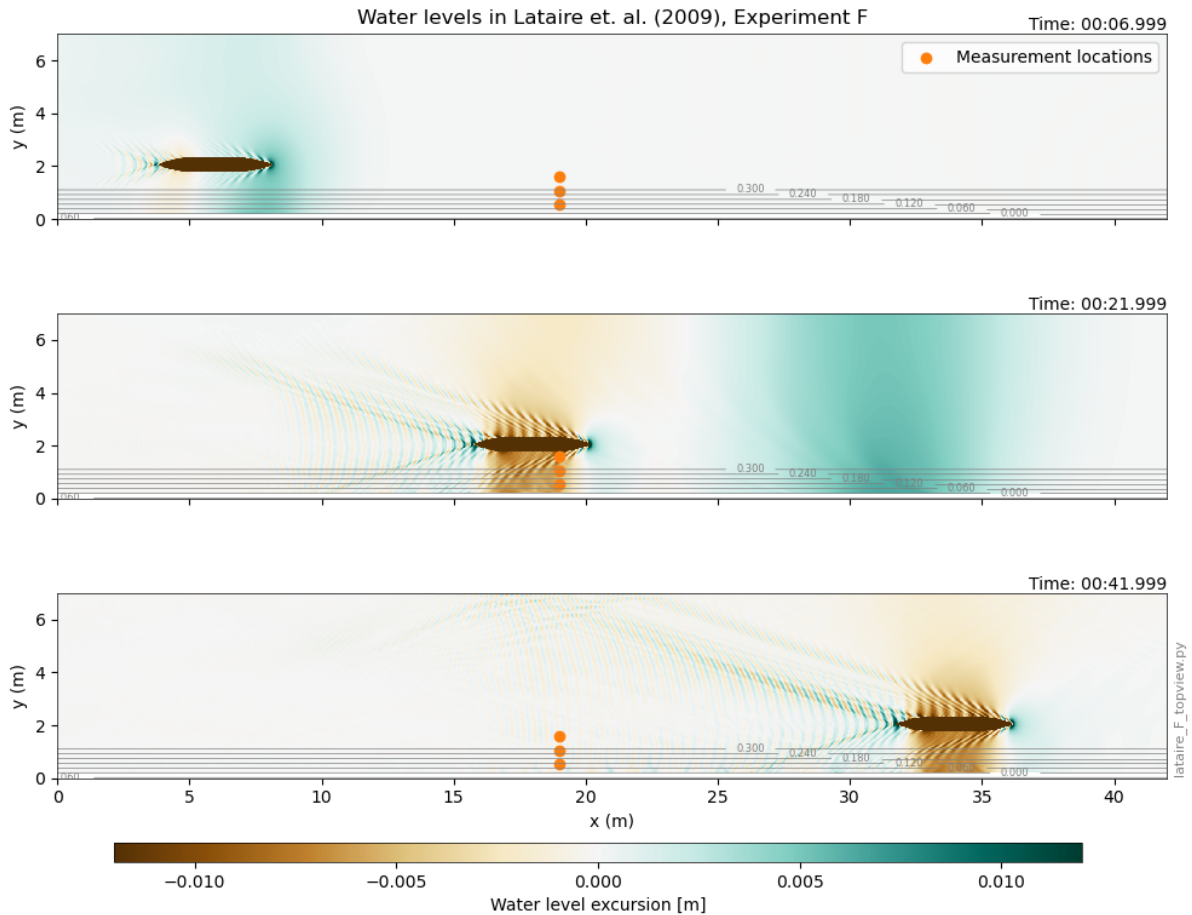


Figure 4.7: Water level excursion in Experiment F from Lataire et al. (2009) as modelled by SWASH. The ship is sailing left to right. Visible are the initial distortion propagating out of the model, the primary wave field along the length of the ship and the secondary waves. The wave signals as recorded in the measurement locations are visible in Figure 4.8.

4.6 Model settings

As described in Chapter 3, studies done on overtopping with SWASH describe grid cell size, bottom friction and viscosity as important settings influencing the overtopping in SWASH. To gain insight in the possibility to model both ship wave generation and overtopping in the same SWASH model, it is relevant to see the interaction of these settings with ship wave generation. In the ideal case, the settings for good overtopping estimation are the same as for good ship wave generation. In this section, the connection between wave generation and wave overtopping settings is described.

4.6.1 Cell size

To test the influence of cell size, two cell sizes have been tested in a recreation of Lataire et al. (2009), experiment F: 5cm and 2cm. The SWASH input file for can be found in Appendix D. The wave signal of these two simulations can be found in Figure 4.8. A visualisation of the wave fields in Figure 4.7.

As expected simulations seem to correctly estimate primary water level depression. The primary water level is visible as the long wave between 47.5 and 52.5 seconds. The depression in the model stays a little longer than in reality. This can be explained by the higher block-coefficient of the ship in the model. For a more cubic ship, the maximum cross-section is the actual cross-section for larger part of the length. The primary water level depression is dependent on the ratio between ship cross-section and canal cross-section. Therefore, the depression is more prominent for longer time. With regard to the secondary wave height, the figure shows a significant difference between 5 CPW and 13 CPW.

The 5 CPW simulation shows an overestimation of secondary wave height at Gauge 1. At Gauge 3 the waves have decayed so much that the simulation is in line with the measurements. The small number of

Comparison between measurements and modelled results from Latiare et al. (2009) experiment F

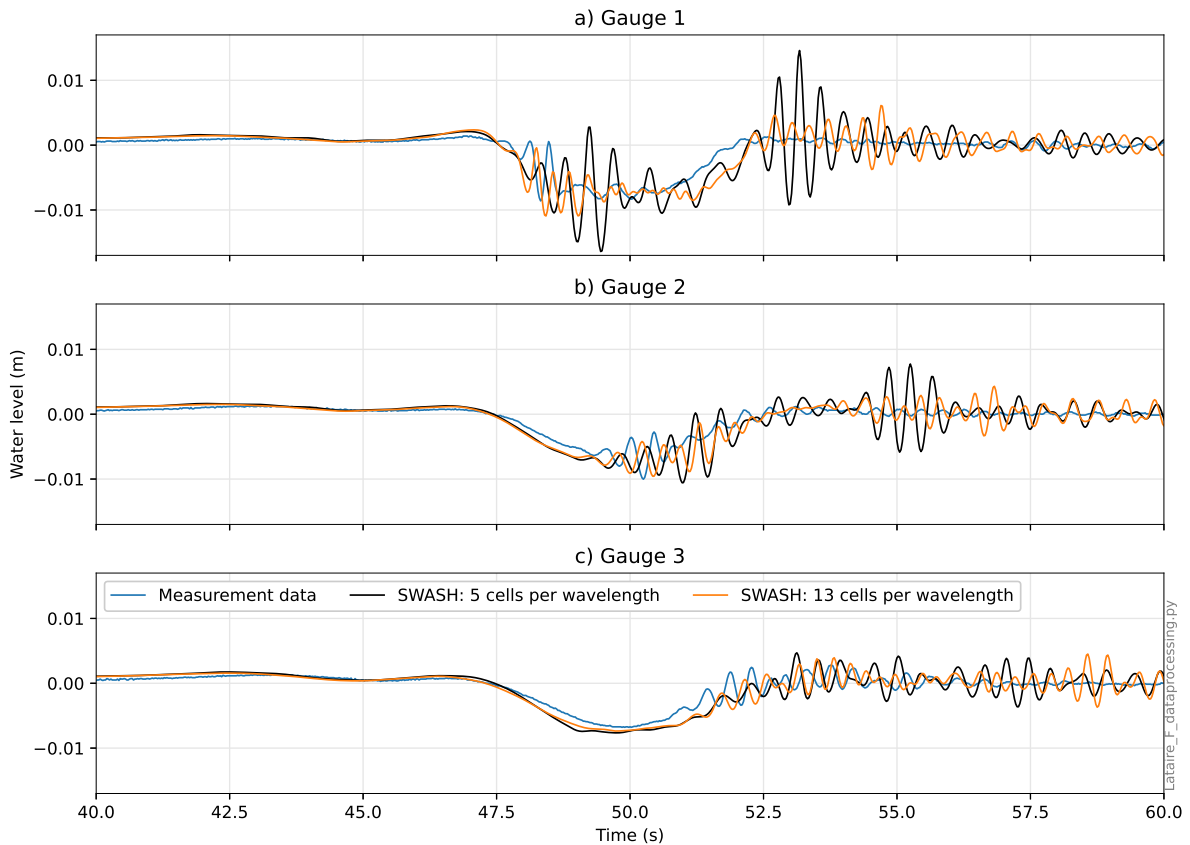


Figure 4.8: The wave signal results for the three gauge locations as depicted in Figure 4.7, plotted for two grid cell sizes.

cells per wavelength causes an overestimation of wave decay. For the 13 CPW simulation, the secondary wave height and wave decay are more in line with expectations. The secondary stern wave that is present in the 5 CPW simulation can be caused by a coarse representation of the ship stern. Next to the wave height, the timing of the secondary waves is influenced by the resolution. At Gauge 1, the 5 CPW simulation shows a delayed secondary wave while the 13 CPW simulation shows the secondary wave closer to the actual timing. This means that the dispersion of the secondary wave is better for a finer grid. In the 13 CPW simulation, the secondary wave still shows some delay giving an indication that the optimal resolution would be even higher.

4.6.2 Bottom friction

For the eventual overtopping volumes, bottom friction has been demonstrated to be an influential parameter (Suzuki et al., 2014). The influence of bottom friction on wave signals as generated by SWASH has been tested on experiment J from the MASHCON dataset. In this experiment, the same ship was used as for F but at a different draught. The speed was also 0.801 m/s. The geometry of Experiment J can be found in Figure 3.6. The tests were done with a grid cell size of 2 cm, so a resolution of 13 CPW. The bottom friction was given a manning coefficient. For one experiment, the bottom friction was set to zero. For the other, the manning friction coefficient was $n = 0.012$ to represent the smooth material that the towing tank was made from. Figure 4.9 shows the wave signals of two tests. Visible is that the wave signals for these two tests completely overlap. This is a bit unexpected as the bottom friction is expected to have an influence on the primary flow effects (BAW, 2010). The lack of influence can be caused by the relatively smooth bottom in combination with the ship sailing in a relatively large channel. The ratio between ship cross sectional area (A_s) and channel cross section (A_c) in MASHCON experiment F is $A_s/A_c = 0.04$, while for an inland channel in the Netherlands it can be up to 0.1. Larger values of the A_s/A_c ratio make the primary flow effects stronger and will therefore increase the influence of bottom

Comparison between measurements and modelled results from Latiare et al. (2009) experiment J

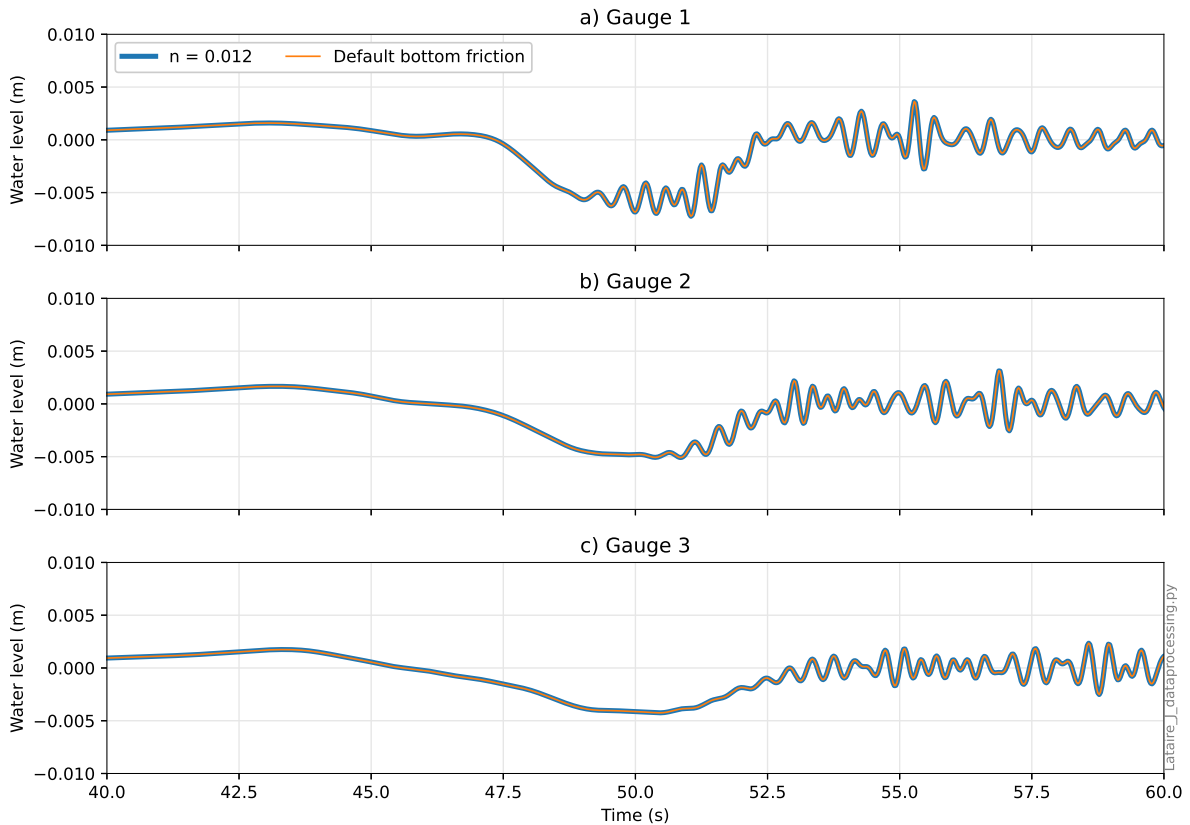


Figure 4.9: Wave signals for the three wave gauges in MASHCON experiment J, plotted for two bottom friction values. Visible is the lack of influence that the bottom friction has on the wave generation.

friction. In line with results from Suzuki et al. (2014), bottom friction is of small relevance for wave generation and transformation and can be tuned when calibrating for overtopping. However, it is not certain that this statement is also true for higher roughness than tested here.

4.6.3 Viscosity

In Zhou et al. (2013), viscosity is used to tune the primary water level drawdown. The same Smagorinsky viscosity model as used there is also tested in SWASH. The viscosity constant is 0.9. Due to time constraints, the simulations are done with the 5 CPW model. The wave signals are plotted in Figure 4.10. As visible, the viscosity model reduces the secondary wave height in Gauge 1 and 2, bringing it closer to the actual secondary wave height. However, in Gauge 3 the viscosity model causes wiggles that are not visible in the measurements. Therefore, the Smagorinsky viscosity model is not considered to increase the performance of SWASH for ship wave generation. Further tests were done using a $\kappa - \epsilon$ turbulence model as also used in the overtopping simulations done by Lashley et al. (2020). However, the model could not be made stable enough to investigate the influence of this turbulence model on the ship wave signal. As no increased performance can be determined, turbulence is left to default (no turbulence model) in further simulations.

Comparison between measurements and modelled results from Lataire et al. (2009) experiment F

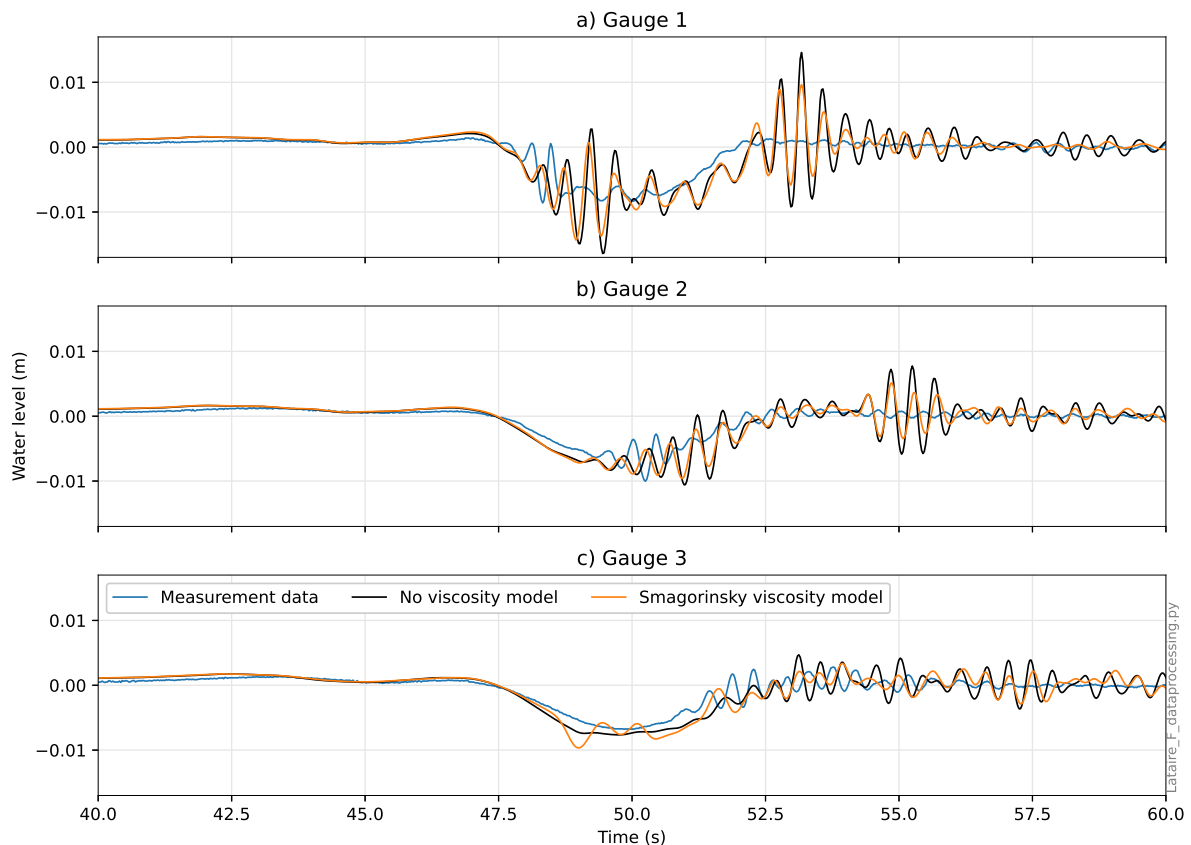


Figure 4.10: Wave signals in MASHCON experiment F as produced with different viscosity models.

4.7 Further implementation characteristics

In this research, the focus lies on modelling ship waves for the purpose of overtopping. However, it is also useful to look at some other characteristics of the model. The first of these characteristics is squat. The second is the model performance regarding calculation time. The performance of SWASH regarding these characteristics will be treated here.

4.7.1 Squat

In SWASH, the usage of the pressure field method makes that the effects of squat are inherently included. A correct estimation of squat by SWASH would increase trust in the mechanics behind the model. Squat will therefore be calculated for Lataire et al. (2009), experiment F and compared to an analytical method in this chapter.

Before calculating squat, some observations can be done on the return current. Figure 4.11 shows the depth-averaged velocity magnitudes during the steady state phase of Experiment F from Lataire et al. (2009). South of the ship, the return current is visible as expected. Behind the ship a line of increased flow velocity is visible. This line is caused by the lack of a propeller and has been observed before in Talstra (2012).

A visualisation of the squat as calculated by SWASH can be found in Figure 4.12. Visible is that under the ship, a pattern of diagonal lines forms. This secondary wave-like pattern is an artefact of the pressure field method. Under a real ship, such a wave pattern doesn't exist. The rigid hull will cause the water to follow the shape of the ship. With a pressure field, the water level under the pressure field can deform. A measure for inaccuracies caused by this deformation is the standard deviation of the water level difference. If the standard deviation is very high, the SWASH model shows high oscillations that cannot be explained by the pressure field. In the displayed model, the standard deviation of the water

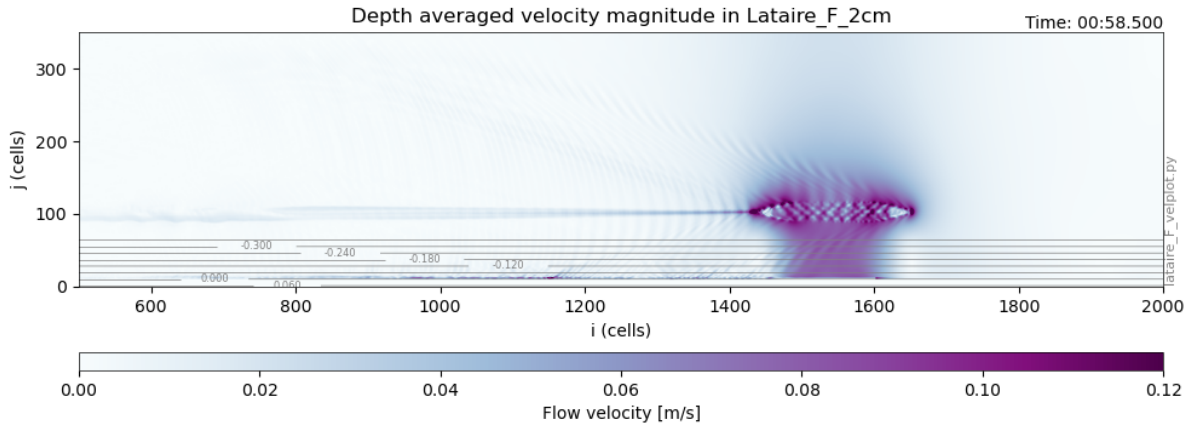


Figure 4.11: Depth averaged flow velocity magnitude in Lataire et al. (2009) experiment F. The main observations here are the return current along the ship, the wave-like pattern underneath the ship and the flow in track of the ship.

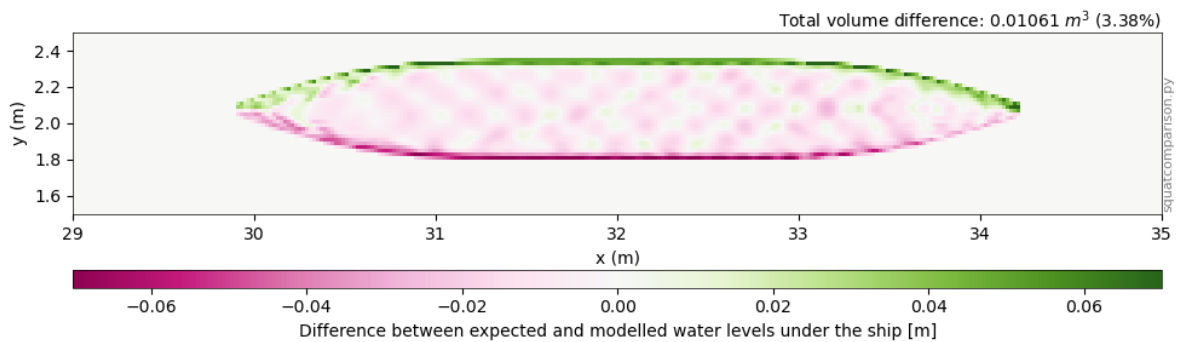


Figure 4.12: Difference between the water level as specified by the pressure grid and actual water levels as calculated by SWASH. The extra depth is the squat, which is 0.55 cm. Visible is the half-cell shift that could also be observed when simulating a stationary ship. Also visible is the mesh-like pattern underneath the ship which is not present in reality.

level difference is 0.0016 m, which is 1% of the draught. This includes the water level differences caused by interpolation at the edges of the ship. The waves under the ship are therefore not expected to have too much influence on the final wave field.

For a conclusion about the correctness of the squat estimated by SWASH, the modelled squat is compared to the measurements and the much used formula as presented by Barrass and Derrett (2012) is used:

$$S_{\max} = \frac{c_b S_2^{2/3} V_s^{2,08}}{30} \quad (4.5)$$

In which S_{\max} is the maximum squat, c_b is the block-coefficient, V_s is the vessel speed and S_2 is the blockage ratio given by:

$$S_2 = \frac{A_w}{A_{ch} - A_w} \quad (4.6)$$

Where A_{ch} is the channel cross-sectional area and A_w is the vessel frontal area. For the experiment at hand, Equation 4.5 predicts a squat of 0.49 cm. For the SWASH model, the total squat is calculated as average difference between depth as modelled by SWASH and depth as expected from the pressure field. With this method, SWASH predicts a squat of 0.55 cm. The measured average squat was 0.6 cm. This means that SWASH is off by 20 %. Compared to the analytical method SWASH overestimates squat by about 10 % which is considered accurate. Compared to the measurements, SWASH underestimates squat by 20 %. This means that although not exactly right, SWASH performs better than a much used analytical method in a simple geometry.

4.7.2 Run time

The run time of a SWASH model depends on the number of grid cells, the number of layers, the model settings and the timestep. Since the timestep is dynamically controlled based on a range of Courant numbers, the timestep depends on cell size, water depth and flow speed.

For SWASH to accurately model the most energetic wave components, the manual advises a resolution of 50 cells per wavelength. For run-up, the advice is to use 100 cells per wavelength. The shortest relevant wave in the ship wave models is the secondary waves. An estimate of the optimal grid cell size is therefore $L_s/50$, with L_s as calculated in equation (2.8).

However, with the PC's used for this research, this grid cell size leads to an unworkable calculation time. To gain insight in estimated calculation time the models ran for this thesis can be used. Figure 4.13 shows the run times of the models. It is visible that there is a strong relation between the number of calculations necessary per core and the run-time. The number of cores over which the calculation is distributed does not seem to influence the run time. Visible is that calculation time depends mostly on the number of calculations per core. There is no slowdown if the workload is distributed over more cores. Based on these observations, the run time of a simulated ship passage in SWASH on current-gen PC's can be estimated by:

$$t_{\text{computing}} = 1.04 * 10^{-19} N^2 + 6.18 * 10^{-9} N - 0.35 \quad (\text{hours}) \quad (4.7)$$

With t as calculation time in hours and N the number of calculations per core, given by:

$$N = \frac{t_e - t_s}{\Delta t} * \frac{mxc * myc * k}{\gamma} \quad (4.8)$$

With t_e and t_s the end and begin time of the calculation, Δt the time step, mxc , myc and k the amount of cells in x, y and z directions and γ the amount of cores that will be used for the calculation. As this formula is based on the data of the runs done for this thesis, it is only valid inside the range of N -values as tested here.

For demonstration purposes, the assumption that Equation 4.7 is also valid for larger models can be done. As shown in Appendix B, simulating the Lataire et al. (2009) experiments with a uniform resolution of 50 CPW will lead to an estimated calculation time of ≈ 20 years. When using a grid locally refined to 50 CPW, this calculation time can be reduced to 238 days. However, if the resolution in the refinement area is increased to the advised 100 CPW, the calculation time again increases to ≈ 6 years.

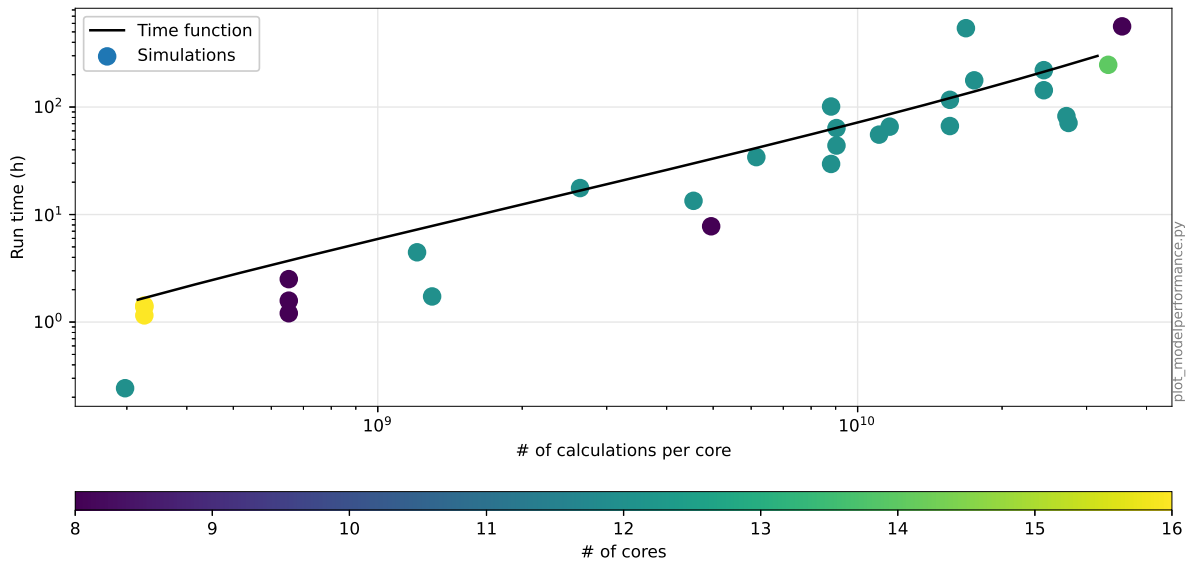


Figure 4.13: The calculation time of the SWASH model for different simulations. Color of the data points is based on the number of cores on which the simulation is ran. Note the log-log scale on the axis, and the lack of influence of the number of cores over which the simulation is distributed.

4.8 Summary

Using time-dependent pressure fields, it is possible in SWASH to recreate ship waves with the pressure field method. A ship sailing through a geometry can accurately be represented with these pressure fields. Stability of the model is an important issue. For the test cases, the numerical scheme as described above is fit for purpose. However, it is not clear if this is also the case for ship passing events that were not tested. Regarding the settings of the model, several aspects are important. First is the warm up of the model. Slowly expanding the ship into the water and then accelerating it is the most disturbance-free method but also computationally the most demanding one. Settings like viscosity and bottom friction are of large influence for overtopping but less for wave generation. They can therefore be tuned to suit the model for overtopping. Most important aspect regarding the settings of the model is grid cell size. Smaller cells mean better estimation of wave height and dispersion. However, the resolution of the model is closely linked to computational time. A user of the model therefore always needs to make a trade-off between accuracy and computational effort. Due to the time constraints in this research, the resolution of the models will be chosen such that the calculation time is always 7-10 days.

5 VALIDATION OF WAVE GENERATION

With the pressure field implemented in SWASH, the next step is to validate the model. Four tests will be done to benchmark the performance of SWASH for ship wave generation. First, a passage from the same measurement series as used for the design of the model will be tested to see SWASH performance in the same towing tank but with a different geometry. Then, a passage from the ROPES measurements will be simulated as well as a passage from the Bath measurements. For a comparison of the performance of SWASH to analytical methods, three passages that have been simulated in SWASH will be modelled with these analytical methods. The chapter will be finalised with a conclusion regarding the performance of SWASH on ship wave signal generation.

5.1 MASHCON towing tank tests

From the MASHCON towing tank tests, Experiment E will be recreated for validation of the waves generated in SWASH. The tank geometry for Experiment E is found in Figure 3.7. In this experiment, the vessel had a speed of $V_s = 0.687 \text{ m/s}$. When using Equation 2.8, this vessel speed gives a secondary wave length of $L_s = 0.20 \text{ m}$. Contrary to test F, the physical model test has been done with the propeller turning at 719 RPM. The propeller is expected to increase primary wave magnitude (Talstra, 2012).

The SWASH model based on this experiment had a resolution of 2 cm, giving $CPW = 10$. As explained in Chapter 4, this resolution will probably cause an overestimation of secondary wave height, and an underestimation of secondary wave dispersion. As the propeller effects are not simulated in SWASH, the primary wave depression is expected to be underestimated by SWASH. The used SWASH input file can be found in Appendix E. The run time of the model was 6 days at 12 cores.

A top view of the wave fields can be found in Figure 5.1. Visible is that the wave fields look realistic: the primary water level depression forms alongside the ship, as well as the secondary waves begin generated at the bow and stern of the ship. The reflection at the closed edges of the tank is also what is expected.

When looking at the wave signal (Figure 5.2) the outcome is largely in line with expectations. In the first gauge, the primary wave is at its maximum for a little too long. Instead of what is expected based on literature on propeller effects, the presence of a turning propeller in the physical model does not create an underestimation of primary wave height in SWASH. Furthermore, in line with expectations, the secondary waves are overestimated. Also the timing of the secondary waves seems a little late. This can all be explained by a too coarse grid. On the bank, the situation is the same. With a lower depth, shoaling makes the secondary waves get shorter so the CPW decreases below the 10 specified earlier. The overestimated wave decay causes the waves in gauge 3 to have the same height as in the physical model.

Using the signal filters as described in Appendix A, the characteristics of both the measured and modelled ship wave have been determined. The wave signal has been analysed in Gauge 1 as in this gauge the waves are most dependent on their generation by the ship and least on deformation by the geometry. For better comparison with the other simulations, this analysis will be done on prototype scale. Figure 5.3 shows that indeed primary water level depression and stern wave height are relatively well estimated, being off by 10 cm. The overestimation of the primary water level depression means that SWASH is conservative on this characteristic. The overestimation is probably caused by the ship in SWASH having a bit more volume than the ship in the measurements. The reason for the underestimation of the primary stern wave remains unknown. The secondary wave height is overestimated. As visible in section 4.6.1, the model overestimates the secondary wave height close to the ship if the horizontal resolution is too coarse. The performance here can probably be increased by refining the resolution of the model.

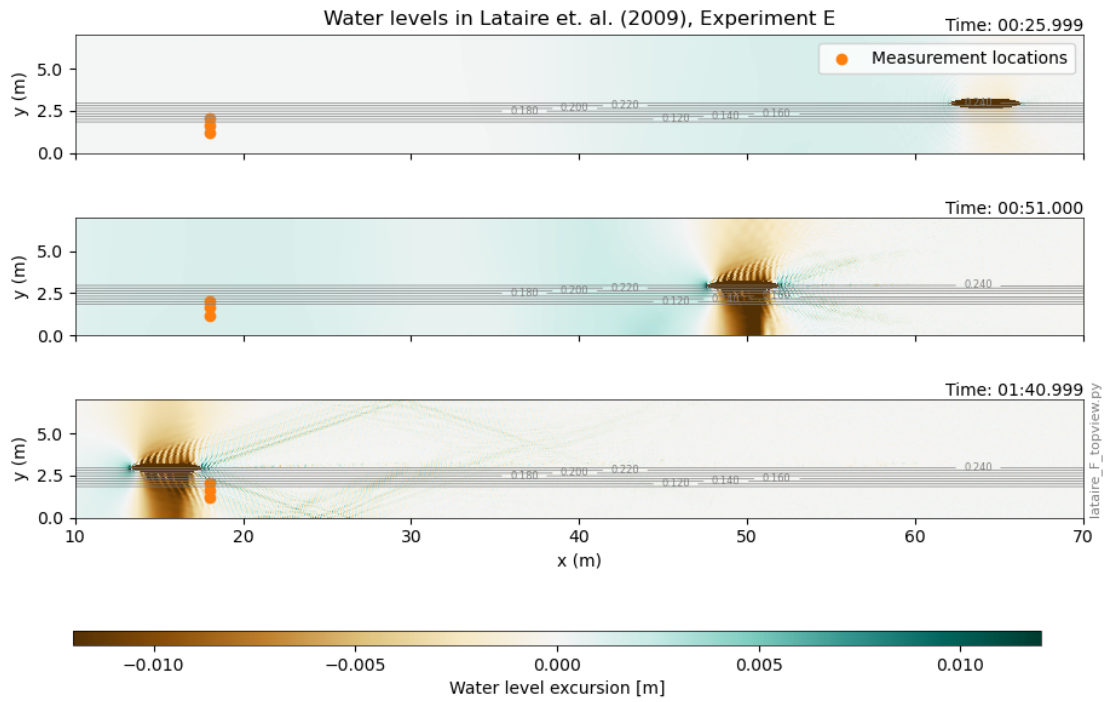


Figure 5.1: Water level excursion over the full domain in Lataire et al. (2009), Experiment E. The ship is sailing right to left.

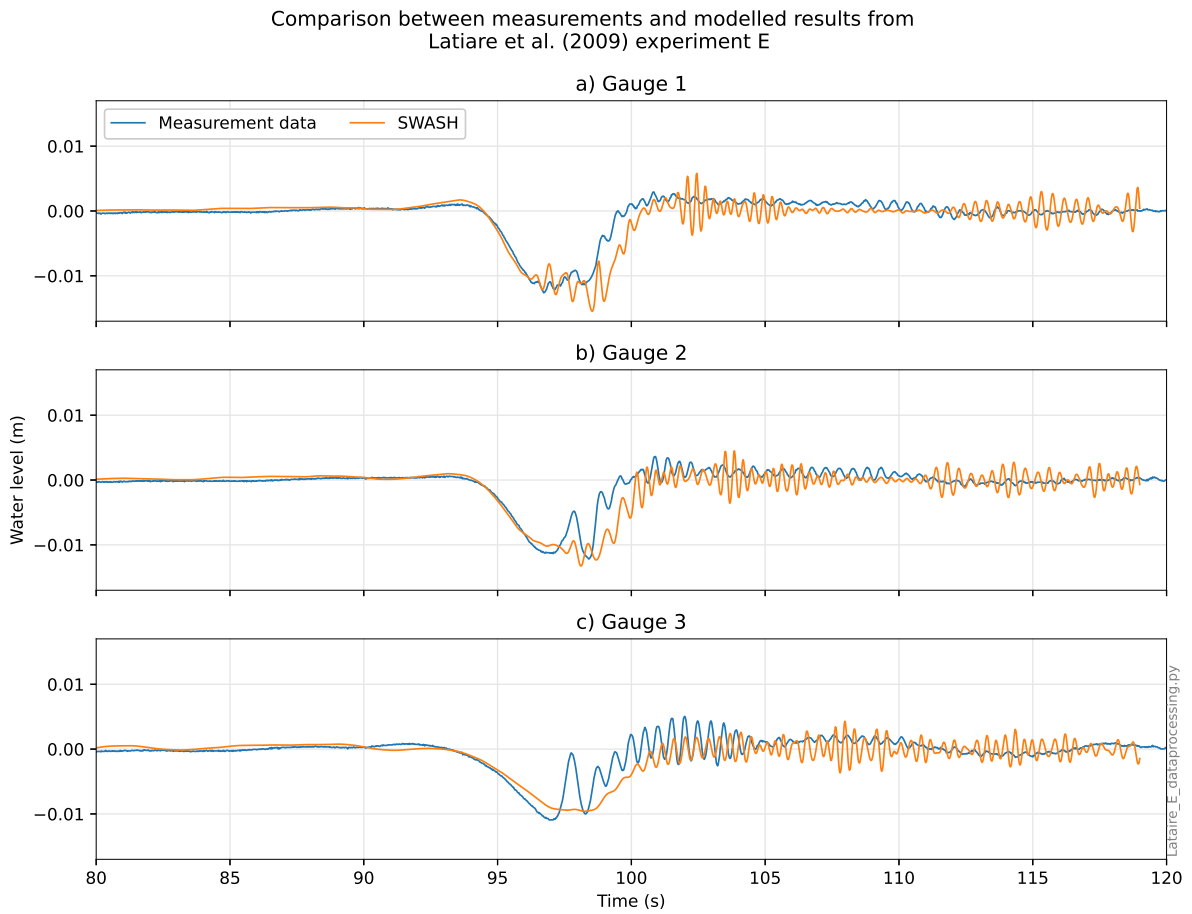


Figure 5.2: Measured and modelled wave signals in Lataire et al. (2009), Experiment E.

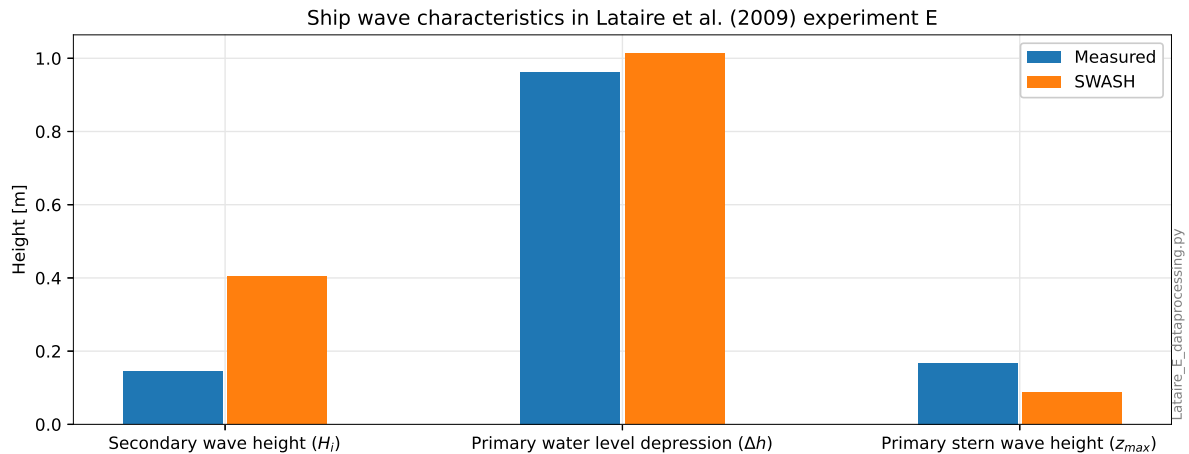


Figure 5.3: Characteristics of the ship wave in Lataire et al. (2009), Experiment E. H_i is the secondary wave

5.2 ROPES measurements

For the simulation, run 902 from the third measurement campaign at the Nieuwe Waterweg Victor (2012) has been selected. The selection of this run was based on two criteria. First was a visual water level signal inspection. A good wave signal has a high signal-to noise ratio, so small surrounding waves, and clearly distinguishable primary and secondary waves. The second criterion for the selection of run 902 is the detailed analysis of this run in the report (Victor, 2012). In this detailed analysis, a picture of the ship track was available. With no GPS data of the ship track, QGIS has been used to draw a spline through the track that was pictured in the measurement report. Figure 3.3 displays the location of the measurements.

5.2.1 Model setup

The first step of the model setup was the selection of the ship. According to the report, a ferry with a length of 142m and a draught of 8m passed the measurement location at 130 m distance with 11.8 knots (6.07 m/s). From the Arcadis ship database, these dimensions match those of the ferry 'Maersk Exporter'. According to the Arcadis ship database, the Maersk Exporter has a width of 23.2 m. Second step in the model setup are the grids. The track and bathymetry are loaded into RGFGrid. For the ROPES case, the used grid measures 3402x486 grid cells. As it is a curvilinear grid, the cell dimensions are not uniform. Figure 5.4 shows the distribution of the cell sizes. Around the measurement area, the cell sizes are below the median of 0.7 and 1.1 m, with the cell size increasing further away from the measurement area. With a speed of 6.07 m/s, the secondary ship wave length is 15.8 m. In the j-direction, this gives a median resolution of 14.3 CPW, and on the i-direction a resolution of 21.1 CPW. The bathymetry as used, ship track and measurement locations are visualised in Figure 5.5. As stated before, measurements were done around the Jaeger Arrow that was moored to the quay. With the Jaeger Arrow moored with the starboard to the quay, the eastern measurement point will be called the bow gauge and the western measurement point will be called the stern gauge. The open boundaries are represented with a Sommerfeld boundary condition. No flow was imposed on the boundaries. The final input grid was a floating object grid representing the Jaeger Arrow moored at the quay. In SWASH, a floating object grid can be specified to indicate a maximum water level on each position. If the water level height is not determined by the free surface condition but by the floating object grid, SWASH switches to pressurized flow. Pressurized flow requires implicit time integration. For the ROPES simulation, the input grid was specified by interpolating the Jaeger Arrow model from the Arcadis ship database onto the computational grid in the location as specified by Victor (2012). The grid cells that were not specified by the ship were set to 2m above still water level to ensure free surface flow. The floating object grid was uniform across time, as SWASH does not allow time-dependent floating object grids. As under the floating object grid pressurized flow forms, implicit time integration is necessary. The implicit time integration is only used for the simulation that included the floating object grid. Third step in the model setup are the passage settings. The launching time was 1 minute and 45 seconds. Acceleration distance was 5 ship lengths so that the ship is at speed at least two ship lengths before it

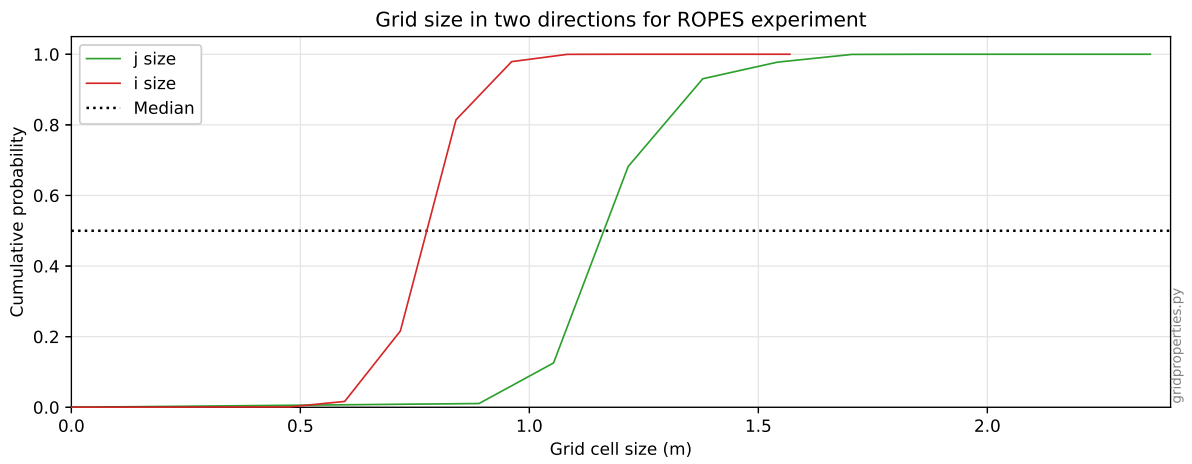


Figure 5.4: Grid size distribution in i and j direction for the grid in the ROPES measurements.

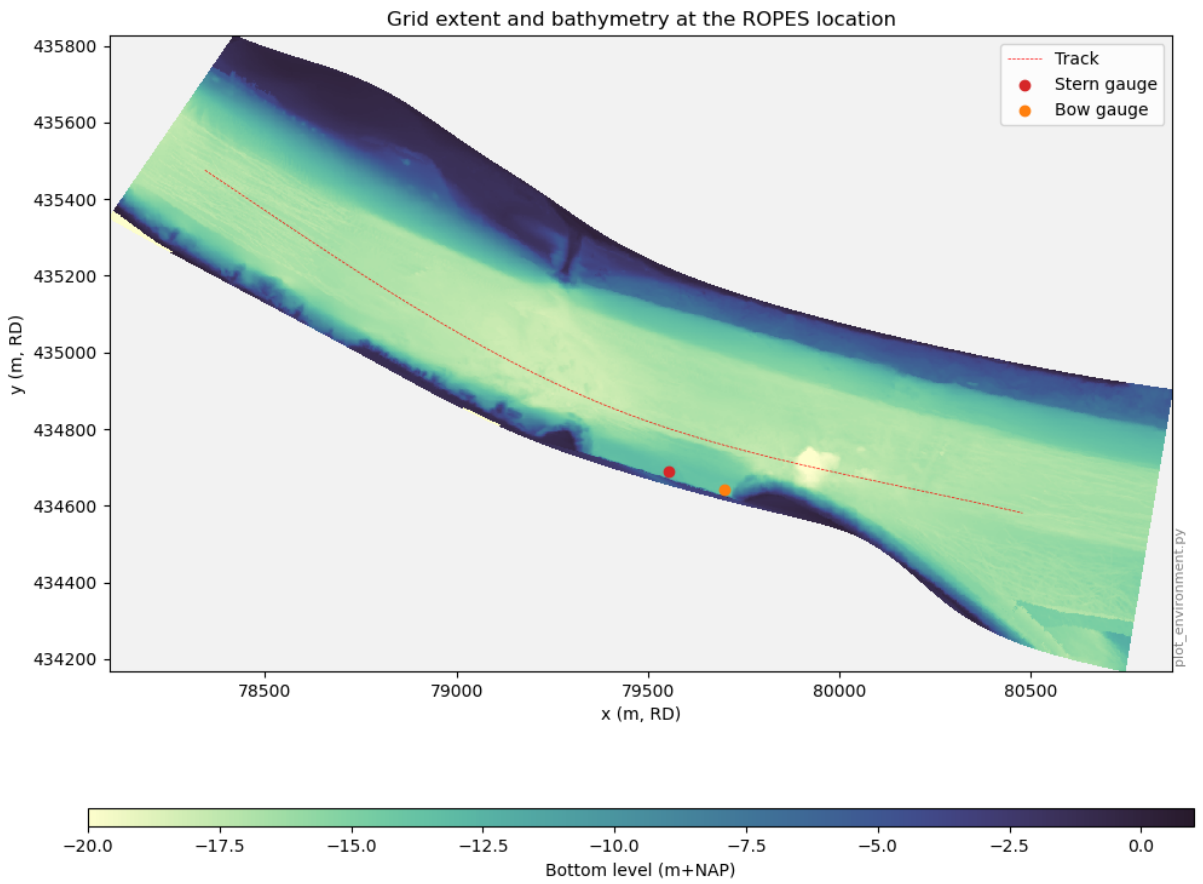


Figure 5.5: Bathymetry, ship track and measurement locations for the ROPES simulation

Table 5.1: Simulations done for the ROPES experiment. As visible only simulation 2 ran successfully, so this simulation is used in further analysis.

Simulation	Launch procedure	Simulated time	Run time (h)
1	2	9.54 min.sec	Error
2	1	5.40 min.sec	116
3	1	5.40 min.sec	Error

passes the measurement locations. Pressure grids were defined every 0.75 seconds. Total simulated time was 9 minutes and 53 seconds.

The model described above was ran three times. Two times to simulate both launching procedures as described in Section 4.5.1, both excluding the floating object grid representing the moored ship. Once it was ran with the floating object grid representing the Jaeger Arrow. A summary of the simulations and their different settings can be found in Table 5.1. The SWASH input file used in simulation 1 can be found in Appendix F.

5.2.2 Results

Unfortunately, the first simulation would not get stable for long enough to simulate the full passage. Due to the parallelization, the output stored by SWASH could not be used to analyze the location of the instability. Depending on the location, the solution for the instability would differ. If the instability problems occurred at the bank, the solution would likely be grid refinement. If the instability occurred in the waterway or around the ship, the solution would likely be a change in the numerical scheme. Due to the launching procedure, the second simulation needed less simulated time. However, at the moment the ship passed the measurement locations the disturbances from launching had not clearly separated from the disturbances caused by the ship sailing at a steady speed. As the launch-induced disturbances were mainly visible as long waves, they may influence the primary wave height. The third simulation was included as a ‘best case’ scenario. This simulation included the floating object grid whereas the other simulations did not. If successful, the simulation would provide extra insight into the influence that the moored Jaeger Arrow has on the measurements in the bow gauge. Including the floating object grid made implicit time integration necessary, as it caused pressurized flow under the ship. Unfortunately, setting an implicit time-integration scheme caused the water to disappear from the model after 38 simulated seconds. No useful output was obtained from this simulation. The instabilities of the the first and third simulations mean that the only usable output is from the second simulation. Despite the drawbacks of the large disturbances caused by the launching procedure, the second simulation is used for further analysis.

Figure 5.6 shows a top view of the water level excursions during the passage. Several things are visible here. To start there is the wave field. When looking at the primary and secondary wave components, both seem relatively well estimated. The primary waves form perpendicular to the ship and the secondary waves at an angle. The primary wave-induced depression at the southern bank is caused by the narrowing of the channel cross-section at the end of the quay. Less positive is the formation of the ring-shaped waves along the track behind the ship. These waves could be an indication of a too coarse resolution, as they also formed during the test runs with a coarser resolution in Chapter 4. In reality, the waves along the track of the ship would be dampened by propeller-induced turbulence. Finally, just west of the stern gauge, some reflections of the secondary waves on the quay are visible.

The water level signals from the measurement points are presented in Figure 5.7. Besides the primary and secondary ship waves that are in line with the typical signal as presented in Figure 1.3, also some noise and long wave components are visible. The noise is probably caused by wind, while the long wave components may be artefacts of waves generated elsewhere and propagating along the canal. It should be noted that in the simulation, the ship moored to the quay was not present. With the passing ship sailing west to east, the bow gauge is likely to be much influenced by the moored ship as it is ‘behind’ the ship. The results of this influence will be visible after the ship has passed, so from around 10:58:10. Likely, the flow effects from the primary wave can still be visible to some extent as the return flow can form under the ship. The secondary waves will reflect on the hull sides will therefore experience more influence from the moored ship. The figures confirm this. At the bow gauge, no secondary wave is present while at the stern gauge there is. The primary wave is visible at both gauges. Due to the influence of the moored ship on the bow gauge, the stern gauge will be used for determination of the wave characteristics. Next to the primary wave of the studied passage, some other long waves are visible. These can be caused

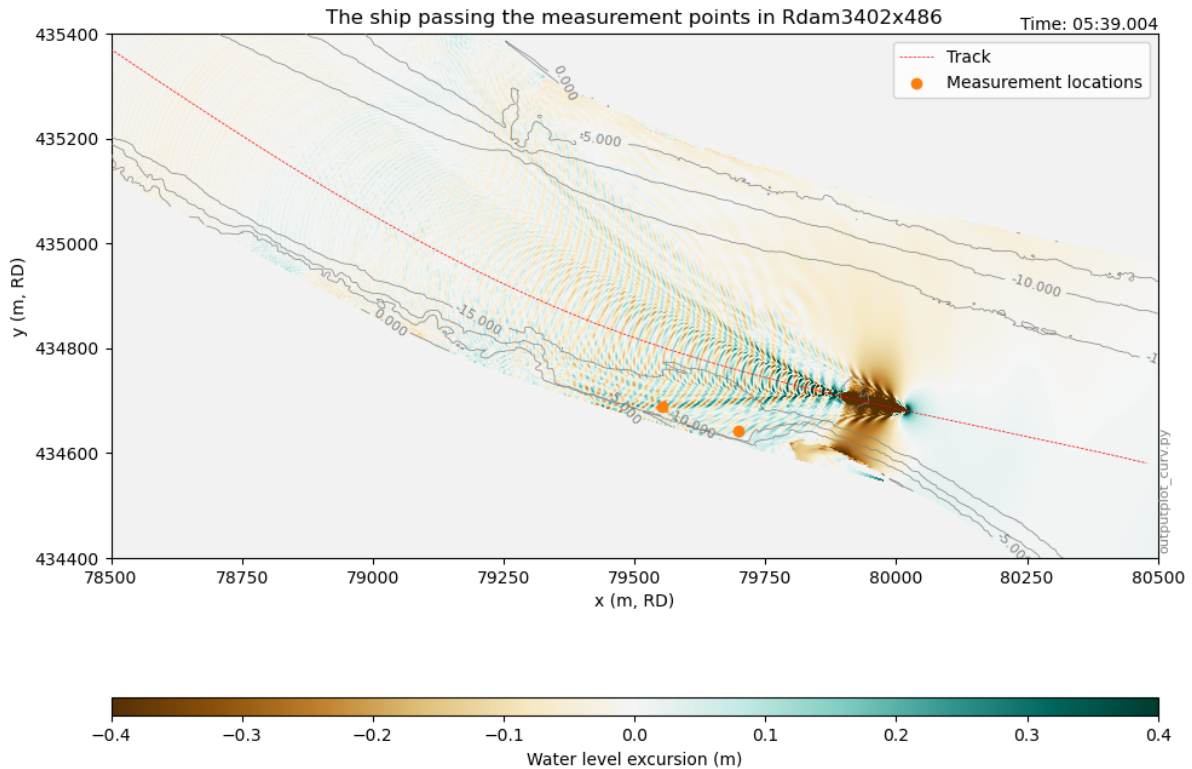


Figure 5.6: Water level excursions as modelled in the ROPES passage. When looking at the wave fields, both primary and secondary waves look to be modelled well. Behind the ship, the ring-waves that show up during simulations with a too low resolution are visible.

by sources further away from the quay, but the exact source cannot be determined from the data or the data report. Luckily for the analysis, the extra long wave components are smaller than the primary wave depression. Therefore, the signal analysis will not base the primary wave characteristic on these artifact waves.

In the stern gauge signal (Figure 5.7 b), primary and secondary wave components are distinguishable. Up till 10:57:10, there is a clear difference between the measured and simulated signal. The measured signal shows the long waves discussed earlier, while the SWASH signal shows a consistent elevation above SWL. The combination of the launching procedure and the lack of propeller jet are a likely cause for this elevation. The launching procedure will create a long wave in front of the ship. As discussed in the literature, the lack of a propeller causes the water level in front of the ship to be elevated so that the necessary return flow can form. Ideally, the time between launching and sailing past the measurement location would have been larger, so that the wave from the launching procedure would have passed before the primary bow wave arrives. However, due to the instabilities no statements can be done on a sufficient distance between launching and measurement points. In the measurement signal, the additional long wave components interfere with the primary bow wave. From 10:57:20, the primary wave as measured properly coincides with the primary wave as simulated.

The secondary waves are visible in the stern gauge signal from 10:58:00. Here, the consistent wave train of increasing and decreasing wave heights as described in literature (see Section 1.1.5) is not clearly visible. A likely cause for this is the reflection of the secondary waves against the quay wall. Reflection of the secondary waves occurs more commonly, see for example Figure 5.1, frame 3. Because the measurement points are close to the quay, the wave train will not have passed the measurement point when the reflection from the quay reaches it. Therefore, there is interference of secondary waves and reflected secondary waves.

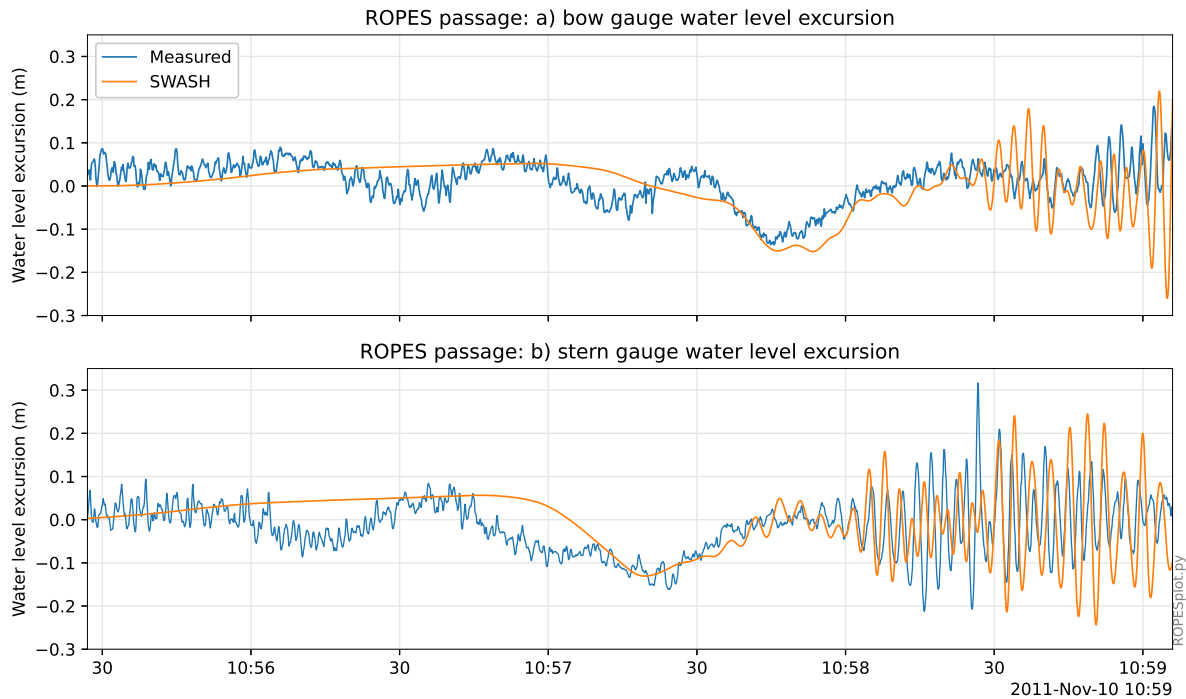


Figure 5.7: Water level excursions in the measurement gauges for ROPES run 902. The time axis alternately hours:minutes or seconds.

The characteristics of the waves in this passage are found in Figure 5.8. Looking at the figure, SWASH seems to underestimate the secondary wave height. This is not in line with observations done earlier regarding the resolution of the model, where SWASH would overestimate secondary wave height at a coarse resolution. However, one could also argue that the measured secondary wave height is due to an outlier being classified as a secondary wave. At 10:58:25, the secondary wave signal in the measurements shows a large peak. In the signal analysis process, this peak is taken as the secondary wave height. However, in this case, the peak could also be caused by interference between the secondary wave and its reflection. Usually, the peak is part of a clear train with increasing and decreasing wave heights around the peak. That is not the case here. The train is not leading up to the height of this peak. If this peak is taken out of the signal analysis, the maximum secondary wave height becomes 0.19 m. Then SWASH would overestimate the secondary wave height which is expected if the resolution of the model is too coarse.

Moving on to the next characteristics, we see that the primary water level depression is estimated well. SWASH is off by 5%. The slight underestimation is in line with expectations. The SWASH model does not take propeller effects into account while in the measurements the ship was likely sailing using its propeller. As the propeller increases primary water level depression, SWASH is expected to underestimate the effect (see Section 1.1.4).

The third characteristic is the primary stern wave. In SWASH, the primary stern wave height is underestimated by 54%. For the purpose of overtopping, underestimating the stern wave height is not ideal, as the stern wave can have a large influence on the overtopping flow characteristics if it coincides with the secondary waves at the bank. The underestimation of the secondary wave can have several reasons. First is the ship model. It is known that the shape of the stern of the passing ship influences the stern wave height. As the ship model is taken from the database it may not be the same shape as the ship that passed during the measurements. The solution to these underestimations may be to use a bit larger and bulkier ship model in the simulations. The size increases the primary wave effects, and the bulkiness of the ship increases secondary wave effects.

Finally, it should be noted that in the SWASH model, tidal flows were not taken into account. This was done to for the simplicity of the model. According to the tide table for the nearby Maassluis Watersportalmanak.nl (2011), there was a flow of 0.71 m/s against the direction of the ship at the moment of measurement. An ebb flow in the opposite direction of the ship would increase its speed through the water and therefore the magnitudes of the wave components. This lack of flow may be another cause

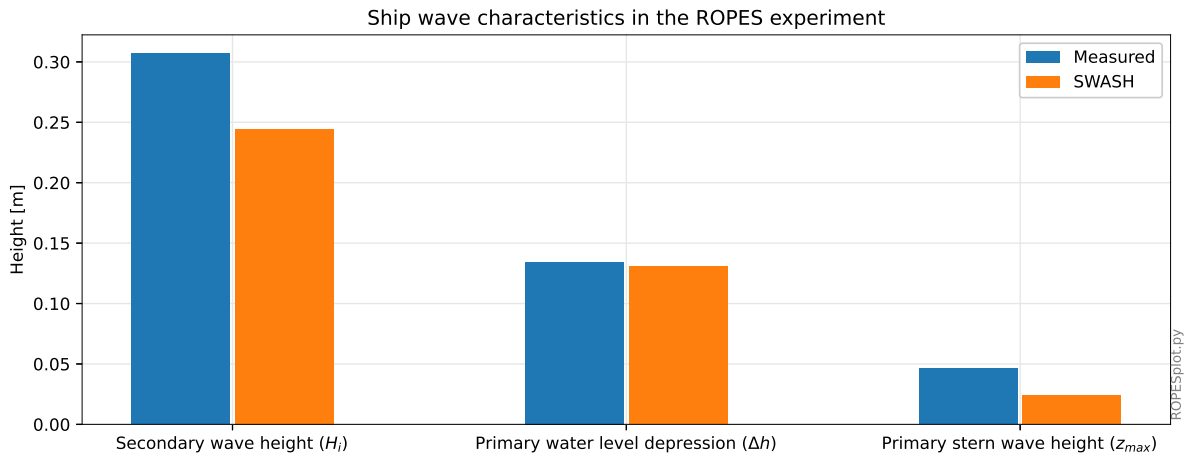


Figure 5.8: Ship wave characteristics at the stern of the Jaeger Arrow for ROPES run 902. The differences between measurements and SWASH will be discussed in the text.

for the underestimation of secondary wave height and primary stern wave height but it is not clear what exactly the effects of this flow are. In future research, it would be useful to study the effects of tidal or river flows on the ship-induced water motions as modelled in SWASH.

Overall, it can be said that SWASH is able to reproduce the ROPES measurements relatively well. Despite the launching procedure causing disturbances, the modelled wave signal resembles the measured wave signal relatively well. Reflection effects may have had an influence on the secondary wave height. The primary wave is estimated almost exactly correct, both in the wave signals as in the magnitude. The underestimation of the primary stern wave leads to questions for further research.

5.3 Bath measurements

The second full-scale validation case is the recreation of measurements done near Bath. The data set is described in section 3.2. Figure 3.4 displays the location of the measurements. The procedure for model setup and results presentation is described in section 3.4.

5.3.1 Model setup

The grid for this simulation consisted of 1701x486 cells. The size distribution of these cells can be found in Figure 5.9. The median dimensions of 1.5x1.7m, in combination with a secondary wave length of 24.5 meter gives a resolution of 14.4 CPW. Which should be sufficient for reliable results (section 4.6.1).

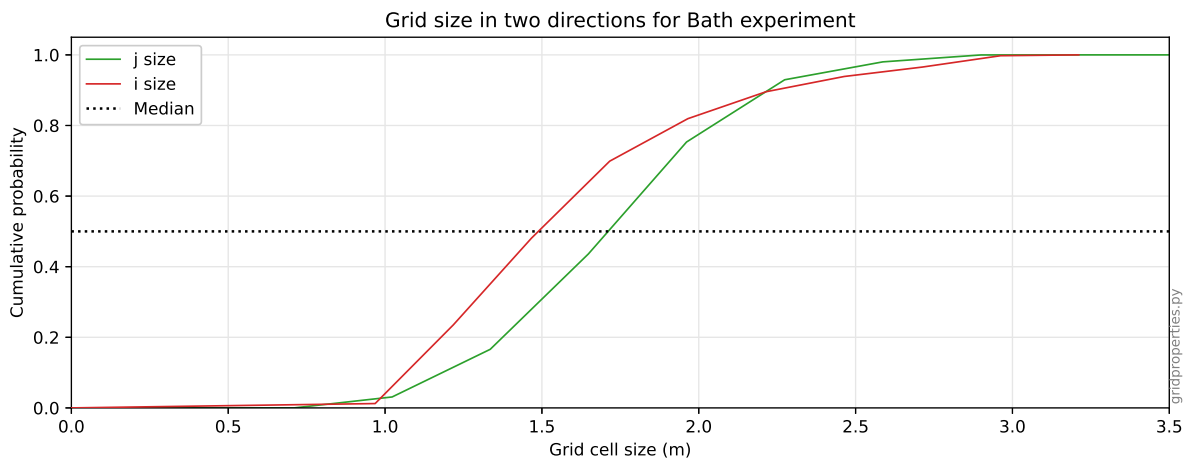


Figure 5.9: Cumulative grid cell size distribution for the simulation done at Bath.

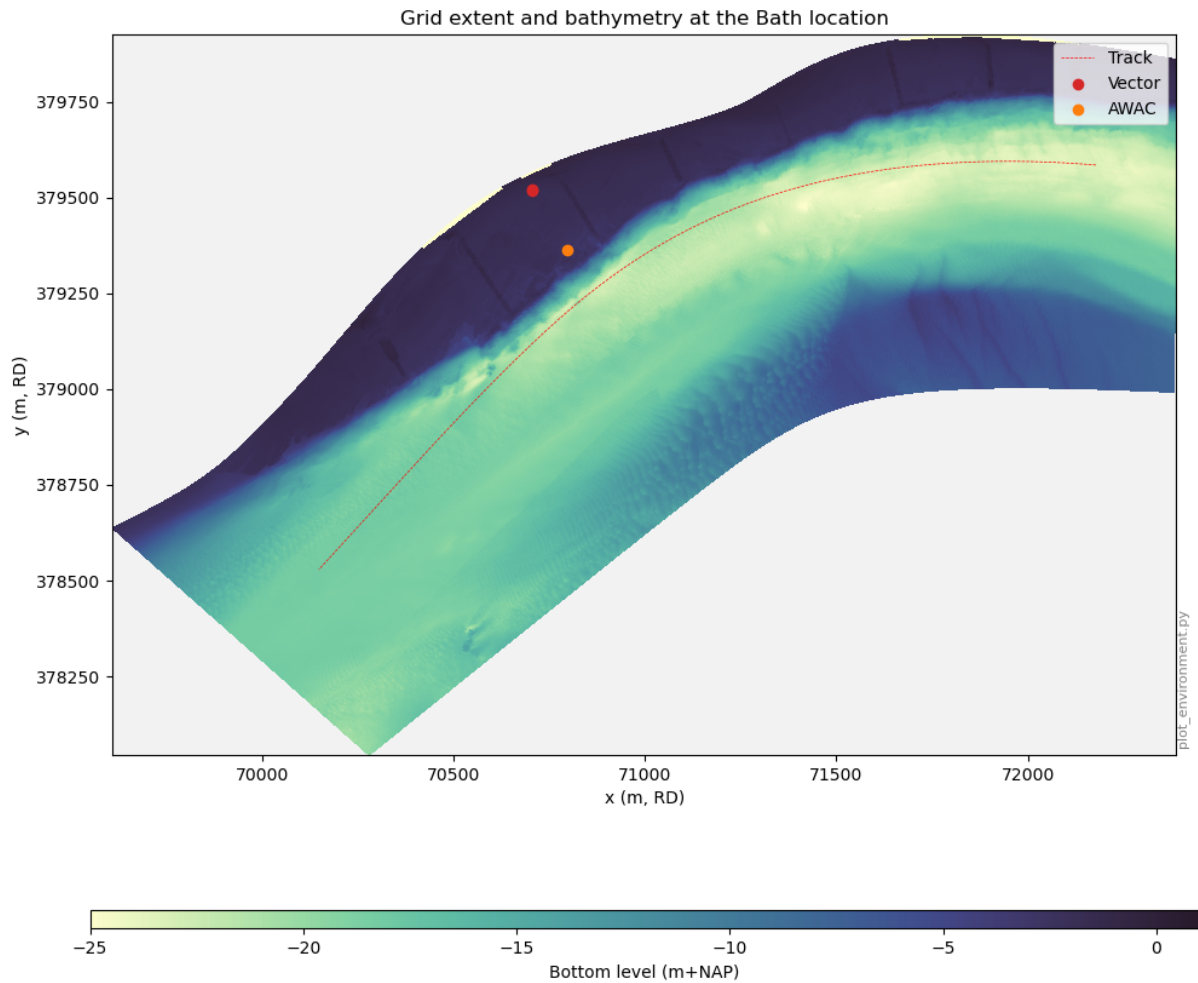


Figure 5.10: An overview of the Bathymetry, ship track and measurement locations for the Bath measurement. The measurement location close to the channel is the location of the AWAC. The measurement location further on the bank is the location of the Vector.

However, this wavelength is calculated next to the ship. On the banks, bottom effects can cause the waves to get shorter, decreasing the number of cells per wave length.

The ship model is selected based on the ship dimensions from the measurement data description. From the Arcadis ship database, the model without a bulb that most closely resembled the 'Margrit Rickmers' was selected. The procedure for creating the track can be found in section 3.4.2. An overview of the model setup is presented in Figure 5.10. The model was ran two times, to simulate both launching procedures described in section 4.5.1. The settings are summarized in Table 5.2. The SWASH input file used for simulation 1 can be found in Appendix G.

5.3.2 Results

Of the two simulations described above, second simulation needed less simulated time than the first and therefore took a shorter period to run. However, at the moment the ship passed the measurement loca-

Table 5.2: Simulations done for the Bath experiment

Simulation	Launch procedure	Simulated time	Run time (h)
1	2	8.50 min.sec	65.7
2	1	4.40 min.sec	34.2

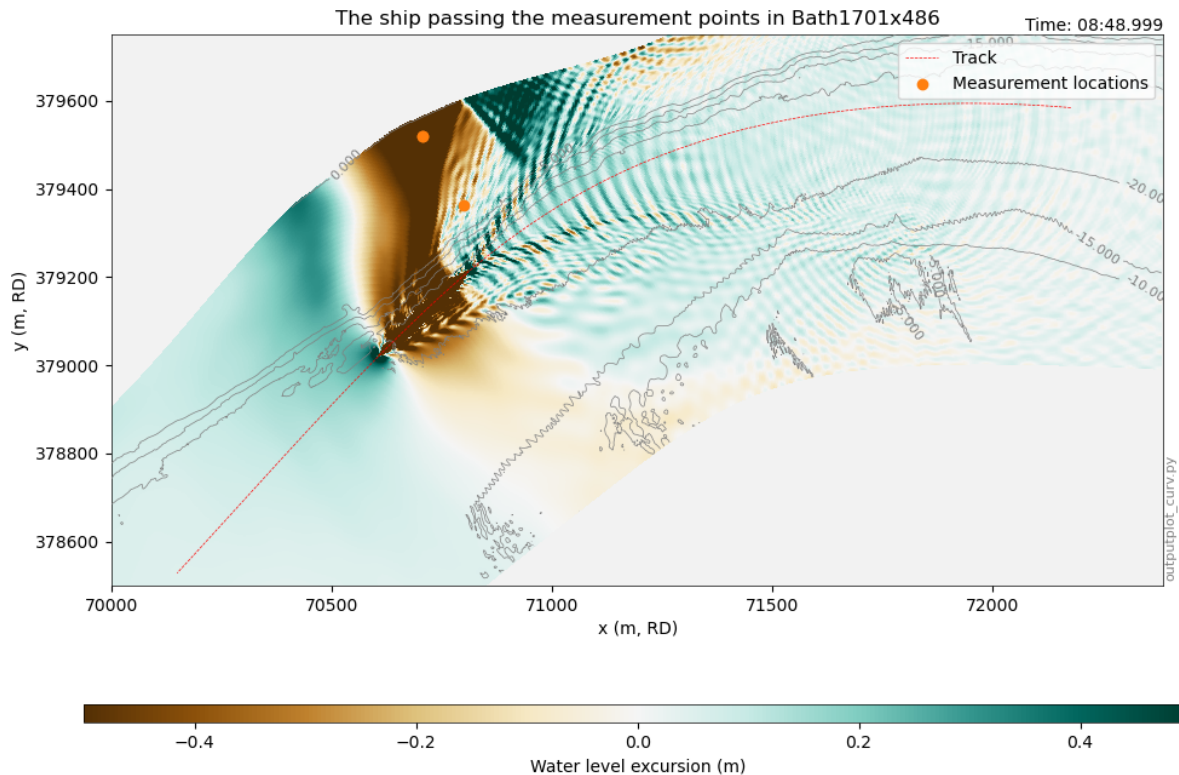


Figure 5.11: A visualisation of the water level excursion as modelled in the Bath passage. Visible is that in the channel, the dispersion of the primary and secondary waves is modelled well. On the banks, the lower water depth decreases wavelength and therefore also decreases the dispersive accuracy of the SWASH model.

tions it was not completely clear that the model had already reached a steady state. The first simulation was therefore selected for analysis.

Figure 5.11 shows a top view of water level excursion during the passage. From this figure, several observations can be made. On the south side of the ship, the primary and secondary wave fields look as expected: the primary wave propagating along the ship in the channel and the secondary waves dispersing from the bow and stern of the ship. Also, the water level difference between the area in front of the ship and behind the ship is as expected. As also noted in the literature, the lack of a propeller causes a small water level difference between the area in front of the ship and the area behind the ship so that the necessary return flow can form. Along the northern bank an exceptionally deep water level depression forms, followed by a high stern wave. The magnitude of the depression may be explained by several effects. First is that a bore forms on the bank. This bore has been observed for several passages during the measurements Huisman et al. (2010). The steep front is well visible behind the depression as it returns to 0 m+SWL in a very short distance. The second possible contributor is the boundary of the model. As the bathymetric data was only available for a short distance shoreward of the measurement location, the boundary of the model was chosen relatively close to the measurement point. At the north boundary, the bottom level was at 0 m+NAP and the SWL at 3.03 m+NAP. This created an open boundary on which a Sommerfeld radiation condition was applied to radiate away the long waves. Initially, this was expected to represent a proper open boundary. However, it is possible that the boundary still influences the water movements. The final observation concerns the secondary waves. The secondary stern waves look realistic. The secondary bow waves in the depression area look realistic as well. However, further on the bank the secondary waves look to be gone. This can be either caused by the bore and the flow effects around the bore, or the disappearance of the secondary waves can be caused by their decreasing length causing a lowered CPW value. As observed in section 4.6.1, a too low CPW value causes excessive decay of the secondary waves. The exact influence of both effects remains unknown. An interesting follow-up simulation would be to extend the grid further shoreward and increase the resolution on the bank.

Further analysis of the wave signal can be done by comparing the SWASH generated signal with the

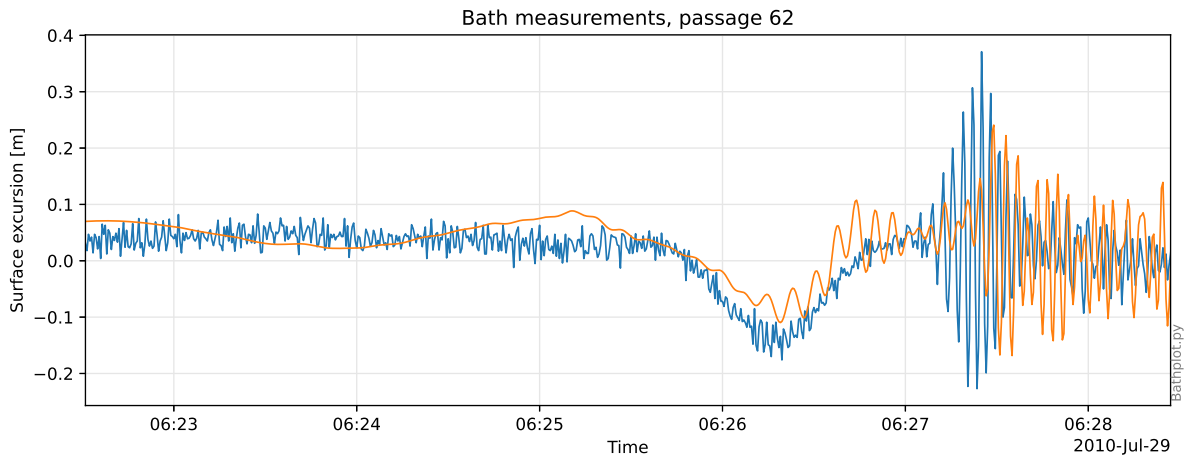


Figure 5.12: Water level signal in the location of the AWAC as measured and modelled by SWASH. Visible is that SWASH underestimates the water level depression. This can be caused by the lack of propeller influence in the SWASH model. The delay of the secondary wave can be caused by a too coarse resolution of the model. This explanation is supported by the noise behind the ship which is visible in all SWASH models with a coarse resolution. The secondary wave height is lower than measured. This can be due to a number of reasons. For example the shape of the bow as the real ship has a bulb while the ship in the model does not, but interference with the wind waves can also play a role.

water levels measured at the AWAC. Both signals are displayed in Figure 5.12. Chronologically, the first observation is before the start of the primary wave. Up till 06:25:40, the measured signal shows only background noise caused by the wind waves. The SWASH signal shows two long waves. The first wave, up till 06:24:00, the wave is caused by the launching procedure. The second long wave, after 06:24:00, the wave is caused by the water level difference necessary to generate the return current. With no propeller implemented in the model, a water level difference between the front and the back of the ship is necessary to generate the return current. At 06:25:40, the primary wave starts. In both the SWASH model and the measurements, the primary wave has the shape of a far-field primary wave. The measured primary wave is a little deeper than the primary wave as created by SWASH. This can be caused by either differences between the real ship and the ship model, or the estimated ship track being further away from the measurement location than the real ship track, or a combination of both. After the deepest point in the primary wave, the SWASH model shows some relatively long oscillations that were not present during the measurements. Starting at 06:27:00, the secondary wave field becomes visible. A few things are noted here. First is that in SWASH, the secondary waves are delayed compared to the measurements. In chapter 4, this has been shown to be the case for a too coarse resolution, but it can also be caused by the real track of the ship being further from the measurement location than the estimated track. Secondly, the secondary wave field is lower in SWASH, and that it not as clearly one wave group as it is in the measurements. A possible explanation for possible reflection of the secondary waves on the boundary that is not there in reality.

From the wave signals, the wave characteristics can be extracted using the process as described in Appendix A. The resulting wave characteristics can be found in Figure 5.13. The characteristics will be described in the order that they are presented in the figure. First is the secondary wave height. For the underestimation of the secondary wave, several factors can be at play. As noted above, the underestimation of the secondary wave height can be caused by a too coarse resolution of the model. As seen in Chapter 4, a too coarse resolution causes an overestimation of secondary wave decay. The relatively large distance between the AWAC and the ship (122 m) can cause an initial overestimation of the secondary wave but an underestimation at larger distances. Another possible cause of this underestimation can be the difference in bow shape between the SWASH model and the measurements. The SWASH model uses a ship model without a bulb. As a bulb is mostly optimized for deep-water sailing, the secondary wave height may be higher than for a model without a bulb like in the SWASH model. The second characteristic in the figure is the primary wave height. Here, the resolution or the bow shape is unlikely to be the case of the underestimation. More likely is that the uncertainty in the track of the ship is a big factor in the difference between observed and modelled primary water level. As the track is based on general observations from literature and the wave signal, the error in the track could be relatively large. If the modelled track is further away from the measurement location than the secondary waves will be delayed and the primary wave will be underestimated, both of which are visible

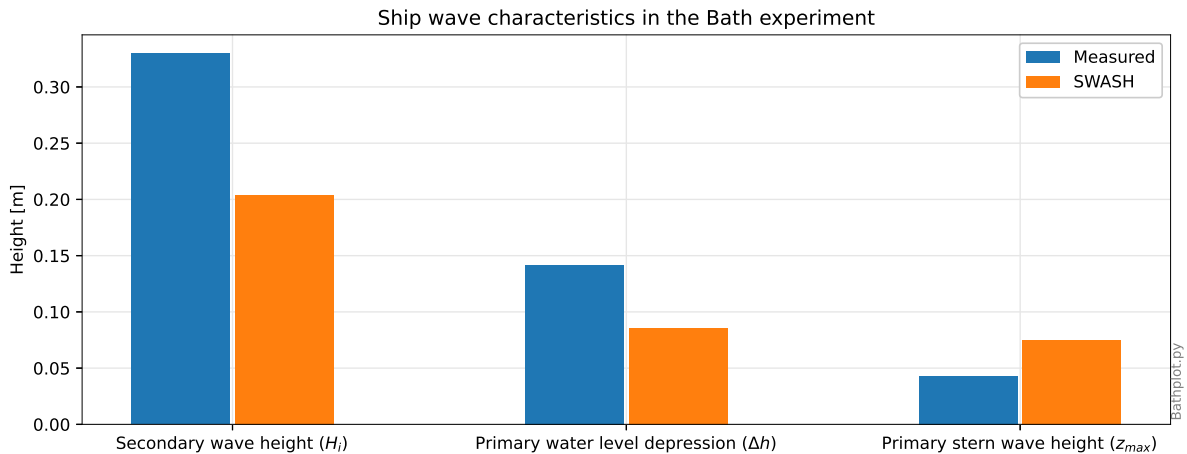


Figure 5.13: Characteristics of the ship wave components for the Bath experiment. Visible is that SWASH underestimates secondary wave height and primary water level depression. Primary stern wave height is overestimated.

in the wave signal and characteristics. Additional possibly influential factors are the propeller effects and tidal flows, but for this case these factors are expected to be of minor influence. The propeller influence diminishes as distance between measurement location and ship increases. Here the ship is relatively far away from the measurement locations. Tidal flow speed was registered at 0.15 m/s at the AWAC at the moment of the passage which is relatively little in comparison to the ship speed of 7.56 m/s. The last characteristic is the primary stern wave. The stern wave is overestimated by 50%. In combination with the underestimated primary wave this is an interesting observation. It is not fully clear what could cause the overestimation.

Aside from the three results presented for all measurements (top view, water level signal and wave characteristics), also the flow velocities at the bottom have been measured for the Bath simulation. As flow velocities are also modelled in SWASH, the results from the simulation can be compared to measurements. If SWASH correctly estimates these velocities, this is further proof for the correctness of the mechanics in the SWASH model. Figure 5.14 shows a comparison between measured and modelled flow velocities in u - and v -directions. The coordinate system here is bound to the channel and rotated by 32° anti-clockwise to the Cartesian coordinate system. The positive u -direction is eastward parallel to the channel. The positive v direction is perpendicular away from the channel. From SWASH, the output was taken at the center of the bottom layer. In the u -direction, parallel to the boundary, SWASH captures the shape of the signal in both AWAC and Vector. In the AWAC, SWASH misses the noise that is probably caused by non-ship-induced waves. In the Vector, SWASH has a too long period of high velocity. It also overlooks the secondary waves. In the v -direction, SWASH captures the essence of the signal but with the wrong sign. It is unknown if this is because of a wrongly understood coordinate system or because of differing flow effects. Overall, there may be two factors that have a large influence on the differences between the measurements and SWASH. First, is the boundary being close to the vector. If flow over the boundaries is not exactly representing reality, the boundary can influence the flow direction in the Vector. SWASH being unable to represent flow in the v -direction (perpendicular to the boundary), this may be an indication that the boundary influences the flow effects at the measurement location. The second is the unequal layer distribution. In the model, the vertical layers are distributed non-equidistantly. From top to bottom, the four layers make up respectively 10, 20, 30 and 40 percent of the water column. This means that the bottom layer is 40% of the total water column height. This coarser resolution can create inaccuracies in the flow effects near the bottom, as the model behaves more like a depth-averaged model here. With only one simulation done, it is not clear what the main causes of the shortcomings of SWASH are. Interesting follow-up simulations if the computational time could be increased would be simulations with the model boundary further shoreward and an increased number of layers near the bottom.

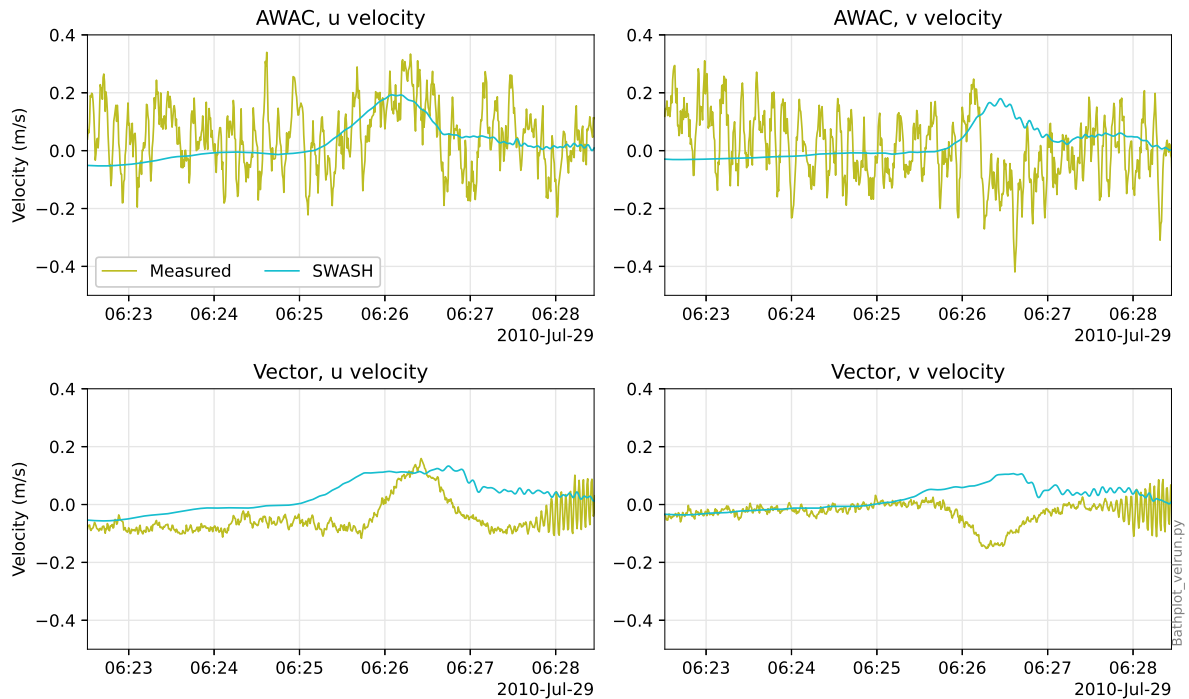


Figure 5.14: The flow velocities as measured by the AWAC and the Vector in the Bath passage. The coordinate system is bound to the channel. The positive u direction is parallel to the channel aiming east, the positive v direction perpendicular away from the channel. For SWASH, the average velocity in the bottom 40% of the water column is displayed. For the measurements, the velocity is measured close to the bottom. Visible is that SWASH captures the shape of the signal in the u direction, but not in the v direction.

5.4 Validation to analytical results

Up till now, the outcomes of SWASH has been compared to measurement results. This gave insight in the ability of SWASH to reproduce these measurement signals. But how well does SWASH perform when compared to existing calculation methods? To gain insight into the answer to this question, the passages that are simulated in SWASH are recreated using two methods: DIPRO+ (Waterloopkundig Laboratorium, 1997) and the BAW code of practice (BAW, 2010). Per passage, the input in DIPRO+ will be discussed followed by the input in the BAW guidelines. Finally, the magnitudes of the components will be discussed.

5.4.1 MASHCON

To recreate the MASHCON experiment in SWASH, some assumptions needed to be done. Firstly due to the scaling in the Lataire et al. (2009) experiments. Due to length and ship power errors, it was necessary to scale the experiment from 1/80 to 1/2. It was not possible to recreate the experiment in full-scale as DIPRO+ limitations wouldn't allow a calculation for such a waterway and ship size. Scaling was done using Froude scaling, so that the ship sails at the same Froude number in the DIPRO+ calculations as it does in the other calculations. The result is that all dimensions increased by a factor 40, while the vessel speed increased by a factor $\sqrt{40}$. After calculation, the results were scaled back to the experiment scale. DIPRO indicated that the vessel speed exceeded the valid formula limits. Further, DIPRO+ is based on measurements done where vessel length is larger than canal width, which isn't the case in the recreated experiment. Because of this, the outcomes of DIPRO+ are also outside of the range for which it was validated. It has before been shown that DIPRO+ is less accurate outside of its range of validity Verheij and van Prooijen (2007).

In the BAW guidelines, the main input characteristic is the schematization of the waterway. Here, the waterway is schematized as a rectangular profile having the same cross-sectional area as the real towing tank. For the uncertainty range, wave height coefficient A_W is chosen as its minimum and maximum value. The same is done for the stern wave influence factor C_h .

For Lataire et al. (2009), Experiment F, the calculated characteristics are given in Table 5.3 and visu-

Table 5.3: Ship wave characteristics in Lataire et al. (2009) Experiment F, as calculated by the different calculation methods.

Simulation	H_i	Δh	z_{max}
Measured	0.0052	0.0073	0.0009
SWASH, 5 CPM	0.0131	0.0077	0.0016
SWASH, 13 CPM	0.0055	0.0077	0.0021
DIPRO+	0.0335	0.0162	0.0162
BAW	0.0112	0.0153	0.0301

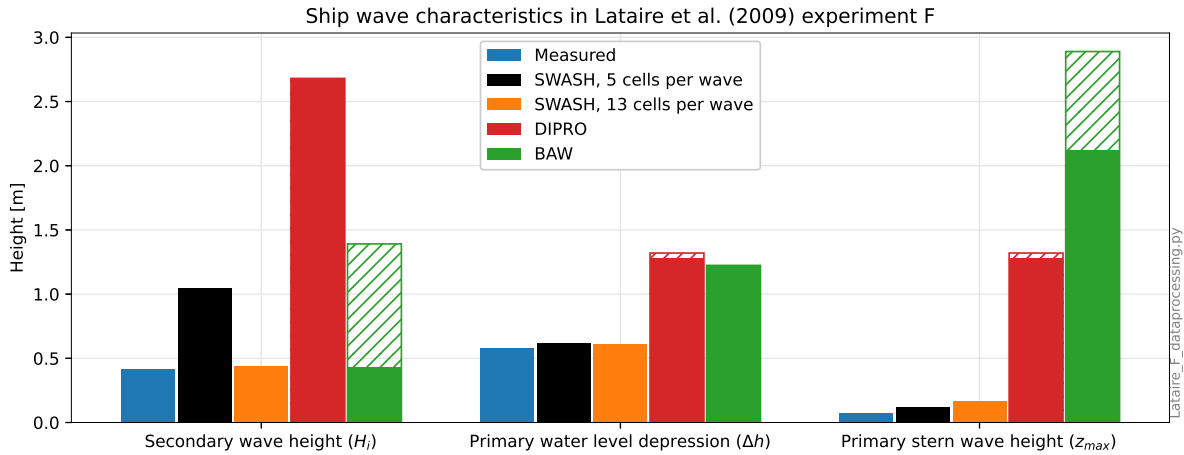


Figure 5.15: Comparison between the measured wave characteristics and the characteristics calculated by different methods for Lataire et al. (2009), experiment F.

alised on prototype scale in Figure 5.15. As visible, with both resolutions SWASH outperforms DIPRO+ and the BAW guidelines for estimating all tested wave characteristics. For the secondary wave height, SWASH performs best with the 13 CPW resolution. This resolution is on par with the estimation done with the BAW guidelines. However, the BAW guidelines see a large uncertainty due to coefficients that need to be chosen by the designer. Regarding the primary water level depression, SWASH gives a good result for both resolutions. The results from DIPRO+ and the BAW guidelines are comparable. This is expected as the formulations in both guidelines are both based on Schijf (1949). Regarding the primary stern wave, SWASH overestimates the magnitude but both DIPRO+ and the BAW guidelines show an overestimation far larger than the overestimation by SWASH. SWASH is therefore the best performing calculation method for this characteristic. For DIPRO+, the difference between measurements and calculated outcomes is expected as the geometry in the experiment is outside of the range of validity. However, no alternative is available that does encompass this geometry. The visible uncertainty is caused by variation in the mid-ship block-coefficient. The BAW guidelines indicate that the 2.5 m stern wave is unrealistically high. However, no alternative is offered to improve the estimation. The uncertainty is caused by variation in the wave height coefficient (A_W) and the ship-type influence factor (C_H).

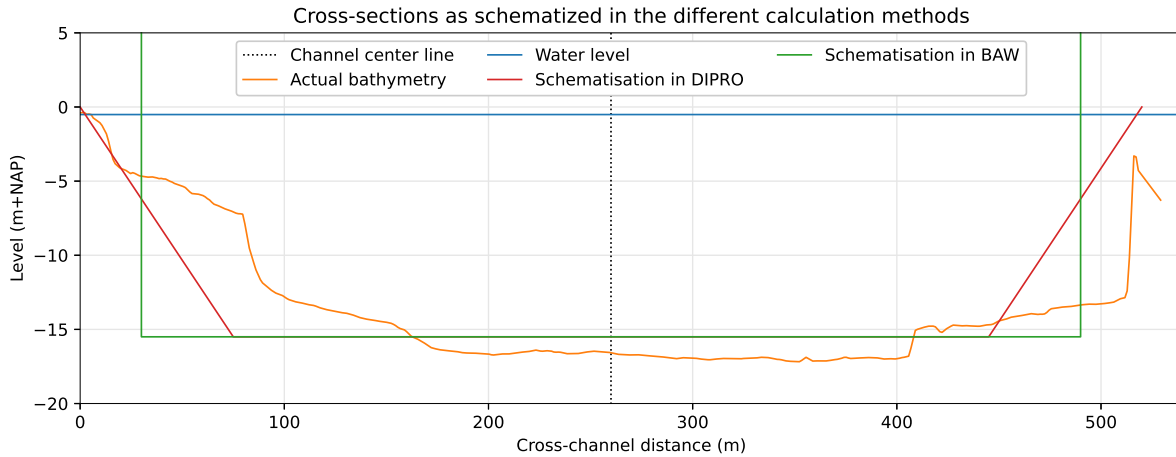


Figure 5.16: The cross-sections of the ROPES geometry as used in the different calculation methods. In the case of DIPRO+, the displayed cross-section represents the average cross section.

Table 5.4: Ship wave characteristics in the ROPES passage, as calculated by the different calculation methods. The values presented here are the average values between favourable and conservative estimates.

Simulation	H_i	Δh	z_{max}
Measured	0.307	0.134	0.046
SWASH	0.245	0.131	0.024
DIPRO+	1.990	1.320	1.320
BAW	0.592	0.444	0.319

5.4.2 ROPES

For the ROPES experiment, the first relevant outcome of the calculation process is the cross-section chosen to schematize the actual geometry. The chosen cross-sections are displayed in Figure 5.16.

In DIPRO+, the software indicates that the calculation is outside of the range of validity for waterway geometry, vessel size and vessel speed. For an uncertainty estimate, the waterway is schematized as a trapezoid that exactly surrounds the actual geometry as well as a trapezoid that fits just inside the actual geometry. Also, the ship is schematized as having a mid-ship block-coefficient C_M of 0.8 and 0.9.

In the BAW guidelines, the same process is used for the waterway. Both a schematized geometry exactly surrounding the actual geometry as well as a schematized geometry fitting just inside the actual geometry have been used. Further, the ship-influence factor f_b has been varied between its minimum value of 1.5 and its maximum value of 3.0. Finally, the ship-type influence factor C_H has been varied between its minimum value of 1.1 and its maximum value of 1.5.

For the ROPES passage, the outcomes of the different calculation methods are given in Table 5.4 and Figure 5.17. Visible is again that SWASH outperforms both DIPRO+ and the BAW guidelines. For DIPRO+, this is in line with expectations as the passage is outside of the validity limits for DIPRO+ on geometry dimensions, ship dimensions and ship speed. For both guidelines, one or more wave components are above the maximum realistic ship wave heights as given by ENW (2007). Here, a height of 1m for all components is given as exceptional height. The calculated outcomes are therefore deemed unreliable. Visible is also that with favorable input, the BAW guidelines are able to estimate the magnitude of secondary wave height and primary water level depression accurately. For the primary stern wave height, DIPRO+ performs better than the BAW guidelines. However, the uncertainty is still large. In the DIPRO+ results, the uncertainty is mainly caused by the different geometry schematizations. In the BAW guidelines, uncertainty is mainly caused by the range in the coefficients.

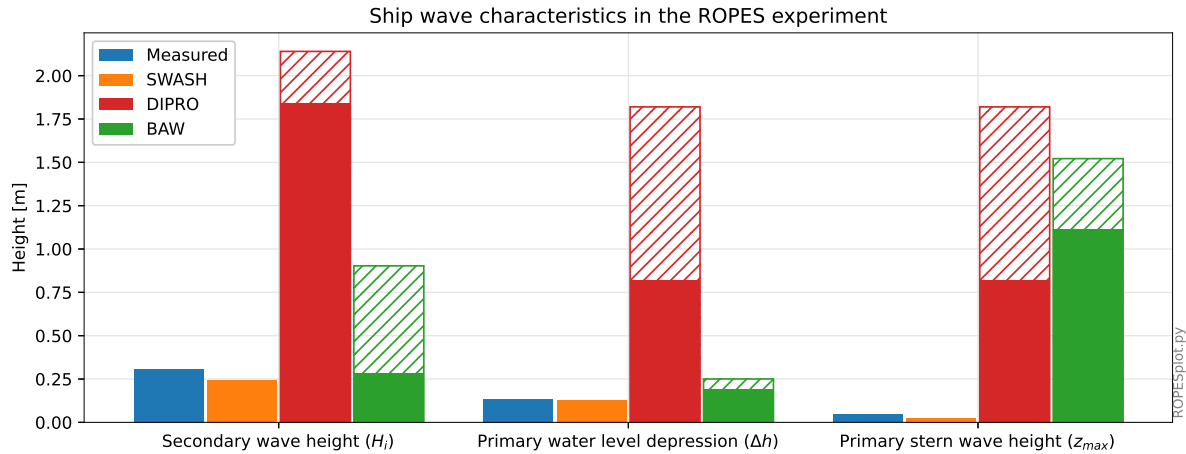


Figure 5.17: Comparison between the measured wave characteristics and the characteristics calculated by different methods in the ROPES passage. As the channel geometry and ship characteristics need to be simplified, some uncertainty exists in the DIPRO and BAW calculations. In this figure, the filled part of the bars represents the most favourable input. The striped part of the bars represents the uncertainty range.

5.4.3 Bath

For the Bath experiment, the first relevant outcome of the calculation process is the cross-section chosen to schematize the actual geometry. The chosen cross-sections are displayed in Figure 5.18. Visible is that the cross-sections in DIPRO+ and the BAW guidelines represent mostly the main channel. The distance between the ship and the bank edge is kept constant in all simulations.

In DIPRO+, the software indicates that the calculation is outside of the range of validity for waterway geometry, vessel size and vessel speed. For an uncertainty estimate, the waterway is schematized as a trapezoid that exactly surrounds the actual geometry as well as a trapezoid that fits just inside the actual geometry. Also, the ship is schematized as having a mid-ship block-coefficient C_M of 0.8 and 0.9.

In the BAW guidelines, the same process is used for the waterway. Both a schematized geometry exactly surrounding the actual geometry as well as a schematized geometry fitting just inside the actual geometry have been used. Further, the ship-influence factor f_b has been varied between its minimum value of 1.5 and its maximum value of 3.0. Finally, the ship-type influence factor C_H has been varied between its minimum value of 1.1 and its maximum value of 1.5.

The outcomes of the different calculation methods are given in Tabel 5.5 and Figure 5.19. Here, the trends are largely the same as for the ROPES passage. From all calculation methods, SWASH shows the best performance. DIPRO+ and the BAW guidelines overestimate all wave components. In line with the ROPES passage, the wave components as estimated by DIPRO+ and the BAW guidelines exceed the ENW (2007) maximums. For the secondary wave height, BAW performs better than DIPRO+. For the primary water level depression, performance is comparable. For the primary stern wave heighth, DIPRO+ performs better than the BAW guidelines. Uncertainty in the DIPRO+ results is caused by the mid-ship block-coefficient and the waterway geometry. In the BAW guidelines, the uncertainty is caused by the possible coefficients.

Table 5.5: Ship wave characteristics in the Bath passage, as calculated by the different calculation methods. The values presented here are the average values between favourable and conservative estimates.

Simulation	H_i	Δh	z_{max}
Measured	0.329	0.142	0.043
SWASH	0.204	0.086	0.075
DIPRO+	5.065	0.635	0.635
BAW	1.136	0.821	2.522

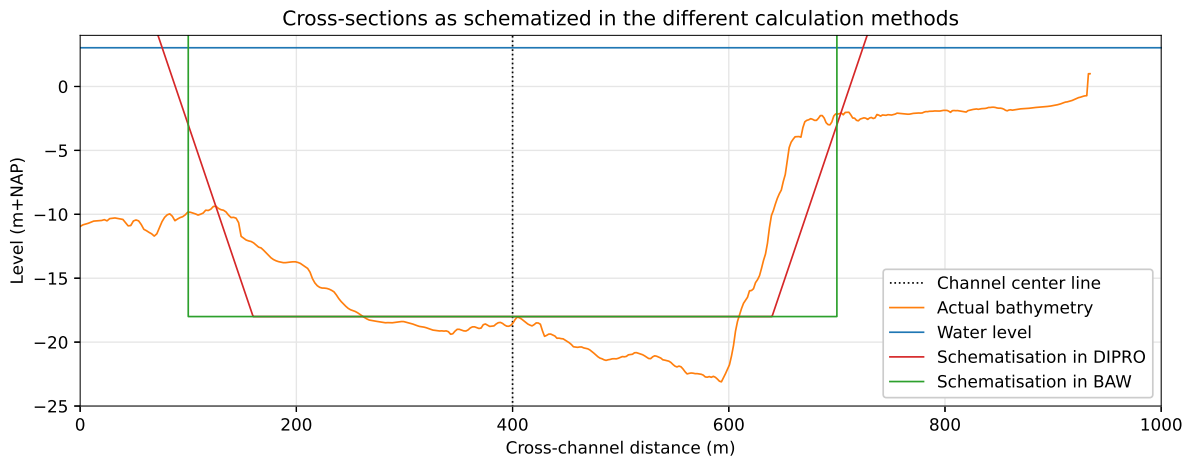


Figure 5.18: The cross-sections as used in the different calculation methods. In the case of DIPRO+, the displayed cross-section represents the average cross section.

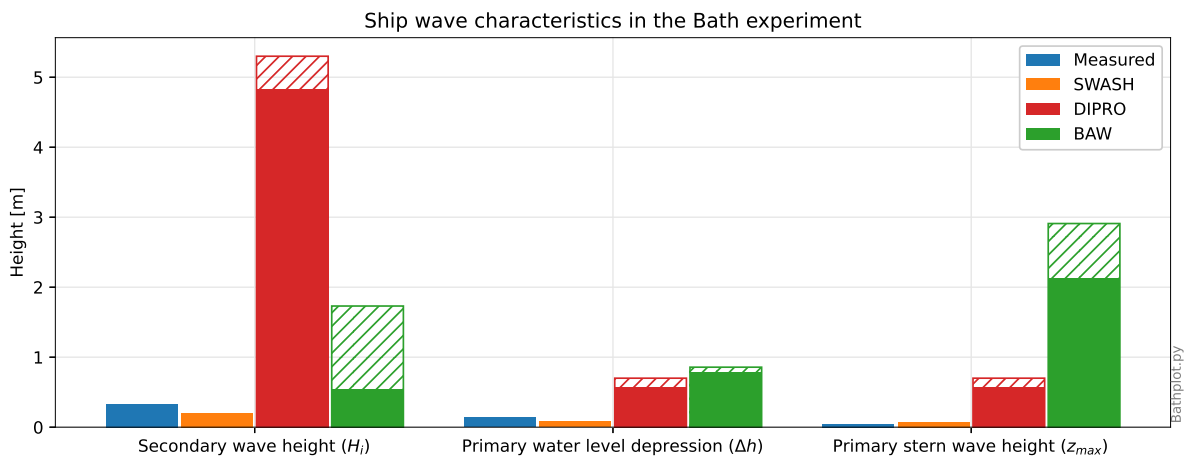


Figure 5.19: Comparison between the measured wave characteristics and the characteristics calculated by different methods in the Bath passage. As the channel geometry and ship characteristics need to be simplified, some uncertainty exists in the DIPRO and BAW calculations. In this figure, the filled part of the bars represents the most favourable input. The striped part of the bars represents the uncertainty range.

5.5 Summary

This chapter studied the validation of the pressure field method as implemented in Chapter 4. For this goal, three passages were recreated in SWASH. The outcomes of SWASH were displayed in three ways: a top view, a plot with the water level at the measurement locations and a comparison of the magnitudes of the components. A comparison with analytical methods gave insight in the performance of SWASH in relation to existing calculation methods.

The top-views showed that SWASH can produce a realistically looking ship-induced wave field in all three simulations. The primary water level depression and secondary waves were generated and propagated as expected.

The gauge-signal plots indicated that SWASH could model the water level signals at the bank relatively well. The shape and magnitude of the modelled primary water level depression resembles that in the measurements. The modelled secondary roughly the same behaviour as in reality. As expected due to the resolution of the model, the modelled secondary waves arrive later than the measured secondary waves and their magnitude is underestimated.

The characteristics plots show that SWASH correctly estimates the relations between the ship wave components relevant for overtopping. However, there can still be a difference between the magnitudes in SWASH and those in the measurements. SWASH does not consistently overestimate the wave characteristics.

Regarding the comparison between SWASH and conventional calculation methods, it is clear that SWASH outperforms both DIPRO+ and the BAW guidelines. This is in line with expectations. For the DIPRO+ and BAW guidelines, a lot of simplifications are necessary. Also, the modelled passages lie outside of the validity range of DIPRO+.

All in all, the validation shows that using SWASH, a considerable improvement over existing calculation methods can be acquired. Not only does SWASH estimate the ship wave characteristics better than conventional calculation methods, it also offers more information and has a wider range of applicability. The accuracy of SWASH seems to be limited by the resolutions used for this research. If more computational time is available, a SWASH model with a finer resolution is likely to produce better results.

The fact that SWASH did not always overestimate ship wave components limits the engineering applicability of SWASH. To develop a true engineering methodology, these uncertainties need to be taken out. Further research can therefore focus on the effects that geometry and ship parameters have on the resulting wave signals and characteristic magnitudes.

6 FIRST STEP TOWARDS MODELLING SHIP-INDUCED OVERTOPPING

As demonstrated before, it is possible to recreate the generation of ship waves in SWASH. However, when creating a model to simulate ship-induced two main issues arise: resolution and stability. This chapter describes a case study that illustrates the resolution problem. Options to overcome this problem are then discussed, and the chapter will be finalized by a summary of the first step towards extending the model to include overtopping.

6.1 Illustrative case study

For illustration of resolution problems when modelling ship-induced overtopping with SWASH, a case study is developed. For the basis of this case, an at-risk area which is easily modelled in SWASH is the most accessible option. As discussed in Chapter 2, the at risk areas are mostly narrow canals and rivers with low-lying quays.

Regarding the geometry to be studied a simple canal geometry is the easiest option. A straight canal would make easy comparison to other calculation methods possible, as well as simple grid designs. Preferably the canal is also deep as this allows higher ship speeds (see Figure 2.3).

The 'Eemskanaal' is a good starting point for geometry design, since it is relatively deep, straight and has a simple geometry. For this illustrative case, the location is chosen near Woltersum, Groningen. Figure 6.1 presents the location on a map.

A representative ship for this geometry is a CEMT class Va as this is the largest inland ship allowed on the main waterway that the Eemskanaal is part of. The dimensions of this ship in loaded condition are 135x11.5x3.5 m LxBxD. The used model is plotted in Figure 6.2. The dimensions of the ship create a blockage ratio of $A_s/A_c = 0.044$, and a limit speed of $V_l = 5.22$ m/s.

Appendix C shows the translation of this canal into a SWASH model with a grid cell size of 0.5m in both x and y direction. A first run was done with a vessel speed of 4.9 m/s, which gives a resolution of CPW = 20.6. This is higher than the resolutions used above. This first simulation clearly shows that for overtopping, the chosen resolution is too coarse. Figure 6.3 shows the minimum and maximum run-up in a test simulation with a uniform resolution of 0.5m per grid cell, and a dike height of 0.3m. As visible, the run-up only floods two cells during the passage. This not only creates an inaccurate estimation of overtopping characteristics, but also creates stability issues in the overtopping box. However, further refining the entire grid quickly creates an unworkable calculation time. Other options need to be found.

6.2 Options for refinement

With a finer resolution necessary, but refining the entire grid not an option, a solution needs to be found in another way. To preserve all interactions between ship and water, local refinement of the grid could be an option. Another option is solving the wave generation and overtopping independently. The ship-induced wave signal can be generated in SWASH and then output for solving the overtopping using a refined SWASH model or a different model. Both options will be discussed here.

6.2.1 Local refinement

One option for creating a larger accuracy without too much extra computational effort is local refinement of the grid. For implementation of this local refinement in SWASH, a curvilinear grid with varying grid cell size can be used. For this illustrative case study, the grid will be refined to a resolution of 0.1x0.1 m

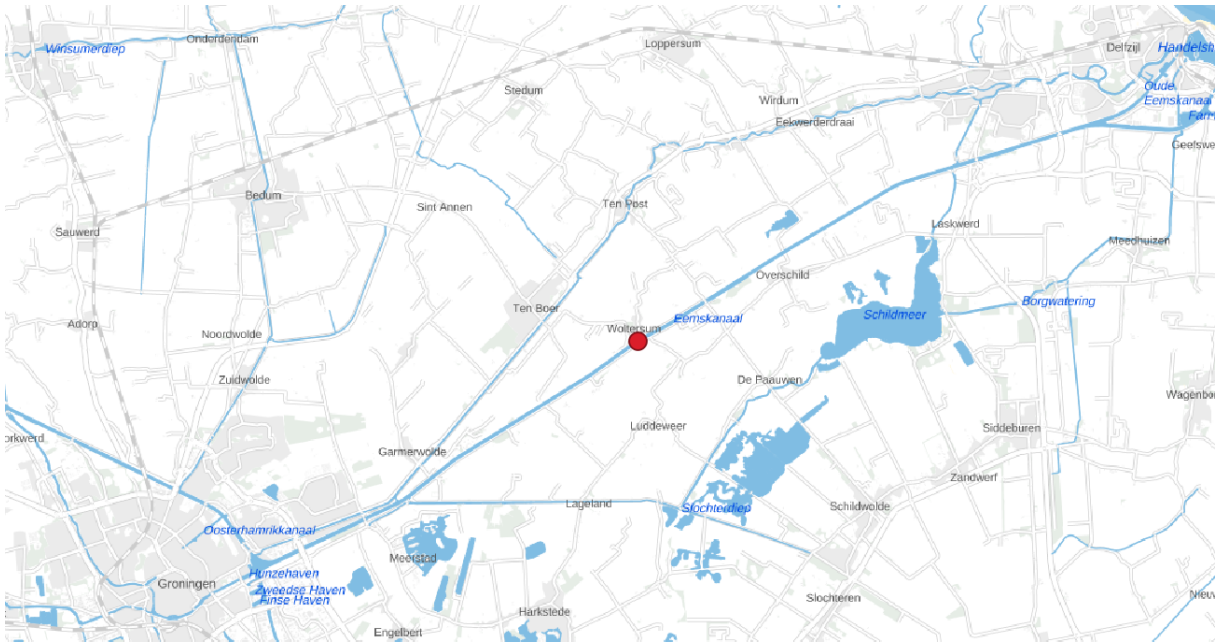


Figure 6.1: Location of the basis for the overtopping case study cross sections

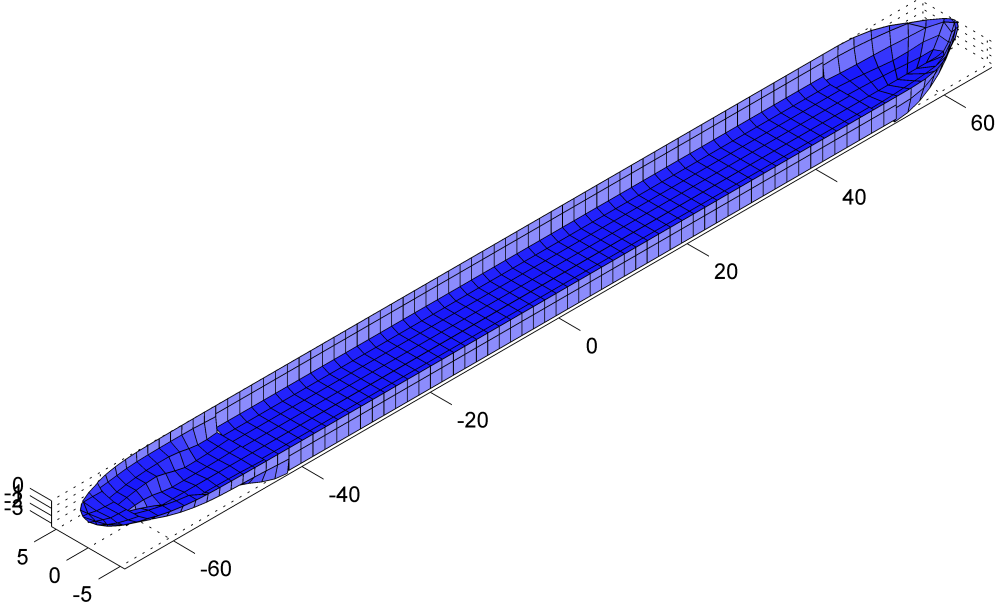


Figure 6.2: The model of a CEMT-Va ship that is used in the case study

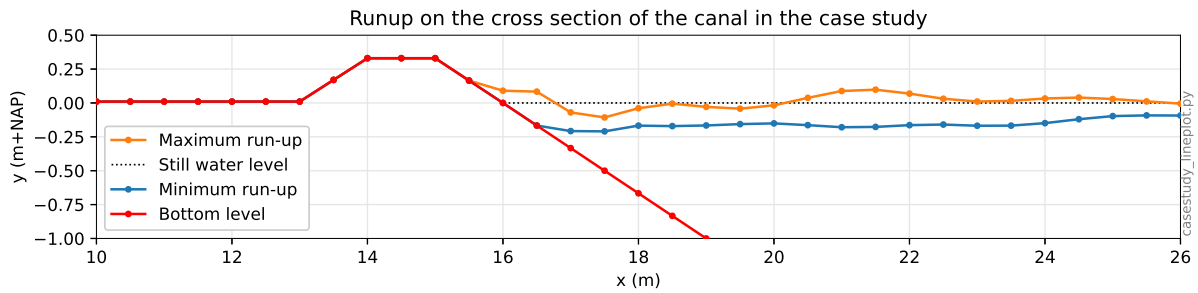


Figure 6.3: Run-up on the 0.5m resolution test grid for the casestudy.

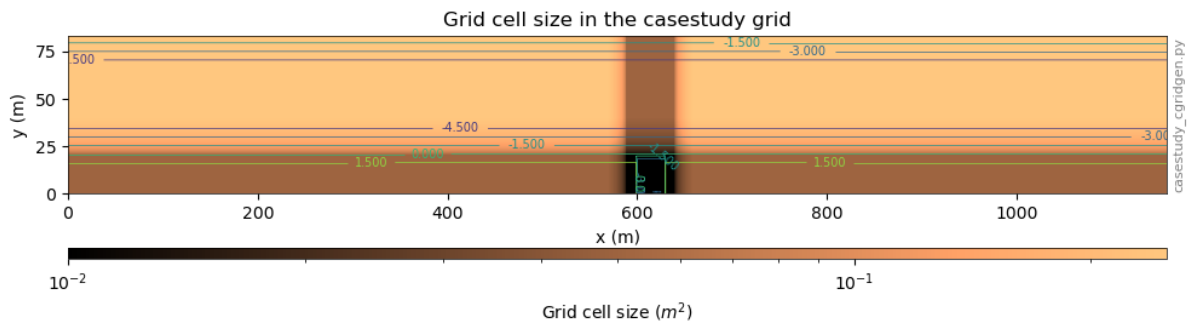


Figure 6.4: Grid cell area in the overtopping case study. Visible is the local grid refinement around the overtopping box.

around the overtopping box. This refinement is still not as fine as the resolutions proposed by Lashley et al. (2020), but more refinement would make the time step so small that the computation effort becomes too large. The refinement takes place linearly over 65 cells. Figure 6.4 shows the grid cell size and bottom contours for the proposed grid. The grid dimensions are 2769x358 grid cells. To speed up simulations, the top of the banks in the non-overtopping area are excluded from simulation, which means a reduction by 2140x150 grid cells. With an allowed range of $0.05 < C_r < 0.3$, SWASH chooses a timestep of 0.0025 s. With $Fr = 0.5$, the whole passage needs a simulated time of 6.50 min.sec. Equation 4.7 yields an estimated run time of $6.96 * 10^2$ hours, or 29 days at 12 cores.

6.2.2 Splitting the model

For the splitting of the model, no illustrative case study has been done. However, a good basis for further steps is research done on splitting the model. As stated earlier in this chapter, with the ship-induced wave signals generated in SWASH it becomes possible to calculate the overtopping using a separate method. These methods can span the full range of models as described by Lashley et al. (2020). The simplest option is using empirical relations developed for wind-waves to estimate the overtopping characteristics. A drawback of this method would be that the interactions between the different ship wave components are lost as these are not properly implemented in relations for wind waves. More accurate would be to couple the SWASH model for wave generation with a separate SWASH model for overtopping. The SWASH model for overtopping could use the full wave signal for overtopping estimation and therefore give an accurate representation of the relevant overtopping characteristics. This SWASH-SWASH coupling has not been done before. What has been done before is coupling of SWASH in 1D with more computationally intensive models like DualSPHysics (Vanneste et al., 2014) or OpenFOAM (Vandebeek et al., 2018). If this coupling can be extended towards a 2D model, the full wave signal can be taken into account. When splitting wave generation and overtopping, a couple of questions arise. First is where to draw the boundary. For computational efficiency, the boundary needs to be placed as close to the shore

as possible, but also in a place where the boundary doesn't influence overtopping characteristics. The second question is how to handle reflection caused by the lack of overtopping in the ship-wave generated signal. If this reflection influences the wave signal on the boundary it can cause unwanted results. The answer to these questions requires further research.

6.3 Summary

As shown in the Eemskanaal case, a resolution suitable for modelling ship wave generation is insufficient for modelling overtopping. The first step towards extending the ship-wave model to include overtopping is therefore finding a method to increase the resolution at the overtopping location while keeping the computational time acceptable. One option is a local refinement of the grid. Using a locally refined grid creates a more accurate grid in the relevant location and makes sure that all interactions between ship and waterway are taken into account. However, the calculation time becomes relatively long, and taking into account the instability that were experienced earlier makes this option an uncertain option. An alternative therefore is to split the model in a wave generation part and an overtopping part. The wave generation can then be done in SWASH while for the overtopping a range of different models can be used. Previous research has shown that coupling between SWASH and other models is possible and produced reliable results. While this method creates some problems with the interaction between the wave generation and overtopping, it is still a promising path to follow.

7 DISCUSSION

This chapter discusses the use of SWASH for the estimation of ship-induced overtopping. First, the insights and limitations of the current study will be discussed. Then the focus will shift to the implications of this study for the engineering applicability of SWASH and the focus of future research.

7.1 Potential insights and limitations

This study aimed to test the applicability of SWASH for modelling ship-induced waves for overtopping with a final goal to contribute to better estimation of ship-induced overtopping hazard at low-lying quays and dikes. Concerning this goal, this study has provided some valuable insights but also sees some limitations.

The main thing to note is the successful creation of a model that can estimate ship-induced wave conditions at the bank for the purpose of overtopping. It is possible to implement the pressure field method in SWASH and thereby to simulate a ship passage. It has been shown that the ship will be properly simulated. The parameters shown to be relevant for overtopping in Suzuki et al. (2014), Suzuki et al. (2017), Vanneste et al. (2014) and Lashley et al. (2020) do not have a large influence on the generated ship wave signal. In line with expectations from literature, the instability of SWASH is a problem. Also, as the secondary waves are very short, the grid cells need to be very small, creating a calculation-intensive model.

With the implementation of the pressure field being successful, the model was validated to three test cases. In these test cases, SWASH produced wave fields as they could be expected in reality, was able to replicate the measured wave signals and estimate wave characteristics better than with existing methods. This leads to the idea that SWASH is a useful tool for modelling ship-induced waves. However, there is still some uncertainty surrounding the validation. This is due to both the limited availability and limited quality of the measured validation data as well as the uncertainties in the model. These uncertainties make this research proof of concept and not an applicable engineering methodology.

The first source of uncertainty is the measurement data. No extensive model validation data set was available. Although being very useful, the data sets that were used for validation were all not gathered for validating a model for the purpose of overtopping. The data from Lataire et al. (2009) was gathered to find the effects of banks on ships manoeuvring in confined waters. The surface excursion measurements were a side product of this research and flow velocity measurements were not available. For the data gathered for the ROPES project (Wictor, 2012), the goal was to find the effects that passing ships have on a moored ship. The surface excursion measurements were a side product of this research. For the data gathered at Bath, the goal was to quantify the impact that passing ships have on bank erosion (Huisman et al., 2010). Most relevant for this is the bottom shear stress. The surface excursion measurements were a side product of this research. In all data sets, this translates to sub-optimal data for model validation. In the Lataire et al. (2009) measurements, flow speeds would have been a useful addition for model validation. For the ROPES measurements, the measurement location was sub-optimal for wave signal validation. The close presence of a reflective quay and a moored ship may have distorted the free wave signal. In the Bath measurements, the unknown track of the ship made the input of SWASH uncertain. In the last two cases, also the lack of the actual bottom data made the geometry uncertain while the geometry can have a large effect on the ship waves. The solution to these limitations would be to do a measurement campaign to gather data with overtopping in mind. In this measurement campaign, the relevant data regarding the waterway is the waterway geometry, water level and flow velocities. Regarding the ship, it is ship-shape, track and velocity. Regarding the waves, the measurement resolution should be fine enough to capture the secondary wave effects. For the overtopping, run-up measurements or flow-velocity and layer thickness on top of a structure are relevant.

The second reason to consider this research proof of concept is the uncertainty in the mechanics behind

the outcomes. Mainly the primary stern wave is subject to a lot of uncertainty. In the MASHCON and ROPES simulations, the primary stern wave is underestimated while in the Bath simulation, the primary stern wave is overestimated. The reason for this can be a multitude of effects. It is therefore unclear what causes over or underestimation. The large computational cost of the simulations made extensive bench-marking impossible in the time frame of this research. For better trust in the model, a sensitivity analysis to environmental parameters like water level and flow velocity would increase the certainty that the ship wave components are overestimated by SWASH. A sensitivity analysis to passage parameters like ship size, shape and track would also decrease uncertainty in the outcomes compared to the results now and therefore increase confidence in the outcomes of the model.

Despite all uncertainties, SWASH already performs better than existing methods for estimating ship waves at the bank. It offers added information in the flow field that it produces, it can produce a wave signal and the magnitudes of the ship wave components relevant for overtopping are better estimated with SWASH than with existing methods.

With the insights as gained above, this study is an extension of the existing literature on ship-induced wave effects. Pre-existing methods like DIPRO+ (Waterloopkundig Laboratorium, 1997) and the BAW guidelines (BAW, 2010) offer only wave characteristics as calculated using standard ships in a simplified geometry. The current model in SWASH can estimate the full wave-signal of a real ship model in the actual geometry. Aside from offering the extra information that the wave signal provides, it has also shown to be an accuracy improvement when used to calculate ship wave magnitudes. The model is therefore a useful starting point for further research on ship-induced water motions.

7.2 Engineering applicability

The applicability of existing ship wave estimation methods is very limited. For example, DIPRO+ is designed for straight channels which can be schematized as a trapezoid. It can explicitly not calculate water movements above a berm or bank. For all cases which do not fall in the validity range of DIPRO+, no good alternative is available. And even if the case at hand fits the limitations of DIPRO+, the output is only wave components and not their dependence. The same goes for the BAW guidelines. Also here, the waterway cross-section is schematized as a rectangle. While being valid for a wider range of waterway widths than DIPRO+, the BAW guidelines don't always offer an increased accuracy.

SWASH can instead be used for more complex geometries and for geometries where wave transformation is important because of the distance between ship and bank. Further, SWASH can estimate not only wave components but the full wave-signal. Instead of guessing the timing of the different wave components at the bank, it can now be estimated using SWASH. This is a significant improvement over pre-existing engineering methods. Aside from overtopping, the wave signal can be used to get the combined effect of primary and secondary waves on bottom shear stress bank protections.

However, caution should still be applied when using SWASH for engineering applications. As this research has shown, SWASH does not consistently overestimate wave components. Also, the timing of the secondary waves can be off if the horizontal resolution of the model is too coarse. Therefore, a safety factor should still be applied when using SWASH to estimate ship wave signals.

But the biggest uncertainty for engineering applications is the instability of SWASH. The risk lies in the chance of spending time to develop a model that doesn't produce any results due to instability. In this research, the instability mainly existed for cases with surface piercing banks. For applications where there are no surface piercing banks, the instability risk is limited. To decrease this risk, research should be done on the causes of the instability in SWASH and ways to mitigate this instability.

In the current state, SWASH is a tool which has potentially a broader application area and a better accuracy than pre-existing tools. However, the unknown necessary safety factor as well as the instability make it only suitable for projects with a large budget. Further research into these elements is necessary to create a design methodology based on SWASH.

7.3 Further research and opportunities

Regarding ship-induced wave overtopping with SWASH, further research can use this thesis as a starting point for three useful follow-up directions.

The first direction is increasing the engineering applicability of SWASH for estimating ship-induced wave signals. This direction should focus on increasing the reliability of the model, as well as increasing trust in the outcomes of the model. Reliability here means increasing stability. In this research, instability has

caused concessions on for example the launching procedure and ship draughts. For increasing trust in the outcomes of the model, more insight is necessary into the mechanics behind these outcomes and the differences with validation measurements. Currently, the mechanics in the model are uncertain. What causes over or underestimation is necessary knowledge to be sure that the simulation doesn't result in an underestimation of the overtopping hazard. This insight can be gained with further research into modelling ship-induced wave signals with SWASH. A sensitivity analysis would be a useful tool. Further, a more extensive measurement data set for comparison would be a useful addition. For a start, the measurement campaign for this data set would register the waterway geometry, the ship-shape, track, velocity and direction during the passage, as well as flow velocity vector, pressure and water level. Ideally, there would be passages of several ships (inland ships as well as sea-going) at different speeds and eccentricities, as well as measurements on the overtopping caused by these ships.

The second direction is extending the model to include overtopping. Including the overtopping is an important step as the current relations for overtopping are mainly based on wind waves and are not necessarily applicable for ship-induced overtopping. Good first steps for this research would be research local refinement of the model around the overtopping location or extending existing coupling methods between SWASH and other models to 2D space to capture the full wave-signal.

The third direction is studying the applicability of SWASH for other ship-induced water motion effect estimation. As indicated by Schroevers et al. (2011), ship waves can cause or accelerate erosion in estuaries. With SWASH being able to model the full ship waves and relevant hydraulic effects like wave breaking and bores, SWASH is a promising tool for gaining more insight in the morphologic effects caused by ship induced water movements. This research has already shown that SWASH can recreate the wave field and signals, but not that it can accurately estimate the ship-induced bottom shear stress over time. Further research is necessary to expand the applicability of SWASH for other applications.

8 CONCLUSION

This thesis aims to research the applicability of SWASH for the estimation of ship-induced overtopping. For conclusion, the three research questions will be answered, followed by some remarks on the aim of the study.

1: In what way can the pressure field method be implemented in SWASH, and how do the settings that influence overtopping influence ship wave generation?

To input the time-varying pressure fields in SWASH, no adaptations to the source code of SWASH need to be made. In this study, a method was developed that specifies the pressure fields and writes them to be read by SWASH. The pressure fields were created by interpolating ship hull coordinates onto a grid. As SWASH offers no hot-start option, a suitable launching procedure should be chosen for the case at hand. Model stability is a determining factor here. Optimally, a longer and more careful starting procedure produces more reliable output. If the model can't be made stable enough for this long procedure, a shorter starting procedure is also an option. The turbulence model and bottom friction that are relevant for overtopping according to the literature have only little influence on the generated wave signal. The model is very sensitive to grid resolution, which in turn has a high impact on the calculation time. In this study, a resolution of 10-20 cells per secondary wavelength was found to be a good optimum. With these settings, the most relevant results can be obtained while the calculation time is still acceptable.

2: To what extent can SWASH reproduce the ship wave components relevant for simulating overtopping?

To test the extent to which SWASH can reproduce the ship wave components relevant for simulating overtopping, SWASH was validated to three ship passages. The validation showed that SWASH performed better than existing methods for estimating the wave components at the bank. Also, SWASH can estimate the wave field and wave signal which existing methods cannot. For overtopping, the primary stern wave and the secondary bow waves are the most relevant. Next to these characteristics, the primary water level depression functions as a measure of reliability. The quality of the estimation by SWASH is analysed by looking at three results: the wave field, the wave signal and the magnitudes of the wave components. In a towing tank environment, SWASH could recreate the measured wave signal relatively well. The certainty about ship position and environment variables made a proper comparison between SWASH and measurements possible. SWASH overestimated secondary wave height and primary water level depression and slightly underestimated primary stern wave height. The two physical passages were characterised by more uncertainty. The ship track was estimated, and tidal flows and reflection could have had their effect on the differences between the measured wave signals and the wave signals produced by SWASH. For the ROPES measurements done in the Port of Rotterdam, SWASH underestimated all wave components. For the secondary wave, this underestimation can be explained by interference between the waves and their reflection on the quay close by. The primary were underestimated because of tidal flow effects which were not implemented in SWASH. SWASH also showed a delayed arrival of the secondary wave compared to measurements. In the measurements done for the effect of ships on the erosion of tidal flats in the Western Scheldt, SWASH showed the same delay in the arrival of the secondary waves and underestimation of secondary wave height and primary water level depression. SWASH overestimated the primary stern wave. In this simulation, the track of the ship was the largest source of uncertainty. The secondary waves and the bore caused by the ship that is influential in the erosion were visible in the model. To classify the performance of SWASH when estimating ship wave components, the SWASH simulations were compared to Dutch and German guidelines. Here,

SWASH outperformed both. Therefore, SWASH has an added benefit over current calculation methods when estimating the wave components relevant for ship-induced overtopping.

3: What is the first step towards extending the ship-wave model in SWASH to include overtopping?

As illustrated by the schematization of the Eemskanaal in SWASH, a resolution suitable for modelling wave generation is too coarse for modelling overtopping. Not only would it cause inaccuracies due to the limited number of cells per wavelength at the bank, but also does this resolution cause instabilities in the overtopping box. For extension of the model to include overtopping, a method needs to be developed that creates a finer resolution at the overtopping location while still keeping the calculation time acceptable. At first sight, a local refinement of the grid is a good solution as this incorporates overtopping in the same model as the wave generation. The interactions between generation and overtopping are therefore taken into account automatically. For the Eemskanaal, such a model would have a calculation time of about a month. Another possibility is splitting the model between a wave generation and an overtopping part. The overtopping part can then be done with empirical relations, SWASH or other models. This method prevents the risk of instability, but it is harder to solve the interactions between generation and overtopping. The first step towards extending the ship-wave model in SWASH to include overtopping is therefore either to do research on increasing the stability of SWASH for overtopping or to implement a coupling method to couple a wave generation model in SWASH to a separate overtopping model.

Research objective: To find out how SWASH performs when modelling ship-induced waves for the purpose of overtopping, by recreating ship wave generation in SWASH, validating the generated wave signals and putting a first step to modelling ship-induced overtopping with SWASH.

Overall, SWASH has been able to recreate the ship-induced wave signal in the cases simulated for this research. For characterizing the performance of SWASH, some measure is necessary. In this case, the easiest measure for performance lies in the replication measurements. Optimal performance is if SWASH could exactly replicate the measured wave signals. The worst possible performance is if the pressure field method could not be implemented in SWASH. Within this range, SWASH shows good performance when modelling ship-induced waves for the purpose of overtopping. The pressure field method was implemented, and the modelled wave signals resembled the measured wave signals. With the SWASH-generated wave fields looking reliable, the differences between SWASH-generated wave signals and the measured wave signals probably originate from uncertainty in the input of SWASH. Compared to existing methods, SWASH is a considerable improvement. With the wave fields and wave signals looking realistic, SWASH has shown that it can model the secondary waves that could not be modelled in earlier studies. When compared with analytical methods, SWASH shows an improvement in accuracy and a wider range of applicability. For the purpose of overtopping, the model should be extended to include the overtopping as well. First steps towards this are working with a locally refined grid or creating a coupling between a wave generation model in SWASH and an overtopping model.

REFERENCES

- Aldershof, M. (2020). Impact of ship waves on sediment transport at two tidal flats in the Western Scheldt. Technical report.
- Allsop, N. W. H., Bruce, T., Pullen, T., and van der Meer, J. (2008). Direct Hazards From Wave Overtopping – the Forgotten Aspect of Coastal Flood Risk Assessment ? *43rd DEFRA Flood and Coastal Management Conference*, (July):1–11.
- Altomare, C., Gironella, X., Suzuki, T., Viccione, G., and Saponieri, A. (2020). Overtopping metrics and coastal safety: A case of study from the catalan coast. *Journal of Marine Science and Engineering*, 8(8).
- Barrass, C. B. and Derrett, D. (2012). *Ship stability for masters and mates LK*. Elsevier / BH, Amsterdam.
- BAW (2010). BAW Code of Practice Principles for the Design of Bank and Bottom Protection for Inland Waterways (GBB) BAW Codes of Practice and Guidelines Publisher.
- CCNR (2019). Annual Report 2019 - Inland Navigation in Europe Market Observation. Technical report.
- Ciria (2007). *The Rock Manual. The use of rock in hydraulic engineering*.
- de Jong, M. (2010). JIP Ropes, WP1 - Framework and overview. Technical report, Svasek, Deltares, Marin, PHM.
- de Jong, M., Roelvink, D. J., Breederveld, C., and Reijmerink, S. (2013). Numerical modelling of passing-ship effects in complex geometries and on shallow water SKIM : the Sea surface Kinematics Multiscale monitoring satellite mission View project [AWA] Ecosystem Approach to the management of fisheries and the marine environmen. *Liege (BE)*, (June 2014):95.
- Deltares (2020a). Quickin User Manual. page 110.
- Deltares (2020b). RGFGGrid User Manual. Technical report, Delft.
- Dusseljee, D., Klopman, G., van Vledder, G. P., and Riezebos, H. (2014). Impact of harbor navigation channels on waves: a numerical modelling guideline. In *ICCE 2014: Proceedings of 34th International Conference on Coastal Engineering, Seoul, Korea, 15-20 June 2014*, pages 1–12. Coastal Engineering Research Council.
- ENW (2007). Ontwerpbelastingen voor het rivierengebied. Technical report, Ministerie van Verkeer en Waterstaat Expertise Netwerk Waterkeren.
- Guimarães, P. V., Farina, L., Toldo, E., Diaz-Hernandez, G., and Akhmatskaya, E. (2015). Numerical simulation of extreme wave runup during storm events in Tramandai Beach, Rio Grande do Sul, Brazil. *Coastal Engineering*, 95:171–180.
- Habben Jansen, A. C. . (2016). The influence of the bow shape of inland ships on the resistance. Technical report.
- Huisman, B., Schroevers, R., and Wal, M. v. d. (2010). Erosie van het slik van Bath. Technical report, Deltares.
- Hujii, A., Takahashi, S., and Endoh, K. (1994). an Investigation of the Wave Forces acting on breakwater handrails. In *Coastal Engineering*, pages 1046–1060.
- Journee, J. M. J. (2001). SEAWAY user manual. Technical Report February.

- Lashley, C. H., Zanuttigh, B., Bricker, J. D., van der Meer, J., Altomare, C., Suzuki, T., Roeber, V., and Oosterlo, P. (2020). Benchmarking of numerical models for wave overtopping at dikes with shallow mildly sloping foreshores: Accuracy versus speed. *Environmental Modelling and Software*, 130:104740.
- Lataire, E., Vantorre, M., and Delefortrie, G. (2012). A prediction method for squat in restricted and unrestricted rectangular fairways. *Ocean Engineering*, 55:71–80.
- Lataire, E., Vantorre, M., and Eloit, K. (2009). Systematic model tests on ship - Bank interaction effects. In *Proceedings International Conference on Ship Manoeuvring in Shallow and Confined Water: Bank Effects 2009*, pages 9–22.
- Mares-Nasarre, P., Argente, G., Gómez-Martín, M. E., and Medina, J. R. (2019). Overtopping layer thickness and overtopping flow velocity on mound breakwaters. *Coastal Engineering*, 154(September).
- Miani, M., Dissanayake, P., Archetti, R., and Lamberti, A. (2015). Sand dune breaching along the Emilia-Romagna littoral zone: A deterministic approach. *36th IAHR World Congress*, (October):1–7.
- Mulligan, R. P., Take, W. A., and Bullard, G. K. (2019). Non-hydrostatic modeling of waves generated by landslides with different mobility. *Journal of Marine Science and Engineering*, 7(8).
- PZC (2019). Vloedgolf verrast strandgangers in Vlissingen.
- Raven, H. C. (2001). Numerical Wash Prediction using a Free-Surface Panel Code. In *MARIN, P.O.Box 28, 6700 AA Wageningen, The Netherlands, Proceedings of the Technical Conference of 6th China International Boat Show, Shanghai, China, April 2001, Paper: P2001-7 Proceedings.*, pages 2–15.
- Rijkswaterstaat (1990). Rekenregels voor waterbouwkundig ontwerpen. Technical report.
- Schijf, J. (1949). Protection of embankments and bed in inland and maritime waters, and in overflows or weirs. In *PIANC 17th congress 1949, Lisbon, section SI C2*. PIANC.
- Schroevers, M., Huisman, B. J., Van Der Wal, M., and Terwindt, J. (2011). Measuring ship induced waves and currents on a tidal flat in the Western Scheldt Estuary. *2011 IEEE/OES/CWTM 10th Working Conference on Current, Waves and Turbulence Measurement, CWTM 2011*, pages 123–129.
- Suzuki, T., Altomare, C., Veale, W., Verwaest, T., Trouw, K., Troch, P., and Zijlema, M. (2017). Efficient and robust wave overtopping estimation for impermeable coastal structures in shallow foreshores using SWASH. *Coastal Engineering*, 122(January):108–123.
- Suzuki, T., Altomare, C., Verwaest, T., Trouw, K., and Zijlema, M. (2014). Two-dimensional wave overtopping calculation over a dike in shallow foreshore by SWASH. *Proceedings of the Coastal Engineering Conference*, 2014-Janua.
- Talstra, H. (2012). Application of FINEL2D for the computation of vessel- induced currents The relevance of applying an explicit Finite Element Method. Technical report.
- TAW (2003). *Leidraad Kunstwerken*.
- Terlingen, H. (2011). Nog geen maatregelen Maeslantkering.
- van Bergeijk, V. M., Warmink, J. J., and Hulscher, S. J. (2020). Modelling the wave overtopping flow over the crest and the landward slope of grass-covered flood defences. *Journal of Marine Science and Engineering*, 8(7).
- Van der Meer, J., Allsop, N., Bruce, T., Rouck, J. D., Kortenhaus, A., Pullen, T., Schüttrumpf, H., Troch, P., and Zanuttigh, B. (2018). *EurOtop: Manual on wave overtopping of sea defences and related structures. An overtopping manual largely based on European research, but for worldwide application*.
- van Os, W. J. (2016). *Golfoverslag in bebouwd gebied*. PhD thesis.
- Vandebeek, I., Gruwez, V., Altomare, C., Suzuki, T., Vanneste, D., De Roo, S., Toorman, E., and Troch, P. (2018). Towards an efficient and highly accurate coupled numerical modelling approach for wave interactions with a dike on a very shallow foreshore. *the 7th International Conference on the Application of Physical Modelling in Coastal and Port Engineering and Science (Coastlab18)*, (1):1–10.

- Vanneste, D., Altomare, C., Suzuki, T., Troch, P., and Verwaest, T. (2014). Comparison of numerical models for wave overtopping and impact on a sea wall. In *Proceedings of the Coastal Engineering Conference*, volume 2014-Janua, pages 1–14.
- Vasarmidis, P., Stratigaki, V., Suzuki, T., Zijlema, M., and Troch, P. (2020). On the accuracy of internal wave generation method in a non-hydrostatic wave model to generate and absorb dispersive and directional waves. *Ocean Engineering*, (September):108303.
- Verheij, H. and Laboyrie, J. (1988). M1115 - XIX, Aantasting van dwarsprofielen in vaarwegen. Technical report, Deltares (WL).
- Verheij, H., Raven, H., Doorn, N., Borsboom, M., and Lambeek, J. (2001). Numerical Modelling of Ship-Induced Water Motions.
- Verheij, H. and van Prooijen, B. (2007). Verbetering DIPRO Q4264.01. Technical Report July.
- Wal, M. v. d. (1990). Heranalyse van M 1115 onderzoeksresultaten. Technical report, Deltares (WL).
- Waterloopkundig Laboratorium (1997). DIPRO 3.02n.
- Watersportalmanak.nl (2011). Tide table Maassluis.
- Victor, E. (2012). Ropes full scale measurements - Nieuwe Waterweg Measurement Campaign, Part III. Technical report, Marin.
- Zhou, M., Roelvink, D., Verheij, H., and Ligteringen, H. (2013). Study of Passing Ship Effects along a Bank by Delft3D-FLOW and XBeach. *International Workshop on Next Generation Nautical Traffic Models*, (1998):71–80.
- Zijlema, M. and Stelling, G. (2005). Further experiences with computing non-hydrostatic free-surface flows involving water waves. *International Journal for Numerical Methods in Fluids*, 48(2):169–197.
- Zijlema, M. and Stelling, G. (2008). Efficient computation of surf zone waves using the nonlinear shallow water equations with non-hydrostatic pressure. *Coastal Engineering*, 55(10):780–790.
- Zijlema, M., Stelling, G., and Smit, P. (2011). SWASH: An operational public domain code for simulating wave fields and rapidly varied flows in coastal waters. *Coastal Engineering*, 58(10):992–1012.

A WAVE SIGNAL PROCESSING

For more insight in the wave signals, and for comparison with DIPRO and BAW guidelines, the relevant wave characteristics need to be extracted from the measured wave signal. The main characteristics are stern wave (z_{max}) and secondary wave (H_i) height, as these will cause the most overtopping when they coincide. For comparison with other models, water level depression (Δh) is also calculated.

A.1 Filtering method

The main method for extracting the characteristics is a band filter on the signal. As the primary wave and secondary wave have significantly different frequencies, their effects can be separated using a low-pass filter to extract the primary wave and a high-pass filter to extract the secondary wave (Aldershof, 2020). According to Wal (1990), the secondary wave frequency is given by:

$$f_i = \frac{g}{5.1V_s} \quad (\text{A.1})$$

With f_i denoting secondary wave frequency, g the gravity constant and V_s the vessel speed. For the Lataire et al. (2009) towing tank experiment, the distance between ship and measurement points meant that the primary wave was not distorted by propagation. Its frequency is therefore given by:

$$f_p = \frac{V_s}{L_v} \quad (\text{A.2})$$

In this equation, f_p is the primary wave frequency and L_v is the length of the vessel. The cutoff frequency is determined by taking a weighted average of these two frequencies. For the primary wave, the frequency distribution is narrower. A good cutoff frequency is therefore closer to the primary frequency than to the secondary wave frequency. The frequency distribution is given by:

$$f_{cutoff} = \frac{3 * f_p + f_i}{4} \quad (\text{A.3})$$

A.2 Example results

The results of this filter is visible in Figure A.1 and Figure A.2, as well as Figure A.3 and Figure A.4. From these wave signals, the secondary wave height H_i is the absolute maximum of the secondary wave signal. The primary water level depression Δh is the minimum of the primary wave signal. The primary stern wave is the maximum of the primary wave signal, only looking at the part of the signal that was recorded after the primary water level depression was measured.

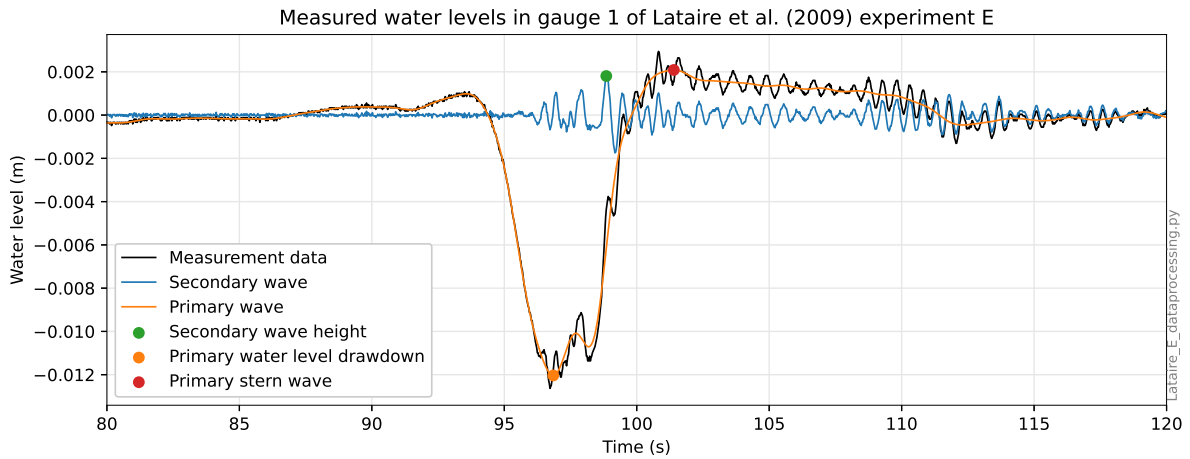


Figure A.1: The wave signals after filtering and the points at which the characteristics were determined, for the measurements in Lataire et al. (2009), Experiment E.

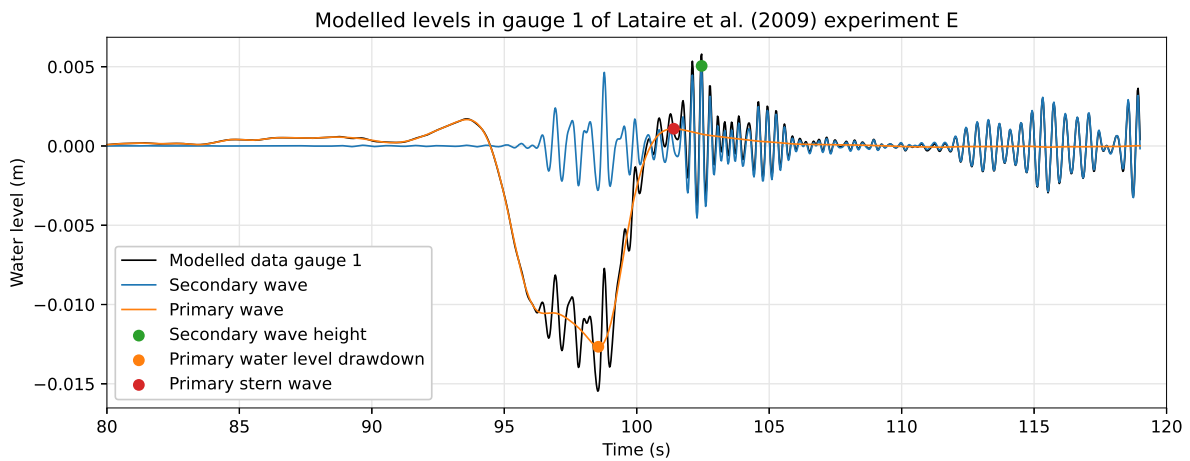


Figure A.2: The wave signals after filtering and the points at which the characteristics were determined, for the model of Lataire et al. (2009), Experiment E.

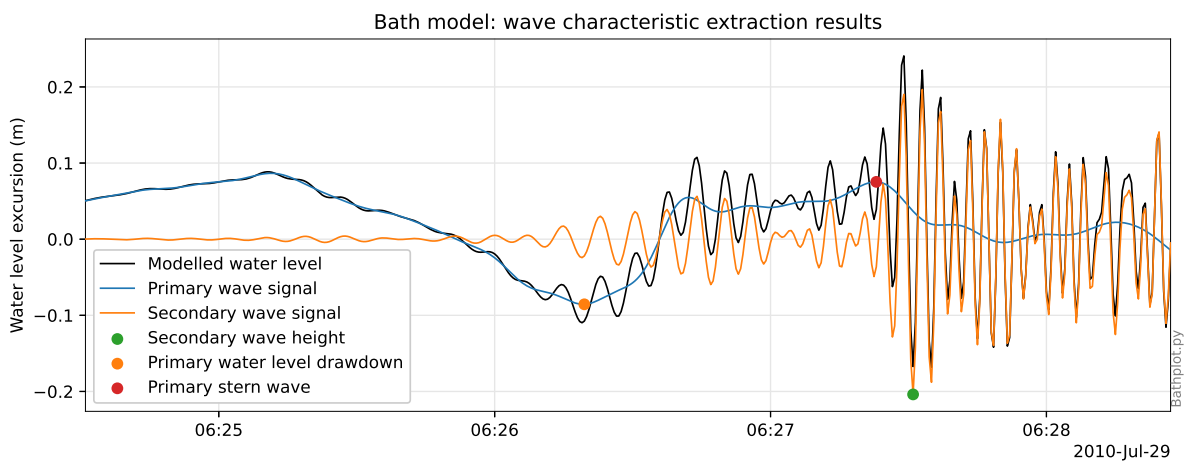


Figure A.3: The wave signals after filtering and the points at which the characteristics were determined, for the measurements on the Bath passage.

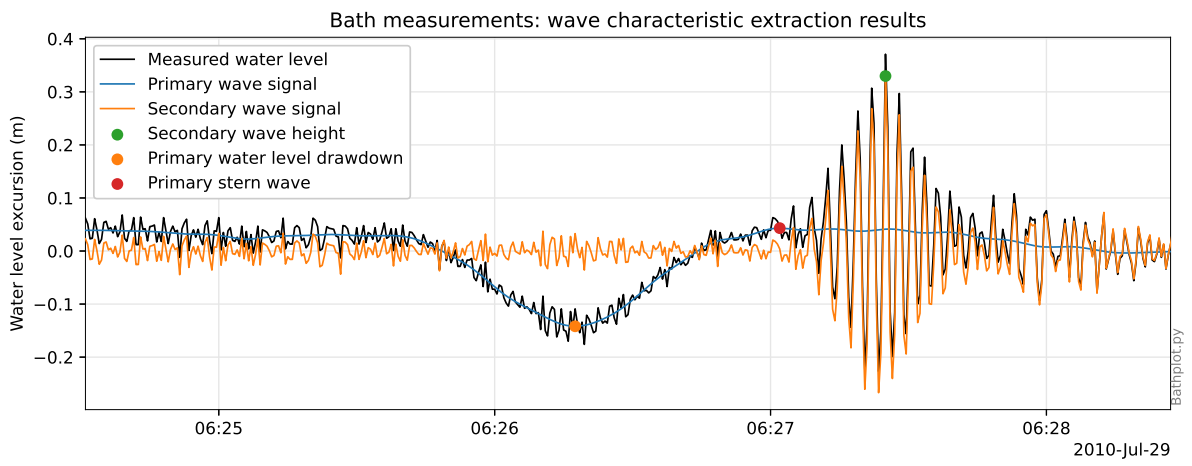


Figure A.4: The wave signals after filtering and the points at which the characteristics were determined, for the model of the Bath passage.

B EXAMPLE CALCULATION TIME ESTIMATION

For the purpose of illustrating the calculation time issue with current gen PC's, two example calculations will be done. The first will be for a uniform grid to show the infeasibility of using the advised resolution everywhere. The second will show the issue when locally refining the grid to the advised resolution.

B.1 Uniform grid

An example calculation for the advised resolution will show the issue with calculation time using current gen PC's. For this example calculation, the duration of the simulation of an experiment from Lataire et al. (2009) on a PC with 12 cores will be calculated. The duration of the experiments is 120 seconds. The dimensions of this towing tank are 7 meters width and 88 meters length. The depth is 0.36m. The maximum speed tested is 0.801 m/s. According to equation 2.8, this speed will give a secondary wave length of 0.275m. The grid cell size will then be: $\Delta x = \Delta y = L_s/50 = 0.0055\text{m}$. Rewriting equation 2.7 gives:

$$\Delta t = \frac{Cr}{(\sqrt{gh} + \sqrt{u^2 + v^2}) \sqrt{\frac{1}{\Delta x^2} + \frac{1}{\Delta y^2}}} \quad (\text{B.1})$$

For the purpose of this example calculation, an optimistic estimate of calculation time will show that a resolution of $L_s/50$ will already lead to an unworkable calculation time. To get the most positive estimation of calculation time that is still realistic, the $Cr = 0.3$ as this is the largest Courant number that is allowed for stability reasons. Further, the calculation will be simplified by neglecting the return current, therefore removing the $\sqrt{u^2 + v^2}$ term. The combination of these assumption will lead to a high estimate of the time step, and therefore a low estimate of the number of calculations necessary. Using the equations and the values as described above gives the following set of outcomes:

$$\Delta t = \frac{0.3}{\sqrt{9.81 * 0.36} \sqrt{\frac{1}{0.0055^2} + \frac{1}{0.0055^2}}} = 6.22 * 10^{-4} \quad (\text{B.2})$$

$$N = \frac{120 - 0}{6.22 * 10^{-4}} * \frac{88}{0.0055} * \frac{7}{0.0055} * 4 = 1.30 * 10^{12} \quad (\text{B.3})$$

$$t_{\text{computation}} = 1.04 * 10^{-19} * (1.31 * 10^{12})^2 + 6.18 * 10^{-9} * 1.31 * 10^{12} - 0.35 = 1.83 * 10^5 h \approx 20 \text{ years} \quad (\text{B.4})$$

It should be noted that this equation is an extrapolation of the trends found in the simulations done for this research. Combined with the spread in the results as visible in Figure 4.13, the uncertainty alone makes the computational time at the wanted resolution too large for any practical purposes. Simplification of the model is therefore necessary, as well as research into the influence simplification has on the outcome of the simulations.

B.2 Locally refined grid

Using a curvilinear grid, it is possible in SWASH to reduce the number of grid cells by only locally refining the grid. For this calculation, the same case as for the uniform grid will be used but with two grid cell sizes: Most of the tank will be simulated at a resolution of 15 CPW, but the 2 m around the measurement location will be simulated at 50 CPW in both x and y direction.

These two resolutions give two grid cell sizes: 0.018m in the 15 CPW area and 0.0055m in the 50 CPW area. With the maximum Courant number being checked for all cells, the smallest cell will determine the timestep. As the smallest cell has the same size in the uniform grid, the timestep will be the same:

$$\Delta t = 6.22 * 10^{-4} \quad (\text{B.5})$$

What will change is the number of calculations necessary, as the total number of grid cells has decreased. The new number of calculations necessary is:

$$N = \frac{120 - 0}{6.22 * 10^{-4}} * \frac{(\frac{2}{0.0055} + \frac{86}{0.018}) * (\frac{2}{0.0055} + \frac{5}{0.018}) * 4}{12} = 2.06 * 10^{11} \quad (\text{B.6})$$

$$t_{\text{computation}} = 1.04 * 10^{-19} * (2.06 * 10^{11})^2 + 6.18 * 10^{-9} * 2.06 * 10^{11} - 0.35 = 5.71 * 10^3 h \approx 238 \text{days} \quad (\text{B.7})$$

Although a large improvement, the estimated calculation time is still unworkably long at 238 days, and this is even using a resolution of 50 CPW. If the refinement is done at 100 CPW, the cell size in the refined area decreases to 0.0027m. This will give the following situation:

$$\Delta t = 3.11 * 10^{-4} \quad (\text{B.8})$$

$$N = \frac{120 - 0}{6.22 * 10^{-4}} * \frac{(\frac{2}{0.0027} + \frac{86}{0.018}) * (\frac{2}{0.0027} + \frac{5}{0.018}) * 4}{12} = 6.96 * 10^{11} \quad (\text{B.9})$$

$$t_{\text{computation}} = 1.04 * 10^{-19} * (6.96 * 10^{11})^2 + 6.18 * 10^{-9} * 6.96 * 10^{11} - 0.35 = 5.46 * 10^4 h \approx 6 \text{years} \quad (\text{B.10})$$

C CASE STUDY LAYOUT

For the illustrative case study in Chapter 6, a SWASH model is designed based on the Eemskanaal near Woltersum. This Appendix describes the design process and the model. It will start with the geometry to be implemented in SWASH. Then the passage settings will determine the length of the model. The final part is the grid layout.

C.1 Geometry

One of the reasons for choosing the Eemskanaal as location for the illustrative case study is the simplicity of the geometry. At the section near Woltersum, the canal is straight and has a trapezoidal cross-section. This cross section is displayed in C.1. Unfortunately, no low-lying quays are present along the Eemskanaal. The low-lying quay and an overtopping box are fictional. The proposed geometries can be found in Figure C.1. Visible is that in the overtopping area, the quay height is 0.1 m. On the side of the canal where no overtopping is expected, the profile stops just below the surface to prevent instabilities here. The width of the canal is 62 m and the depth 5 m. The banks have a slope of 1:3. The bank on the non-overtopping side of the canal ends below the waterline to prevent instability issues at this bank.

C.2 Passage settings

In the SWASH model, three phases can be distinguished in the ship passage:

1. Launching and accelerating,
2. passing the overtopping location,
3. leaving the overtopping domain, creating time for overtopping to take place.

In the first phase, the ship is launched and then accelerated. The acceleration distance is estimated to be three times the ship length. In the second phase the ship passes the overtopping location, generating the waves that will eventually overtop the dike. As found in Chapter 2, the hazards of overtopping ship waves stem mostly from flow speed and layer thickness. These characteristics should therefore be measured

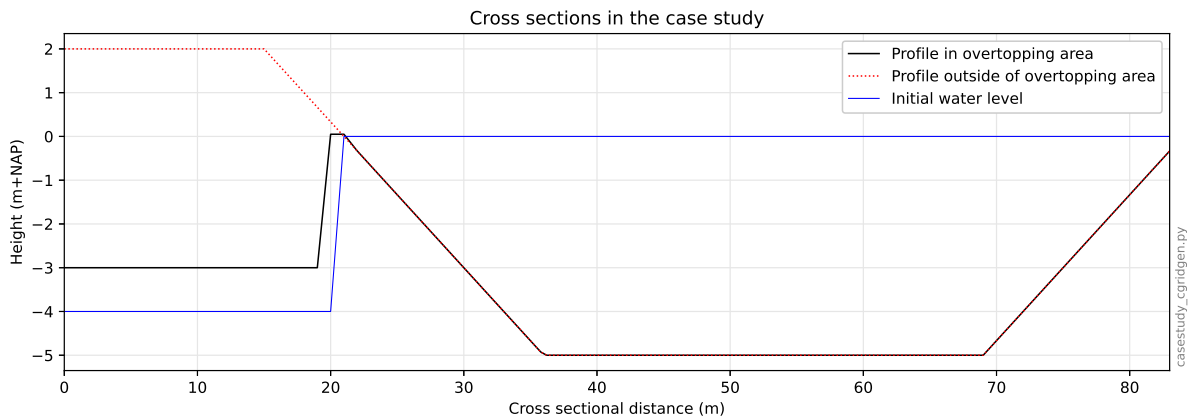


Figure C.1: Cross sections for the overtopping case study. The blue line represents the initially specified water level. If this water level is below the bottom level, a cell is dry.

Table C.1: Speed, secondary wave length and resolution for the different cases in the case study

Froude	V_s (m/s)	L_s (m)	Resolution (CPW)
0.7	4.9	10.3	20.6
0.6	4.2	7.56	15.1
0.5	3.5	5.25	10.5

on top of the dike. At the overtopping location, an overtopping box should be present to make sure that the ship waves can freely overtop. For the estimating the overtopping volumes, an overtopping box is not necessary. To get a steady overtopping away from transition between non-overtopping and overtopping geometries, the overtopping area is taken to be 100 m long. In the third phase, the ship has passed the overtopping location. The waves propagate towards the dike and create the eventual overtopping effects. The distance covered by the ship during this phase is estimated to be five ship lengths. The total length of the geometry is 1400 m.

C.3 Grid layout

The simplest grid is a rectangular grid with uniform grid cell size. For a simulation with an acceptable computational effort, the grid cell size can be 0.5 m in both x and y direction, creating a grid of 1400 by 174 cells. The resolution for the different ship speeds as visible in Table C.1 looks acceptable for wave generation.

D SWASH INPUT FILE: MASHCON EXPERIMENT F

```
$*****HEADING*****
$
PROJ 'lataire_F2' 'run1'
$ 2D tests atmospheric pressure-induced water movements
$ Adapted from sws_master by swsngen.py on 09/09/2020
$
$ --|-----|
$ | This SWASH file is created by swsngen.py for testing |
$ | settings when simulating ship waves using |
$ | the pressure field method |
$ --|-----|
$
$ *****SHIP SETTINGS*****
$ Ship name: container_zhou_3 Length: 4.332m Speed: 0.801m/s
$ Start position: [3, 2.06]m Launch time: [2, 25]s
$
$*****MODEL INPUT*****
$
SET depmin = 0.5e-4 salinity = 0.0
$
MODE NONST TWOD
$
CGRID REG 0. 0. 0. 50.0 7.0 2500 350
$
VERT 4 10 20 30 40 PERC
$
INPGRID BOTTOM 0. 0. 0. 2500 350 0.02 0.02
READINP BOTTOM 1. 'bottomgrid.txt' 1 0 FREE
$
INPGRID PR 0. 0. 0. 2500 350 0.02 0.02 NONSTAT 000000.000 0.1 SEC 000120.000
READINP PR 100 SERI 'pgrid_fnames.txt' 1 0 FREE
$
INPGRID WI 0. 0. 0. 2500 350 0.02 0.02
READINP WI 1. 'windgrid.txt' 1 0 FREE
$
$ * Commands for initial and boundary conditions*****
$
INIT ZERO
$
BOU SIDE E BTYPE SOMM CON 0
BOU SIDE W BTYPE SOMM CON 0
SPON E 1.0
SPON W 1.0
$
$ * Commands for physics *****
$
$ No wind, no bottom friction, no turbulent mixing, no porous layers
```

```

$
$ * Numerics *****
NONHYD BOX PREC ILU
$
DISCRET UPW UMOM MOM H FRO
DISCRET UPW WMOM H FRO
DISCRET UPW UMOM MOM V BDF
DISCRET UPW WMOM V BDF
$
TIMEI 0.05 0.3
$
$***** OUTPUT REQUESTS *****
$
POIN 'GAUGE1' 24.000 2.050
TABLE 'GAUGE1' NOHEAD 'output\gauge1.txt' TSEC WATL PRESS OUTPUT 000001.000 0.025 S
$
POIN 'GAUGE2' 24.000 1.650
TABLE 'GAUGE2' NOHEAD 'output\gauge2.txt' TSEC WATL PRESS OUTPUT 000001.000 0.025 S
$
POIN 'GAUGE3' 24.000 1.185
TABLE 'GAUGE3' NOHEAD 'output\gauge3.txt' TSEC WATL PRESS OUTPUT 000001.000 0.025 S
$
GROUP 'LINE' 1200 1200 1 351
BLOCK 'LINE' NOHEAD 'output\line.mat' WATL OUTPUT 000001.000 0.025 S
$
BLOCK 'COMPGRID' NOHEAD 'output\wl_grid.mat' WATL OUTPUT 000001.000 0.25 S
$
BLOCK 'COMPGRID' NOHEAD 'output\velgrid.mat' VMAG OUTPUT 000001.000 0.25 S
$
$GROUP 'VELVEC' 1 2501 1 351
$BLOCK 'VELVEC' NOHEAD 'output\velvec.mat' VEL OUTPUT 000001.000 0.25 S
$
$ ***** TEST, START AND STOP COMMANDS *****
TEST 1,0

COMP 000001.000 0.002 SEC 000115.000
STOP

```

E SWASH INPUT FILE: MASHCON EXPERIMENT E

```
$*****HEADING*****
$
PROJ 'Lataire_E' 'run1'
$ 2D tests atmospheric pressure-induced water movements
$ Adapted from sws_master by swsngen.py on 24/09/2020
$
$ --|-----|
$ | This SWASH file is created by swsngen.py for testing |
$ | settings when simulating ship waves using |
$ | the pressure field method |
$ --|-----|
$
$ *****SHIP SETTINGS*****
$ Ship name: container_zhou_3 Length: 4.332m Speed: 0.687m/s
$ Start position: [-1, 2.97]m Launch time: [2, 25]s
$
$*****MODEL INPUT*****
$
SET depmin = 0.5e-4 salinity = 0.0
$
MODE NONST TWOD
$
CGRID REG 0. 0. 0. 71.0 7.0 3550 350
$
VERT 4 10 20 30 40 PERC
$
INPGRID BOTTOM 0. 0. 0. 3550 350 0.02 0.02
READINP BOTTOM 1. 'bottomgrid2.txt' 1 0 FREE
$
INPGRID PR 0. 0. 0. 3550 350 0.02 0.02 NONSTAT 000000.000 0.1 SEC 000200.000
READINP PR 100 SERI 'pgrid_fnames.txt' 1 0 FREE
$
INPGRID WI 0. 0. 0. 3550 350 0.02 0.02
READINP WI 1. 'windgrid.txt' 1 0 FREE
$
$ * Commands for initial and boundary conditions*****
$
INIT ZERO
$
BOU SIDE E BTYPE SOMM CON 0
BOU SIDE W BTYPE SOMM CON 0
SPON E 1.0
SPON W 1.0
$
$ * Commands for physics *****
$
$ No wind, no bottom friction, no turbulent mixing, no porous layers
```

```

$
$ * Numerics *****
NONHYD BOX PREC ILU
$
DISCRET UPW UMOM MOM H FRO
DISCRET UPW WMOM H FRO
DISCRET UPW UMOM MOM V BDF
DISCRET UPW WMOM V BDF
$
TIMEI 0.05 0.3
$
$***** OUTPUT REQUESTS *****
$
POIN 'GAUGE1' 18.000 2.050
TABLE 'GAUGE1' NOHEAD 'output\gauge1.txt' TSEC WATL PRESS OUTPUT 000001.000 0.025 S
$
POIN 'GAUGE2' 18.000 1.650
TABLE 'GAUGE2' NOHEAD 'output\gauge2.txt' TSEC WATL PRESS OUTPUT 000001.000 0.025 S
$
POIN 'GAUGE3' 18.000 1.185
TABLE 'GAUGE3' NOHEAD 'output\gauge3.txt' TSEC WATL PRESS OUTPUT 000001.000 0.025 S
$
GROUP 'LINE' 900 900 1 351
BLOCK 'LINE' NOHEAD 'output\line.mat' WATL OUTPUT 000001.000 0.025 S
$
BLOCK 'COMPGRID' NOHEAD 'output\wl_grid.mat' WATL OUTPUT 000001.000 0.25 S
$
BLOCK 'COMPGRID' NOHEAD 'output\velgrid.mat' VMAG OUTPUT 000001.000 0.25 S
$
$BLOCK 'COMPGRID' NOHEAD 'output\velvec.mat' VEL OUTPUT 000001.000 0.25 S
$
$ ***** TEST, START AND STOP COMMANDS *****
TEST 1,0

COMP 000001.000 0.002 SEC 000159.000
STOP

```

F SWASH INPUT FILE: ROPES SIMULATION

```
$*****HEADING*****
$
PROJ 'curv01' 'run1'
$ Sailing along a spline through Rotterdam
$
$ --|-----|
$ | This SWASH file is created by swsgen.py for testing |
$ | settings when simulating ship waves using |
$ | the pressure field method |
$ --|-----|
$
$*****MODEL INPUT*****
$
SET depmin = 0.5e-4 salinity = 0.0
$
MODE NONST TWOD
$
CGRID CURV 3402 486
READGRID COOR 1. 'Rdam3402x486.sgrd' 3 0 FREE
$
VERT 4 10 20 30 40 PERC
$
INPGRID BOTTOM CURV EXC 999
READINP BOTTOM -1. 'Rdam3402x486.bot' 3 0 FREE
$
$INPGRID PR CURV NONSTAT 000000.000 1 SEC 000630.000
$READINP PR 100 SERI 'pgrid_fnames.txt' 3 0 FREE
$
INPGRID WI CURV
READINP WI 1. 'windgrid.txt' 3 0 FREE
$
INPGRID SHIP CURV
READINP SHIP 1 'mooredship.shp' 3 0 FREE
$
$ ***** Commands for initial and boundary conditions*****
$
INIT ZERO
$
BOU SEGM IJ 1 1 1 487 BTYPE SOMM CON 0
$
BOU SEGM IJ 3403 1 3403 487 BTYPE SOMM CON 0
$
$ ***** Commands for physics *****
$
$ No wind, no bottom friction, no turbulent mixing, no porous layers
$
$ ***** Numerics *****
```

```

NONHYD BOX PREC ILU
$
DISCRET UPW UMOM MOM H FRO
DISCRET UPW WMOM H FRO
DISCRET UPW UMOM MOM V BDF
DISCRET UPW WMOM V BDF
$
TIMEI 0.05 0.3
$
$***** OUTPUT REQUESTS *****
$
GROUP 'GAUGE1' 1 1 1 1
TABLE 'GAUGE1' NOHEAD 'output\gauge1.txt' TSEC WATL PRESS OUTPUT 000001.000 0.5 S
$
GROUP 'GAUGE2' 162 162 30 30
TABLE 'GAUGE2' NOHEAD 'output\gauge2.txt' TSEC WATL PRESS OUTPUT 000001.000 0.5 S
$
BLOCK 'COMPGRID' NOHEAD 'output\wl_grid.mat' WATL OUTPUT 000001.000 2 S
BLOCK 'BOTGRID' NOHEAD 'output\bot_grid.mat' WATL XP YP BOTL DEP
$
$ ***** TEST, START AND STOP COMMANDS *****
TEST 1,0

COMP 000001.000 0.05 SEC 001000.000
STOP

```

G SWASH INPUT FILE: BATH SIMULATION

```
$*****HEADING*****  
$  
PROJ 'bath62' 'run1'  
$  
$ --|-----|--  
$ | Recreating the measurements done on ship waves at |  
$ | Bath using the pressure field method |  
$ | |  
$ --|-----|--  
$  
$*****MODEL INPUT*****  
$  
SET level = 3.03 depmin = 0.5e-4 salinity = 0.0  
$  
MODE NONST TWOD  
$  
CGRID CURV 1701 486  
READGRID COOR 1. 'Bath1701x486.sgrd' 3 0 FREE  
$  
VERT 4 10 20 30 40 PERC  
$  
INPGRID BOTTOM CURV EXC 999  
READINP BOTTOM -1. 'Bath1701x486.bot' 3 0 FREE  
$  
INPGRID PR CURV NONSTAT 000000.000 1 SEC 000850.000  
READINP PR 100 SERI 'pgrid_fnames.txt' 3 0 FREE  
$  
INPGRID WI CURV  
READINP WI 1. 'windgrid.txt' 3 0 FREE  
$  
$ ***** Commands for initial and boundary conditions*****  
$  
INIT ZERO  
$  
BOU SEGM IJ 1 1 1702 487 BTYPE SOMM CON 0  
$  
$  
$ ***** Commands for physics *****  
$  
$ No wind, no bottom friction, no turbulent mixing, no porous layers  
$  
$ ***** Numerics *****  
NONHYD BOX PREC ILU  
$  
DISCRET UPW UMOM MOM H FRO  
DISCRET UPW WMOM H FRO  
DISCRET UPW UMOM MOM V BDF
```

```
DISCRET UPW WMOM V BDF
$
TIMEI 0.05 0.3
$
$***** OUTPUT REQUESTS *****
$
GROUP 'AWACW' 779 779 1 487
BLOCK 'AWACW' NOHEAD 'output\awacw.mat' TSEC WATL OUTPUT 00001.000 0.5 S
$
GROUP 'AWACV' 779 779 1 487
BLOCK 'AWACV' NOHEAD 'output\awacv.mat' TSEC VELK OUTPUT 00001.000 0.5 S
$
GROUP 'VECV' 776 776 1 487
BLOCK 'VECV' NOHEAD 'output\vecv.mat' TSEC VELK VEL OUTPUT 00001.000 0.5 S
$
BLOCK 'COMPGRID' NOHEAD 'output\wl_grid.mat' WATL OUTPUT 00001.000 2 S
BLOCK 'BOTGRID' NOHEAD 'output\bot_grid.mat' WATL XP YP BOTL DEP
$
$ ***** TEST, START AND STOP COMMANDS *****
TEST 1,0

COMP 00001.000 0.05 SEC 000850.000
STOP
```